Combustion for Enhanced Recovery of Light Oil at Medium Pressures

Negar KHOSHNEVIS GARGAR

Combustion for Enhanced Recovery of Light Oil at Medium Pressures

Proefschrift

ter verkrijging van de graad van doctor
aan de Technische Universiteit Delft,
op gezag van de Rector Magnificus prof. ir. K.C.A.M. Luyben,
voorzitter van het College voor Promoties,
in het openbaar te verdedigen op donderdag 3 juli 2014 om 15:00 uur

door

Negar KHOSHNEVIS GARGAR

Master of Science in Petroleum Engineering,
University of Calgary and Petroleum University of Technology
geboren te Tabriz, Iran

Dit proefschrift is goedgekeurd door de promotoren:
Prof.dr. J. Bruining
Prof.dr. D. Marchesin

Samenstelling promotiecommissie:

Rector Magnificus	Voorzitter
Prof.dr. J. Bruining	Technische Universiteit Delft, promotor
Prof.dr. D. Marchesin	Instituto Nacional de Matemática Pura e Aplicada Brazilië, promotor
Prof. dr. P.L.J. Zitha	Technische Universiteit Delft
Prof. ir. C.P.J.W. van Kruijsdijk	Shell International, Rijswijk / Technische Universiteit Delft
Dr. A.A. Mailybaev	Instituto Nacional de Matemática Pura e Aplicada, Brazilië
Dr. K.H.A.A. Wolf	Technische Universiteit Delft
Dr. D. van Batenburg	Shell International, Rijswijk
Prof. dr.J.D. Jansen	Technische Universiteit Delft, reservelid

This research was carried out within the context of the first ISAPP programme. This first programme of ISAPP (Integrated Systems Approach to Petroleum Production) is a joint project of the Netherlands Organization of Applied Scientific Research TNO, Shell International Exploration and Production, and Delft University of Technology. In addition, this thesis was also supported by Capes/Nuffic 024/2011. The author thanks TU Delft and the collaboration between TU Delft and IMPA for providing the opportunity for this work.

Cover design by N. Khoshnevis Gargar, Combustion

Printed by CPI-Wöhrmann Print Service – Zutphen

ISBN: 978-94-6203-611-6

To Roozbeh, my father and my mother

Contents

1. Introduction

Today's share of fossil fuels in the global energy demand is estimated (by World Energy Outlook 2013 [50]) at 82%, which is the same as it was 25 years ago. It is anticipated in that report that an increased availability of renewable energies would reduce this to around 75% in 2035 [50]. However, it is expected that the share of renewables (e.g., biofuels, wind and solar) in primary energy use will rise from 13% in 2011 to only 18% in 2035.

The production from current oil fields is declining at an increasing rate; moreover 50% of the initial oil in place is left unproduced. Recovery percentages from oil reservoirs range from 5% for difficult oil to 50% for light oil in highly permeable reservoirs. Other reservoirs contain oil that is difficult to produce by conventional means, e.g., because the permeability is highly heterogeneous or the viscosity is high [87, 20]. One option is using enhanced oil recovery (EOR), in which 30% to 60% of the reservoir's original oil can be extracted [2] compared with 20% to 40% using only primary and secondary recovery [1].

This thesis considers a new process of air injection to enhance recovery of light oil [34, 36, 40, 85, 79, 41, 9, 5]. Since air injection, leads to high temperatures as a result of combustion, it is often categorized as a thermal recovery method, unlike nitrogen injection, which is a miscible and immiscible displacement in different proportions. In this case the oxygen in the injected air burns the heavier components of the oil, thus generating a heat wave leading to cracking of heavier components and vaporization of lighter components. Air injection has the advantage of ready air availability at any location [83]; however, energy costs of air compression necessary for injection are not negligible.

In-situ combustion is generally considered as a technique applicable to heavy oils because of the significant reduction in oil viscosity. However, it also promotes production through thermal expansion, distillation and combustion gas drive; so it can also be used to recover light oils. In this case the air injection process can be employed in deep light oil reservoirs, where it is usually applied at higher pressures and therefore referred to as high pressure air injection (HPAI), whereas the term "in-situ combustion" traditionally has been used for heavy oil reservoirs. An improved understanding of air injection processes, including HPAI, is required in order to prevent the oxygen from reaching the production wells, which is considered a safety hazard [44].

Air injection is potentially one of the most promising and important secondary and tertiary oil recovery methods, which could be applied in numerous projects. Our

interest is in recovering light oil from low permeability heterogeneous reservoirs using air injection leading to oil combustion, as the oil vaporizes away from the lower permeability parts to be collected in the higher permeability streaks. Due to simultaneous vaporization, the combustion at medium pressures, i.e., at medium depth, occurs at medium temperatures. It turns out that the research described here leads to unraveling new mechanisms that prevail during medium temperature oxidation.

It is worth noting that water injection is not an efficient recovery method in low permeability heterogeneous reservoirs due to poor sweep efficiency [87, 20]. There is a large body of literature describing the use of HPAI (high pressure $>$ 100 bars air injection) to recover oil [3, 6, 23, 25, 26, 56, 62, 63, 88, 93]. HPAI was first introduced in 1979 in the Buffalo field [35]. The effectiveness of HPAI depends on many oil recovery mechanisms [28] including sweeping by flue gases, field re-pressurization by the injected gas, oil swelling, oil viscosity reduction, stripping off light components in the oil by flue gas and thermal effects generated by the oxidation reactions. The displacement efficiency of oil recovery in combustion processes is the initial oil-in-place excluding the amount of fuel consumed in combustion, i.e., it produces the residual oil [68]. However to reduce the high compression costs and to avoid fracturing at shallower depth, our focus will be an alternative to HPAI, i.e., to inject air at medium pressures ($\sim 10 - 90$ bars). The main recovery mechanism that we consider for medium pressures is the interaction between vaporization and combustion of light oil.

The mathematical theory of combustion in porous media is well developed for immobile fuels, see, e.g., [16, 23, 71, 82, 88]. When the fuel is liquid and can also vaporize, the problem becomes more complicated. It was shown in [66] that, in the case of liquid fuel, the combustion wave has a resonant structure similar to that encountered earlier in detonation problems, see [37, 58, 84, 92]. This structure occurs both in HPAI and medium pressure air injection. The mathematical theory shows that the recovery is most efficient when resonance occurs. In this case at some point in the internal structure (resonant point) of the wave, the Buckley-Leverett characteristic speed is equal to the combustion velocity.

In this thesis, we extend the model suggested in [67] for air injection in light oil leading to medium temperature oxidation (MTO). The mechanisms operative in MTO have received little attention in the literature [45, 43, 42, 40, 47]. The main purpose of this thesis is to elucidate the prevailing mechanisms in MTO. Therefore we developed a simple 1-D model considering light oil recovery through displacement by air at medium pressures and low injection rates and performed both numerical and laboratory experiments to validate the theory. The presence of liquid fuel, which is mobile and can vaporize or condense, is a challenge for modeling the combustion process [41]. The low air injection rate was chosen to mimic the processes in the main reaction zone (away from the injection well) in an oil reservoir. We only consider the one dimensional flow problem, expecting that its solution contributes to understanding the MTO process and determine the displacement efficiency.

The mathematical model is given by a system of multi-phase flow equations with additional terms describing reaction and vaporization rates, and an energy balance equation. Analytically, the general solution is composed of three types of nonlinear waves, which are a thermal, a combustion and saturation waves [67]. In MTO, all physical processes, reaction, vaporization, condensation and filtration, are active. The name of the wave (MTO) comes from the fact that the maximum temperature is bounded by the liquid boiling temperature and, thus, cannot become very high. One of the main issues investigated in this thesis is the relative importance of vaporization/condensation/oxidation for light oil recovery in an MTO process.

The detailed mechanism depends on diffusive processes (capillary, molecular diffusion and heat conductivity), oil composition, air injection rate, pressure, presence of water and water saturation. It is anticipated that the theory gives the ratio between the oil recovered and the oil burnt, the behavior of oil mixtures (here modeled as two-component mixtures), the produced water, which depend on the presence of initial water, produced water as well as the effect of the diffusive processes. One of the purposes of our research is to investigate whether we can find experimental evidence for the combustion mechanism described theoretically. We perform and interpret experiments involving air injection in a consolidated porous medium filled with one-component oil (hexadecane) at medium pressures and conditions away from the injection well to validate the theory and to find details of the oxidation mechanisms. As we use conditions that are representative further away from the well, we expect to see details relevant in the field that are not visible for experiments operating at high rates and high pressures [13, 47, 40, 63, 45], which are representative in the near well bore region.

The main research questions addressed in this thesis are (1) applicability of air injection at medium pressures and the MTO process efficiency, i.e., the amount of oil produced with respect to the oil combusted, (2) the detailed combustion mechanisms in the presence of vaporization and the relative importance of combustion and vaporization, (3) the location of the bifurcation point between MTO and HTO in two-component mixtures, (4) the relative importance of combustion with respect to initial water, (5) whether it is possible to employ user provided equation based commercial software to solve combustion model equations of interest and can be applied to quantify the effect of diffusive processes, such as capillary diffusion, thermal conductivity and molecular diffusion, (6) can we use experiments to validate the developed models.

The thesis is organized in Chapters, each addressing specific aspects of the research questions, concerning the recovery of light oil using air injection and the role of MTO.

In Chapter 2, we consider exclusively modeling and simulation of the MTO combustion process. We examine a very simplified model, but include mass-, thermal and capillary-diffusion for air injection in light oil reservoirs. We consider only a one-component oil, e.g., heptane in dry porous rock, to improve the understanding of the

oxidation/vaporization/condensation mechanisms and to include diffusive processes to allow comparison to the non-diffusive process, which can be solved analytically [67]. Heptane represents a single pseudo-component as liquid fuel, which is characterized by its average boiling temperature, density and viscosity. It turns out that the oxidation, vaporization and condensation often occur close to each other and move with the same speed in the porous medium [67]. The temperature variation is bounded by the oil boiling temperature and thus not very large. We analyze the effect of capillary pressure, heat conductivity and diffusion and compare the results with the analytical solution in the absence of diffusion processes.

In Chapter 3, we show that it is possible to find the bifurcation point between MTO and HTO by studying a simple model involving a two-component oil mixture, e.g., heptane and decane in dry porous rock. Heptane represents the light component, which both vaporizes and combusts, whereas decane represents the medium fraction in the oil mixture, which we assume to react with oxygen, but disregard its vaporization. The main discerning factor in the MTO combustion process is the ratio between vaporization and combustion in the low injection rate regime.It turns out that also with the two-component mixture, oxidation, vaporization and condensation often occur close to each other in the MTO wave. Vaporization occurs upstream of the combustion zone. The temperature variation is bounded by the oil boiling temperature. As in the single pseudo-component model we also have a bounded temperature regime for the two-component model [55]. We show that a higher concentration of non-volatile components reverts the sequence of oxidation/vaporization in the MTO wave. This leads to much higher temperatures, eventually changing the combustion regime to HTO. The overall flow consists of three waves, viz., the thermal, the MTO, and the saturation waves.

Chapter 4 studies the effects of water on the oxidation/vaporization/condensation mechanisms in the MTO wave by considering a simple three phase model involving a one-component oil (e.g., heptane, pentane or dodecane) and water in porous rock. Heptane (or pentane, dodecane) represents the pseudo-component. We assume that heptane (pentane and dodecane) vaporizes/condenses as well as combusts, whereas water only vaporizes and condenses. The main emphasis of this Chapter is to investigate the relative importance of steam condensation, vaporization/condensation of oil and combustion in the low injection rate regime. It turns out that the solution consists of a thermal wave, a steam condensation front coinciding or downstream of the medium temperature oxidation (MTO) wave (oil vaporization and combustion), and saturation waves involving oil, gas and water. Numerical calculations show that the presence of water makes the light oil recovery more efficient and faster and diminishes the adverse effect of high oil boiling points.

Chapter 5 presents combustion experiments with one-component oil at conditions that are characteristic further away from the well. The initial aim of the laboratory experiments was to validate various aspects considered in Chapters 2-4. As it turns out it will lead to the discovery of a new combustion mechanism prevailing in medium pressure air injection. In this experimental study, the mechanisms involving

air injection in sandstone rock filled with hexadecane have been analyzed through several air and nitrogen injection experiments in a ramped temperature reactor operating at medium pressures and low injection rates. The experiments were done to investigate the mechanisms of the combustion reaction at different pressures and injection rates. The air fluxes used in typical combustion tube experiments and accelerating-rate calorimetry [94] are much higher than in the field, except in the near wellbore region of air-injection wells. At slower rates we expect to see details that are not visible for the experiments operating at high rates and high pressures [13, 47, 40, 63, 45]. The low air injection rate was chosen to mimic the processes in the main reaction zone (away from the injection well) in an oil reservoir, which provides a long residence time for the oxygen to be in contact with the oil. The most important aspect in this Chapter was to determine the nature of the mechanism and products at low temperatures prior to the full combustion reaction. The mechanism of initial uptake of oxygen for later release was established in this work. The experiments showed that an oxygen sorption step takes place at low temperatures in the initial stage before the bond-scission combustion reactions occur. In the low temperature range (below $300°C$), oxygen may bond physically or chemically in the low temperature oxidation zone with hydrocarbon. At a later stage, the oxygen containing compound desorbs the oxygen or further undergoes oxidation reactions to produce CO and CO_2. In the air injection process, the trend of the amount of burned oil divided by the amount of recovered oil obtained by the analytical results of medium temperature oxidation process [67] was validated was by our laboratory air injection experiments. It was also shown that the oil recovery is faster at higher pressures.

We end with some conclusions.

2. Diffusive Effects on Recovery of Light Oil by Medium Temperature Oxidation

Abstract[1]

Volatile oil recovery by means of air injection is studied as a method to improve recovery from low permeable reservoirs. We consider the case in which the oil is directly combusted into small products, for which we use the term medium temperature oil combustion. The two-phase model considers evaporation, condensation and reaction with oxygen. In the absence of thermal, molecular and capillary diffusion, the relevant transport equations can be solved analytically. The solution consists of three waves, i.e., a thermal wave, a medium temperature oxidation (MTO) wave and a saturation wave separated by constant state regions. A striking feature is that evaporation occurs upstream of the combustion reaction in the MTO wave. The purpose of this paper is to show the effect of diffusion mechanisms on the MTO process. We used a finite element package (COMSOL) to obtain a numerical solution; the package uses fifth order Lagrangian base functions, combined with a central difference scheme. This makes it possible to model situations at realistic diffusion coefficients. The qualitative behavior of the numerical solution is similar to the analytical solution. Molecular diffusion lowers the temperature of the MTO wave, but creates a small peak near the vaporization region. The effect of thermal diffusion smoothes the thermal wave and widens the MTO region. Capillary diffusion increases the temperature in the upstream part of the MTO region and decreases the efficiency of oil recovery. At increasing capillary diffusion the recovery by gas displacement gradually becomes higher, leaving less oil to be recovered by combustion. Consequently, the analytical solution with no diffusion and numerical solutions at a high capillary diffusion coefficient become different. Therefore high numerical diffusion, significant in numerical simulations especially in coarse gridded simulations, may conceal the importance of combustion in recovering oil.

[1]Accepted in Journal of Transport in porous Media, 2014.

Nomenclature

A_r	MTO reaction pre-exponential factor, 1/s
c_l, c_g	heat capacity of liquid and gas, J/(mol · K)
C_m	heat capacity of porous matrix, J/(m^3 · K)
D_g	gas diffusion coefficient, m^2/s
f_l	fractional flow function for liquid phase
J	Leverett J-function
k	rock permeability, m^2
k_l, k_g	liquid and gas phase permeabilities, m^2
n	MTO reaction order with respect to oxygen
P_g	gas pressure, Pa
P_l	liquid pressure, Pa
Q_r	MTO reaction enthalpy per mole of oxygen at reservoir temperature, J/mol
Q_v	liquid fuel vaporization heat at reservoir temperature, J/mol
R	ideal gas constant, J/(mol·K)
s_l, s_g	saturations of liquid and gas phases
t	time, s
T	temperature, K
T^b	boiling temperature of liquid at elevated pressure, K
T^{ini}	reservoir temperature, K
T^{ac}	MTO activation temperature, K
u_l, u_g, u	liquid, gas and total Darcy velocities, m/s
u_{gj}	Darcy velocity of component $j = h, o, r$ in gas phase, m/s
u_g^{inj}	injection Darcy velocity of gas, m/s
W_v, W_r	vaporization rate, and MTO reaction rate, mol/(m^3 · s)
x	spatial coordinate, m
Y_h, Y_o, Y_r	hydrocarbons, oxygen and remaining gas molar fractions, mol/mol
Y_o^{inj}	oxygen fraction in injected gas
φ	porosity
κ_l	phase transfer parameter
λ	thermal conductivity of porous medium, W/(m·K)
μ_l, μ_g	viscosity of liquid and gas, Pa·s
ν_l, ν_g	stoichiometric coefficients in the MTO reaction
ρ_l, ρ_g	molar densities of liquid and gas, mol/m^3
σ	liquid oil surface tension, N/m
θ	liquid oil/rock contact angle

2.1. Introduction

Reactive transport in porous media is important for a variety of processes that cover the range from small-scale reaction-diffusion problems in catalyst pellets to large-scale transport problems in geologic reservoirs; one example is in-situ combustion (ISC), also referred to as fire flood. In view of the decline of easy oil and the difficulties encountered in the production of heavy oil, ISC and high pressure air injection (HPAI) are considered as effective ways to enhance the recovery of oil. In these cases the oxygen in the injected air reacts with the heavier components of the oil, generating a hot zone in which cracking and vaporization of lighter components occur. Air injection has the advantage of air availability at any location [83]; however, energy costs of air compression, necessary for injection, are not negligible [33]. Oil combustion is generally considered as a technique that is applicable for heavy oils because of the conspicuous reduction in oil viscosity due to the generated heat, but it also promotes production through thermal expansion, distillation and gas drive caused by combustion gases. The air injection process is often referred to as high pressure air injection when it is applied to deep light oil reservoirs, whereas the term in-situ combustion has been traditionally used for heavy oil reservoirs. The mechanism actually responsible for oil displacement in ISC varies with the type of oil. For light oil, evaporation and condensation are just as important as the oxidation reaction [67]. As opposed to heavy oil combustion, light oil combustion occurs usually at lower temperatures because the oil is only partially oxidized. When evaporation is small and locally all of the light oil is oxidized, relatively high temperatures can still occur. Thermal and mass diffusion as well as capillary forces lead to diffusive processes and are important when steep changes occur in the dependent variables in the wave profile. It is the purpose of this work to determine the effects of capillary pressure diffusion, longitudinal heat conduction and mass diffusion on the combustion recovery process.

Combustion for low and medium viscosity oil [3, 6, 23, 25, 26, 56, 62, 63, 93] are described by different mechanisms. For light oil combustion, coke formation is usually disregarded, although it can occur [53]. At lower temperatures, the crude oil undergoes the oxidation reaction without generating carbon mono- and dioxide. As the temperature rises, distillation coupled with pyrolysis produces hydrogen gas and some light hydrocarbons in the gas phase. A major part of these hydrocarbons are produced without undergoing oxidation [34]. However, oxygen reacts with the remainder of these hydrocarbons and therefore medium-temperature oxidation occurs. Further increase of temperature leads first to deposition and then to combustion of coke.

In summary we have high temperature oxidation (HTO) when heat conducted out of the reaction zone converts the oil to coke before it is combusted, low temperature oxidation (LTO) when the oxygen is incorporated in the hydrocarbon molecules to form alcohols, aldehydes, acids or other oxygenated hydrocarbons [45, 44, 48], and medium temperature oxidation (MTO) [45, 46, 40] when the oxidation reaction leads

to scission of the molecules and formation of small reaction products such as water, CO or CO_2. The focus of this paper is on MTO.

ISC is a complex process that involves the interaction of many physical phenomena that occur at different time and space scales. Indeed, one of the reasons for difficulty in simulating ISC is the disparity in time and space scales at which the dominant mechanisms occur. For instance, the time and space scales associated with advection or heat conduction are much larger than the scales at which chemical reactions happen in the reservoir, which in turn are considered larger than the scales associated with the transfer of components between phases [41]. Only at fine temporal and spatial grid step sizes the impact of numerical errors may be sufficiently reduced to give reasonable predictions of combustion, saturation and heat wave speed. To establish this unambiguously, it is important to compare numerical computations with results from models that allow analytical solutions [90, 91].

There are many papers presenting the results of numerical simulation of combustion tube experiments. These papers deal with the kinetics of the reactions for light and heavy oil [63] and focus less on the evaporation and condensation mechanisms. In most of these papers, the thermal, mass diffusion and capillary forces are disregarded. However, in some works thermal diffusion is included [4]. In the continuity equations for the components, molecular diffusion has not been explicitly considered [18] in view of the dominating effect of numerical diffusion introduced by the finite-difference approximations [86, 75].

The mathematical theory of combustion in porous media is well developed for immobile fuels, e.g., [16, 23, 71, 82, 88, 64]. When the fuel is a mobile liquid and, additionally, undergoes gas-liquid phase transitions, the problem becomes more complicated. It was shown in [66] that, in the case of liquid fuel, the combustion wave has a resonant structure similar to that encountered earlier in detonation problems, see [37, 58, 84, 92]. In this case at some point in the internal structure of the wave (resonant point), the Buckley-Leverett characteristic speed is equal to the combustion wave velocity. In this resonant case, analysis of the internal wave structure (i.e., the reaction zone) is necessary in order to obtain macroscopic parameters of the wave. However, the determining equations appear to be independent of the particular form of the evaporation and reaction rate expressions, as vaporization is usually much faster than combustion.

In this paper we consider exclusively modeling and simulation of the MTO combustion process. We examine a simplified model for light oil recovery by air injection in the absence of water, but including mass-, thermal- and capillary-diffusion for air injection in light oil reservoirs, leading to medium temperature oxidation. This is an extension of the model suggested in [67], which is given by a system of multi-phase flow balance equations with source terms describing reaction and vaporization rates, and an energy balance equation. Despite the fact that water is important in thermal processes, sometimes increasing the oil production [31], we are not yet considering in the current work water that may be present initially or

that condenses from steam originating from the reaction. We consider only a one-component oil, e.g., heptane in dry porous rock, to improve the understanding of the oxidation/evaporation/condensation mechanisms and include diffusive processes to allow comparison to the non-diffusive process, which can be solved analytically [67]. Heptane represents a single pseudo-component as liquid fuel, which is characterized by an average boiling temperature, density and viscosity. It turns out that the oxidation, evaporation and condensation often occur at locations close to each other that move with the same speed in the porous medium [67]. The temperature variation is bounded by the oil boiling temperature and thus not very large. The presence of liquid fuel, which is mobile and can vaporize or condense, is a challenge for modeling the combustion process. We consider only the one dimensional problem, expecting that its solution contributes to understanding of the MTO processes [45, 40, 46] that occur in practice.

The chapter is organized as follows. The model is introduced in Section 2.2. Section 2.3 describes the analytical solution for the non-diffusive model. Section 2.4 presents the numerical results for thermal, capillary and mass diffusive processes. We end with some conclusions.

2.2. Model

We study a two-phase flow problem involving a combustion front when air is injected into porous rock filled with light oil. The temperature of the medium is bounded by the boiling point of the liquid and, thus, remains relatively low. There are numerous references indicating that gas phase reactions in porous media in itself are important [10, 76, 80, 95]. Gas phase reactions can be important for HPAI [12]. We disregard gas-phase reactions, because there are also many references that indicate that gas-phase reactions in in-situ combustion play a minor role [13] with respect to the reactions with liquid or solid fuel. In summary, it is still a matter of debate whether gas phase reactions play a significant role in porous media as annihilation of free radicals at the pore walls will drastically reduce the reaction rates [11, 49, 60, 81, 38].

When oxygen reacts with liquid hydrocarbons at low temperatures, a series of reactions may occur that convert hydrocarbons into oxygenated hydrocarbons (ketones, alcohols, aldehydes and acids). Further oxidation leads eventually to complete combustion of the oxygenated hydrocarbons [38]; in this paper the combined reaction to oxygenated hydrocarbons and the subsequent reaction to gaseous products is simplified into the form of a single reaction modeled as

$$\nu_l(\text{hydrocarbons}) + O_2 \rightarrow \nu_g\,(\text{gaseous products}), \tag{2.1}$$

i.e., one mole of oxygen reacts with ν_l moles of initial (liquid) hydrocarbons generating ν_g moles of gaseous products (H_2O, CO_2, etc.). This system is studied in

one-dimension (flow in the positive spatial direction x), allowing for the presence of oil and gas. The liquid saturation is denoted by s_l and the gas saturation is $s_g = 1 - s_l$. In the gaseous phase, we distinguish the molar fraction of hydrocarbon gas Y_h and the molar fraction of oxygen Y_o. The remaining components with molar fraction $Y_r = 1 - Y_o - Y_h$ consist of reaction products and inert components from the injected gas. The molar mass balance equations for liquid and gas components are

$$\partial_t(\varphi\rho_l s_l) + \partial_x(\rho_l u_l) = -\nu_l W_r - W_v, \tag{2.2}$$

$$\partial_t(\varphi Y_h \rho_g s_g) + \partial_x(\rho_g u_{gh}) = W_v, \tag{2.3}$$

$$\partial_t(\varphi Y_o \rho_g s_g) + \partial_x(\rho_g u_{go}) = -W_r, \tag{2.4}$$

$$\partial_t(\varphi Y_r \rho_g s_g) + \partial_x(\rho_g u_{gr}) = \nu_g W_r, \tag{2.5}$$

where $u_{\alpha j}$ means the Darcy velocity of component j in phase α . There are three components, viz., gaseous hydrocarbon (h), oxygen (o), and the "rest" (r) in the gas phase. Light oil can exist in the liquid phase l and the gas phase g, whereas oxygen and the rest can only exist in the gas phase. The liquid, gas and total Darcy velocities are

$$u_l = -\frac{k_l}{\mu_l}\frac{\partial P_l}{\partial x}, \quad u_g = -\frac{k_g}{\mu_g}\frac{\partial P_g}{\partial x}, \quad u = u_g + u_l. \tag{2.6}$$

In this equation $\mu_l(T)$, $\mu_g(T)$ are the viscosities, P_l is the oil pressure and P_g is the gas pressure. We denote the permeability of phase α by k_α. We disregard the effect of capillary forces on the phase behavior. Moreover we also disregard pressure variations due to fluid flow on the density and thermodynamic behavior. We use the ideal gas law to relate the molar density ρ_g to the pressure P_g, i.e.,

$$\rho_g = \frac{P_g}{RT}. \tag{2.7}$$

The capillary pressure $P_c(s_l) = P_g - P_l$ is given by

$$P_c(s_l) = \frac{\sigma \cos(\theta)}{\sqrt{k/\varphi}} J(s_l), \tag{2.8}$$

where the factor multiplying the Leverett J-function is constant [17, p.445-446]. We will use the derivative of Eq. (2.8) to estimate the order of magnitude of the capillary diffusion coefficient; however we will assume a saturation-independent average value. It is convenient to express the liquid and gas velocities as

$$u_l = u f_l + \frac{f_g k_l}{\mu_l} P_c'(s_l) \frac{\partial s_l}{\partial x}, \quad u_g = u - u_l, \tag{2.9}$$

where the prime denotes the derivative with respect to the function argument, and the liquid and gas fractional flow functions are

$$f_l(s_l, T) = \frac{k_l/\mu_l}{k_l/\mu_l + k_g/\mu_g}, \quad f_g = 1 - f_l. \tag{2.10}$$

The Darcy velocities for gas components are

$$u_{gj} = Y_j u_g - \varphi D_g s_g \partial_x(Y_j) \quad (j = h, o, r). \tag{2.11}$$

As a first approximation, we use the same diffusion coefficient D_g for all gas components (see, however, the Stefan–Maxwell relations in [19] for the full composition dependence).

The phase permeability functions for the liquid phase and gas phase are taken as

$$k_l(s_l) = k \left(\frac{s_l - s_{lr}}{1 - s_{lr}} \right)^2 \quad \text{for} \quad s_l \geq s_{lr}, \quad \text{and} \quad 0 \quad \text{otherwise} \tag{2.12}$$

$$k_g(s_l) = k (1 - s_l)^3 \tag{2.13}$$

where we assume that the residual gas saturation is zero.

The temperature dependence of the gas and liquid viscosity μ_g and μ_l in cP is given as [77]

$$\mu_g = \frac{7.5}{T + 120} \left(\frac{T}{291} \right)^{3/2} \quad \text{and} \quad \mu_l = 1.32 \times 10^{-2} \exp\left(\frac{1006}{T} \right). \tag{2.14}$$

By adding up (2.3)–(2.5) and using (2.11) with $Y_h + Y_o + Y_r = 1$, the total mass balance of the gases is given by

$$\partial_t(\varphi\rho_g s_g) + \partial_x(\rho_g u_g) = W_v + (\nu_g - 1)W_r. \tag{2.15}$$

Assuming that the temperature of solid rock, liquid and gas are equal, we write the heat balance equation as

$$\frac{\partial}{\partial t}\left(C_m + \varphi c_l\rho_l s_l + \varphi c_g\rho_g s_g\right)\Delta T + \frac{\partial}{\partial x}(c_l\rho_l u_l + c_g\rho_g u_g)\Delta T = \lambda\frac{\partial^2 T}{\partial x^2} + Q_r W_r - Q_v W_v, \tag{2.16}$$

where $\Delta T = T - T^{ini}$ with initial reservoir temperature T^{ini}. The heat capacities for the sand matrix, the liquid phase and gas phase are C_m, c_l, c_g respectively; they are all assumed to be constant and independent of composition. We use λ to denote the effective thermal conductivity. We disregard heat losses, which are usually very small in field applications (however, taking into account heat losses becomes essential for interpreting laboratory experiments).

Our implementation for the liquid and gas Darcy velocities is described by

$$u_l = -\frac{k_l}{\mu_l}\frac{\partial P_l}{\partial x} = -\frac{k_l}{\mu_l}\frac{\partial(P_g - P_c)}{\partial x} = -\frac{k_l}{\mu_l}\frac{\partial P_g}{\partial x} + \frac{k_l}{\mu_l}\frac{\partial P_c}{\partial x} \approx -\frac{k_l}{\mu_l}\frac{\partial P_g}{\partial x} - D_{cap}\frac{\partial s_l}{\partial x}, \tag{2.17}$$

where we use the average value D_{cap} to avoid degenerate diffusion effects

$$D_{cap} = -\int_0^1 \frac{k_l}{\mu_l}\frac{\sigma\cos(\theta)}{\sqrt{k/\varphi}}J'(s_l)\mathrm{d}s_l, \tag{2.18}$$

where the quantities are evaluated at the initial temperature T^{ini}, the parameters are given in Table 2.1 and we use typical values for the interfacial tension $\sigma \approx 0.03N/m$ and the contact angle $\theta = 0$. To estimate the capillary diffusion it is assumed that the derivative of the Leverett J-function is equal -0.3. Therefore the capillary diffusion coefficient is estimated as $D_{cap} = 1.0 \times 10^{-7}$ m^2/s. Then the mass balance

equations (2.2)–(2.5) read

$$\begin{aligned}
\partial_t(\varphi\rho_l s_l) + \partial_x(\rho_l u_{ll}) - \partial_x(D_{cap}\rho_l\partial_x(s_l)) &= -\nu_l W_r - W_v \,, \\
\partial_t(\varphi\rho_g s_g) + \partial_x(\rho_g u_g) &= W_v + (\nu_g - 1)W_r \,, \\
\partial_t(\varphi Y_o\rho_g s_g) + \partial_x(\rho_g Y_o u_g) - \partial_x(\varphi\rho_g D_g s_g\partial_x(Y_o)) &= -W_r \,, \\
\partial_t(\varphi Y_r\rho_g s_g) + \partial_x(\rho_g Y_r u_g) - \partial_x(\varphi\rho_g D_g s_g\partial_x(Y_r)) &= \nu_g W_r \,,
\end{aligned} \tag{2.19}$$

where

$$u_{ll} = -\frac{k_l}{\mu_l}\frac{\partial P_g}{\partial x}, \quad u_l = u_{ll} - D_{cap}\frac{\partial s_l}{\partial x} \,, \quad u_g = -\frac{k_g}{\mu_g}\frac{\partial P_g}{\partial x}. \tag{2.20}$$

The energy balance is given by

$$\begin{aligned}
\partial_t((C_m + \varphi c_l\rho_l s_l + \varphi c_g\rho_g s_g)\Delta T) + \partial_x((c_l\rho_l(u_{ll} - D_{cap}\partial_x s_l) + c_g\rho_g u_g)\Delta T) = \\
\lambda\frac{\partial^2 T}{\partial x^2} + Q_r W_r - Q_v W_v \,.
\end{aligned} \tag{2.21}$$

The partial pressure of the gaseous hydrocarbon in liquid-gas equilibrium is given by the Clausius-Clapeyron relation and Raoult's law as

$$Y_h^{eq} P_g = P_{atm}\exp\left(-\frac{Q_v}{R}\left(\frac{1}{T} - \frac{1}{T^{bn}}\right)\right), \tag{2.22}$$

where T^{bn} is the (normal) boiling point measured at atmospheric pressure P_{atm}. Taking $Y_h^{eq} = 1$ in (2.22), one recovers the actual boiling temperature $T = T^b$ at the elevated gas pressure $P_g > P_{atm}$. We can see that Y_h^{eq} increases with temperature and $Y_h^{eq} \to 1$ as $T \to T^b$. Even if there are better boiling point relations than Clausius-Clapeyron (see [77]), this relation is sufficiently accurate for our purpose.

We consider the reaction rate as

$$W_r = A_r\varphi\rho_l s_l\left(\frac{P_g Y_o}{P_{atm}}\right)^n \exp\left(-\frac{T^{ac}}{T}\right), \tag{2.23}$$

where A_r is the frequency factor for the oxidation rate of the oil. We use T^{ac} to denote the activation temperature for the oxidation rate. The activation temperature is related to the activation energy E_{ac} as $T^{ac} = E_{ac}/R$. We choose $T^{ac} = 7066$ K.

We use an evaporation rate given by

$$W_v = \kappa_l (Y_h^{eq} - Y_h)\rho_g s_l^{2/3}, \tag{2.24}$$

where we assume that the evaporation rate is proportional to the deviation of the mole fraction of the light oil component in the gas phase from its equilibrium value and proportional to $s_l^{2/3}$, which is related to the surface area. The empirical transfer parameter is denoted as κ_l. This formulation can be considered a consequence of non-equilibrium thermodynamics (see for instance [78], [60]). If κ_l is large this approach describes the situations close to local thermodynamic equilibrium [22] for the gaseous hydrocarbon mole fraction Y_h, i.e., instantaneous vaporization. The vaporization rate W_v vanishes under the conditions

$$W_v = 0 \qquad \text{when} \qquad s_l > 0,\ Y_h = Y_h^{eq} \quad \text{or} \quad s_l = 0. \tag{2.25}$$

2.2.1. Initial and boundary conditions

The initial reservoir conditions are taken as

$$t = 0,\ x \geq 0: \quad T = T^{ini},\ s_l = s_l^{ini} R(x),\ Y_h = Y_h^{eq},\ Y_o = 0, \quad P_g = P_{ini}(x). \tag{2.26}$$

where $R(x)$ is Ramp function. It is necessary for simulation purposes to specify the initial pressure curve $P_{ini}(x)$. In the entrance domain $0 \leq x < x_e$ where oil saturation is initially zero the initial pressure is given by

$$P_{ini}(x) = P_0 + \mu_g u_{inj} \left(\frac{x_e - x}{k} + \frac{l - x_e}{k_g(s_l^{ini})} \right) \tag{2.27}$$

and in the rest of the domain, i.e., for $x_e \leq x \leq l$, where l is the length of the system

$$P_{ini}(x) = P_0 + \frac{(l - x)\mu_g u_{inj}}{k_g(s_l^{ini})}\ . \tag{2.28}$$

We use the parameters from Table 2.1 and $x_e = 15\text{m}, \quad l = 50\text{m}$.
The injection conditions at $x = 0,\ t \geq 0$ are

$$s_l = Y_h = 0, \quad T = T^{ini}, \quad Y_r = 1 - Y_o^{inj}, \quad u = u_{inj}, \quad Y_o = Y_o^{inj}, \tag{2.29}$$

corresponding to the injection of an oxidizer (air) at the reservoir temperature. The condition $u = u_{inj}$ leads to an injected flux of $u_{inj}\rho_g$. It is assumed that there are no gaseous hydrocarbons in the injected gas, i.e., $Y_h = 0$. The production conditions at $x = l$, $t \geq 0$ are

$$\partial_x s_l = \partial_x Y_o = \partial_x Y_r = \partial_x T = 0, \quad P_g = P_0. \tag{2.30}$$

A_r	=	4060 1/s	P_0	=	10^6 Pa	T^{ini}	=	300 K
c_g	=	29 J/mol K	Q_r	=	440 kJ/mol	u^{inj}	=	8.0×10^{-7} m/s
c_l	=	224 J/mol K	Q_v	=	31.8 kJ/mol	Y_{inj}	=	0.21
C_m	=	2 MJ/m ^{3}K	R	=	8.314 J/mol K	λ	=	3 W/m K
D_{cap}	=	1×10^{-7} m^2/s	s_l^{ini}	=	0.9	ν_g	=	1.36 [mol/mol]
D_g	=	1×10^{-6} m^2/s	s_{lr}	=	0.1	ν_l	=	0.090 [mol/mol]
k	=	10^{-10} [m^2]	T^{ac}	=	7066 K	ρ_l	=	6826 mol/m^3
n	=	0.5	T^{bn}	=	371 K	φ	=	0.3

Table 2.1.: Values of reservoir parameters for heptane. We use D_{cap} to denote the average capillary diffusion coefficient.

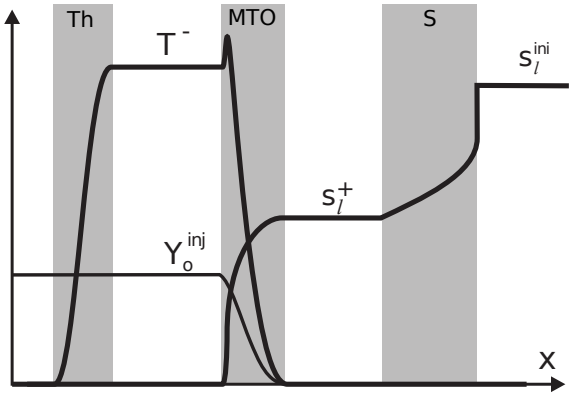

Figure 2.1.: Wave sequence solutions with the thermal (Th), MTO and saturation (S) region. Indicated are the distributions of the temperature T, oleic saturation s_l and oxygen fraction Y_o [67].

2.3. Analytical solution - wave sequence solutions

It is the purpose of this paper to compare numerical to analytical results obtained previously. The analytical expressions are derived with zero molar diffusion, capillary diffusion and thermal diffusion coefficients. We summarize the results of the analytical solution [67] for reasons of easy reference. The analytical solution describes the combustion of a light oil by MTO. Our interest is the behavior at large times. The solution consists of a sequence of waves separated by constant states. As shown in Fig. 2.1, the solution consists of three waves, i.e., the thermal, MTO, and saturation wave. The thermal wave is the slowest wave due to the high heat capacity of rock. The constant states at the upstream side of the thermal wave are determined by the injection boundary conditions. As shown in Fig. 2.1 the temperature in the thermal wave changes from $T = T^{ini}$ upstream to some value T^- further downstream. The equation for the calculation of T^- can be found in [67].

The MTO region contains the most interesting traveling waves, possessing the same speed v. In this region, all the dependent variables T, s_l, u, Y_h, Y_o depend on a

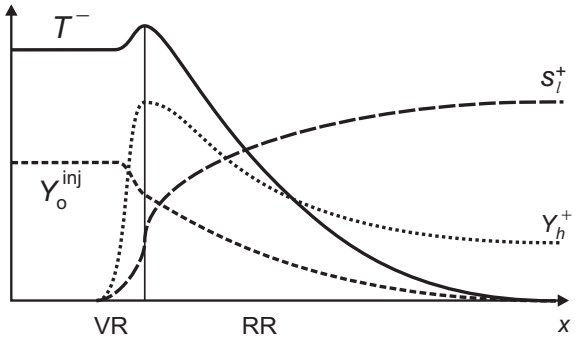

Figure 2.2.: Schematic graphs of the MTO wave profile. Indicated are changes in the temperature T, liquid fuel saturation s_l, oxygen fraction Y_o and fuel fraction Y_h in the gas. The thin region VR is dominated by vaporization and the much wider region RR is dominated by MTO reaction (with slow condensation). The VR is much thinner than the RR, because it is assumed that vaporization rate is much faster than the reaction rate [67].

single traveling coordinate $\xi = x - vt$, i.e., in a moving frame of reference with speed v the profiles are stationary. Reference [67] uses the solution of the traveling wave to relate quantities at the upstream side (T^-, s_l^-, u^-, Y_h^-, Y_o^-) to those at the downstream side (T^+, s_l^+, u^+, Y_h^+, Y_o^+). It turns out that the wave speed v can also be obtained from these quantities [67]. The region upstream of the MTO wave contains injected gas with an oxygen fraction $Y_o^{inj} > 0$ and no gaseous hydrocarbons, $Y_h = 0$. Our interest is in situations where the reaction rate w_r vanishes both at the upstream and downstream sides of the MTO region; we find the condition $s_l = 0$ (no fuel) at the entrance and no oxygen at the production side. Downstream of the MTO wave there are liquid hydrocarbons with saturation $s_l^+ > 0$ and temperature $T = T^{ini}$. The equilibrium conditions $W_r = W_v = 0$ require $Y_o = 0$ and $Y_h = Y_h^{eq}(0)$. Expressions for the five unknown quantities in the limiting states, i.e., T^-, s_l^+, the Darcy velocities u^-, u^+, and the wave speed v of the MTO wave are given in [67]. Finally, the saturation region travels downstream of the MTO wave, see Fig. 2.1. In this region, the temperature is constant and equal to $T = T^{ini}$. Therefore, we have equilibrium between liquid heptane and heptane vapor, i.e., $Y_h = Y_h^{eq}(T^{ini})$, and there is no net vaporization and condensation. The oxygen has been consumed completely in the MTO region. Therefore, we have $Y_o = 0$ in the saturation region and no reaction occurs. The saturation region contains a Buckley-Leverett solution constructed using the standard procedure involving the Welge tangent construction [89]. Briefly, from upstream to downstream it consists of a rarefaction, a shock and a constant state, see also [73]. Recall that in the analytical solution, thermal, mass and capillary diffusion are disregarded.

We continue to detail the behavior of the MTO region. The mathematical analysis is simplified in an essential way by the physical assumption that the vaporization rate is much faster than the reaction rate. Under this assumption we can divide the wave

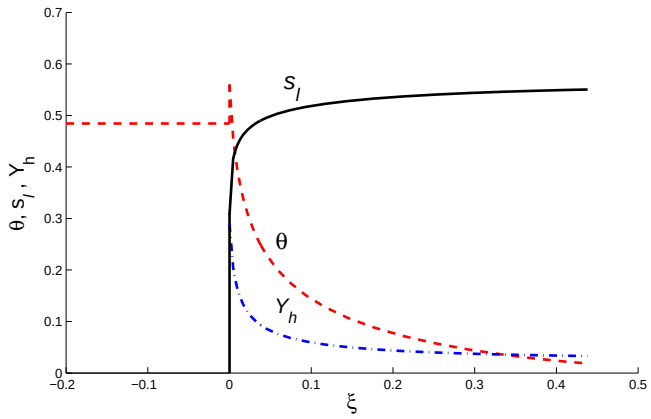

Figure 2.3.: The blown up analytic diffusionless MTO wave profile for parameters in Tab. 2.1. The horizontal span corresponds to 15 mm. Shown are the variables T, s_l and Y_h as functions of the dimensionless traveling wave coordinate ξ (the dimensional length scale is $x^* = 0.022\,\mathrm{m}$). The dimensionless quantity $\theta = (T - T^{ini})/(T^b - T^{ini})$ is used to rescale the temperature. The Figure was obtained with quadratic permeabilities [67], i.e., $k_l = (s_l - 0.25)^2$ and $k_g = (1 - s_l)^2$, as opposed to the relative permeability functions (2.12), (2.13), used in our simulations. The very thin VR appears as a peak of temperature, see also Fig. 2.2.

profile into the vaporization region (VR) and reaction region (RR), see Fig. 2.2. The VR is very thin, as its width is approximately proportional to the ratio between the reaction and vaporization rates. The surprising feature of MTO is that the thin vaporization region is located upstream of the RR. Here the fraction Y_h of gaseous fuel raises from $Y_h = 0$ in the injected gas to the equilibrium value $Y_h = Y_h^{eq}(T^{res})$ at the downstream end of the VR (see Fig. 2.2). Since this region is very thin and the reaction rate is not large at the prevailing low fuel concentration, the oxygen consumption is negligible and we neglect the reaction process in the VR. Downstream of the VR, we have the RR. In the RR, most of the MTO reaction occurs, as well as slow condensation due to the temperature decrease in the direction of gas flow. Along the RR, the equilibrium condition $Y_h = Y_h^{eq}(T)$ holds approximately.

Plots of the diffusionless analytical profiles shown in Fig. 2.3 confirm that the form of the wave profile in the RR remains qualitatively similar in the general case, i.e., the variables T, Y_h, Y_o decrease in the direction of gas flow in the RR, while s_l increases. The downstream liquid saturation stays around the value $s_l^+ \approx 0.6$, for a large interval of pressures. Temperature, pressure and MTO wave speed increase together.

2.4. Numerical modeling

We consider a fully coupled, implicit numerical solution approach based on finite-elements. We solve the finite-element problem with COMSOL software, which gives numerical results that can be compared to the analytical solution. We apply the mathematical module of COMSOL to introduce the model equations in weak form. We use fifth order Lagrange elements, which means that the basis functions in this finite element space are polynomials of degree five. In other words, on each mesh element the solution is a polynomial of degree five and the entire solution is a sum of piecewise fifth order polynomials. The grid size in the numerical simulation is 0.01 m, which is fine enough to capture the multi-scale processes and is capable of resolving the salient features. The spatial resolution of 5000 is fine enough.

Let us consider reservoir parameters values given in Tab. 2.1. The values correspond to heptane (C_7H_{16}) as a fuel. Parameters of the MTO reaction rate vary considerably depending on specific conditions. The availability of reaction rate data is limited. In Tab. 2.1 we present the MTO rate parameters compatible with experimental results obtained in [39]. In our solutions, the wave speed and limiting states are fortunately weakly dependent on the elusive kinetic parameters. As shown in Fig. 2.4 the numerical solution exhibits two regions (thermal and MTO) in the same way as the analytical solution. The saturation region has moved out of sight to the right. The analytical and numerical solution look similar, in spite of the presence of diffusion terms in the numerical solution. For the parameters used by us, the thermal wave is the slowest wave. Therefore, the thermal wave travels in the region of the reservoir from which the liquid and gaseous hydrocarbons were already displaced, i.e., $s_l = 0$. Also, $Y_h = 0$, as the injected gas contains no gaseous hydrocarbons. Therefore, the liquid fractional flow function f_l, the reaction rate w_r and the evaporation rate w_v are all zero. Since there is no reaction in the upstream part of the MTO wave, the oxygen fraction $Y_o = Y_o^{inj}$ is constant. The temperature in the thermal wave changes from the injection value $T = T^{ini}$ upstream to some value T^- in the plateau. The gradual increase is due to the non-zero value of the thermal conductivity. A steeper increase is illustrated in Fig. 2.10, where a very low thermal conductivity is used. The Darcy velocity upstream of the thermal wave is the injection Darcy velocity $u = u_{inj}$. The MTO region contains the most interesting waves in our solution, viz., evaporation and combustion. The saturation region travels downstream of the MTO wave. In this region, the temperature is equal to the initial temperature $T = T^{ini}$. Downstream of the MTO region there is liquid-gas equilibrium $Y_h = Y_h^{eq}(0)$, and there is neither vaporization nor condensation, see (2.24). The oxygen has been consumed completely in the MTO region. No reaction occurs downstream of the MTO region as the oxygen mole fraction is zero ($Y_o = 0$), see (2.23) and no reaction occurs upstream of the MTO region due to lack of fuel. Since the volume of each phase remains constant, the total Darcy velocity is also constant in regions of constant temperature.

When one compares the analytical (Fig. 2.3) and numerical computations (Fig. 2.4)

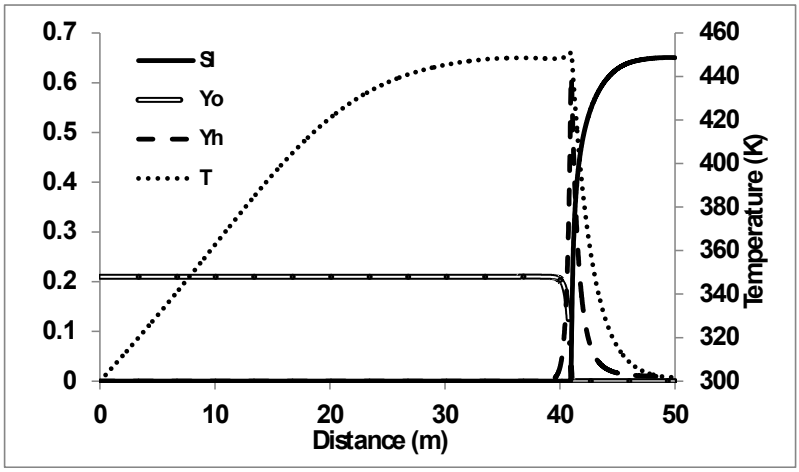

Figure 2.4.: Wave sequence solution with the thermal and MTO regions. Indicated are the distributions of the temperature T, liquid saturation s_l , oxygen mole fraction Y_o and gaseous hydrocarbon mole fraction Y_h at $t = 4 \times 10^7 sec$ in base case related to Table 2.1. Note near $x = 40$ the abrupt decay of the oxygen concentration, the narrow peak of the Y_h concentration, and the rapid decay in temperature. Consequently the reaction region (RR) and the vaporization region (VR) are also narrow and partly overlapping.

one must keep in mind that different relative permeabilities were used. The width of the reaction region (RR) evaluated by the decline of the oxygen concentration is of the order of one meter in the diffusive simulation shown in Fig. 2.4, while the width in the diffusionless analytical solution (Fig. 2.3) is of the order of millimeters. This discrepancy is due to both physical (molecular, capillary and thermal diffusion) and numerical diffusion, all present in the simulation. The vaporization rate is made very fast by the application of a high transfer function in the numerical computations or by using thermodynamic equilibrium in the analytical computations. In the RR, the wave profile is characterized by steep changes in all variables at higher temperatures, followed by slower variations at lower temperatures downstream (see Fig. 2.3). Note also that the temperature T attains a maximum at a peak that determines the resonance state. At this state the heat consuming vaporization at the VR is replaced by the heat providing combustion process in the reaction region (RR). As shown in Fig. 2.3, the oxygen mole fraction Y_o, the gaseous hydrocarbon mole fraction Y_h and temperature T change more steeply in the RR wave than the corresponding profiles in Fig. 2.4. Note that T^- is equal to $T^{ini} + 0.85(T^b - T^{ini})$ in Fig. 2.4, which means that the temperature at the upstream part of the MTO region T^- is 177^{o}C. This value is between the boiling point T_b and the temperature T^- upstream of the MTO region in Fig. 2.3. Indeed, the temperature upstream of the MTO region increases to become close to T^b by taking into account the diffusive processes to the model, as was already conjectured in [67]. The liquid saturation downstream of the MTO region, s_l^+ in Fig. 2.4, is about 0.65 as opposed to 0.56 in

the analytical solution.

2.4.1. Effect of gas diffusion

There is no diffusion in the liquid phase, because there is only one component. However there is diffusion in the gas phase. As stated above we use a single diffusion coefficient in Eqs. (2.19). Because diffusion coefficients are usually small, their physical impact can easily be masked by such processes introduced by the numerical models. The finite element code uses algorithms that minimize such processes; diffusion effects are explicitly introduced by adding a diffusion term to the equations. When the injection velocity is small, diffusion effects are well represented by our numerical model. In the base case with a diffusion coefficient $D_g = 10^{-6}$ m^2/s, as shown in Fig. 2.4, the effect of diffusion is small. However, it is clearly visible in the oxygen concentration Y_o profile, where the oxygen concentration decreases steeply, but smoothly to zero. The gaseous hydrocarbon profile Y_h is a peak with a finite width. At the upstream side of the MTO region, hydrocarbon evaporates, whereas it condenses at the downstream side. The curve is asymmetric and has a tail, where slow condensation occurs. If we choose a smaller diffusion coefficient, e.g., $D_g = 10^{-9}$ m^2/s, the oxygen mole fraction shows a much steeper decline (see Fig. 2.5). The peak representing the gaseous hydrocarbon is much steeper, in particular at the upstream side of the MTO region. However, the downstream side looks very similar to the case with base diffusion coefficient. Simulations with higher diffusion coefficients ($D_g = 10^{-5}$ m^2/s) show a slower decline of the oxygen concentration and a hydrocarbon peak that is also slowly increasing at the upstream side of the MTO region, Fig. 2.6. Moreover higher diffusion coefficient lowers the maximum temperature and gives rise to a small temperature spike in the evaporation region. The general appearance of the solution is preserved when the gas diffusion is increased within the range of physically accepted values. Within this range, the amount of recovered oil by the MTO region does not change significantly.

2.4.2. Effect of capillary pressure

Large capillary forces cause the gas displacement to be the main recovery mechanism and a small amount of oil is left behind for the combustion. As shown by a comparison of Fig. 2.4 and Fig. 2.7, a lower capillary diffusion leads to a lower temperature and a lower gaseous hydrocarbon concentration (the integrated mole fraction of gaseous hydrocarbon in Fig. 2.7 is 0.43 m, which is smaller than 0.74 m in Fig. 2.4). For a higher capillary diffusion (above physically reasonable values), the results of which are displayed in Fig. 2.8, the temperature is higher and a larger amount of gaseous hydrocarbons (the integrated mole fraction is 1.45 m) are produced. In this case, the liquid saturation is really low, which means that higher capillary forces decrease the amount of oil available for MTO. Large capillary forces

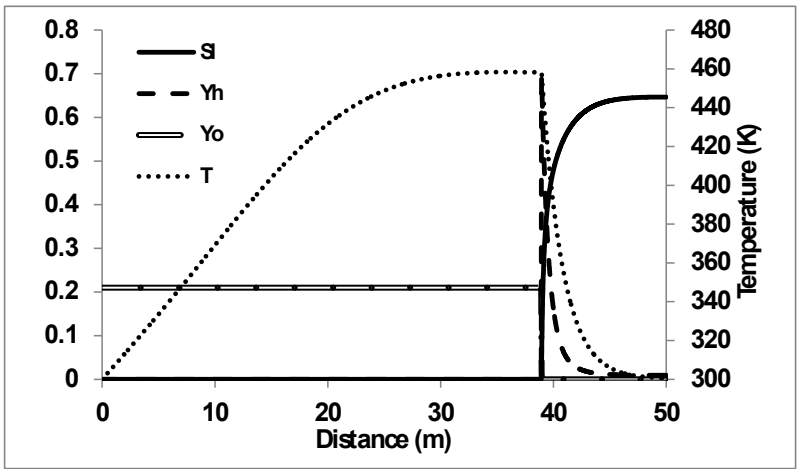

Figure 2.5.: Wave sequence solution with the thermal and MTO regions. Indicated are the distributions of the temperature T, liquid saturation s_l, oxygen mole fraction Y_o and the gaseous hydrocarbon mole fraction Y_h at $t = 4 \times 10^7 sec$ in the case of extremely small gas diffusion, i.e., $D_g = 1 \times 10^{-9}[m^2/s]$.

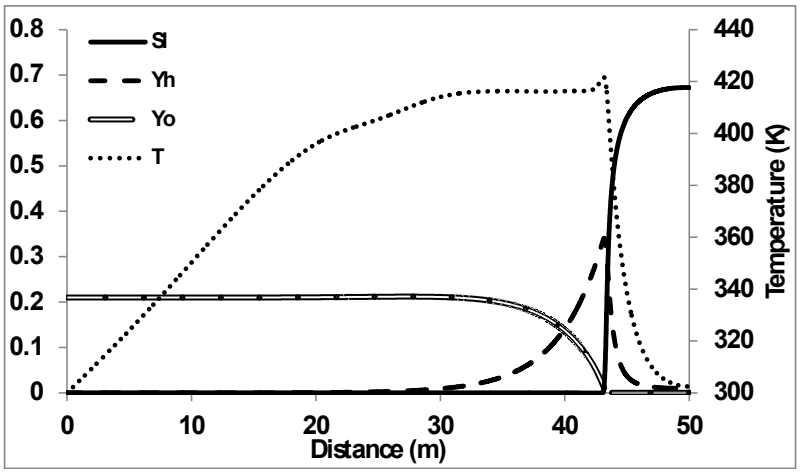

Figure 2.6.: Wave sequence solution with the thermal and MTO regions. Indicated are the distributions of the temperature T, liquid saturation s_l, oxygen mole fraction Y_o and gaseous hydrocarbon mole fraction Y_h at $t = 3.4 \times 10^7 sec$ in the case of large gas diffusion $D_g = 1 \times 10^{-5}[m^2/s]$.

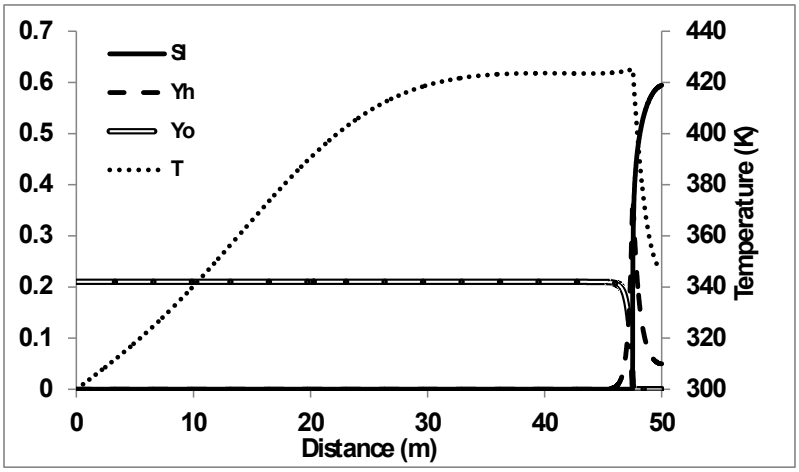

Figure 2.7.: Wave sequence solution with the thermal and MTO regions. Indicated are the distributions of the temperature T, liquid saturation s_l, oxygen mole fraction Y_o and gaseous hydrocarbon mole fraction Y_h at $t = 4 \times 10^7 sec$ in the case of small capillary diffusion $D_{cap} = 1 \times 10^{-10}[m^2/s]$.

decrease the velocity of the MTO region and therefore increase the temperature (see Fig. 2.8).

Larger capillary forces sweep more oil ahead of the the vaporization/combustion zone. Now the dominant displacement mechanism is capillary mixing away from the MTO region. The smaller amount of oil that enters the MTO region is partly combusted and partly evaporated. Increasing capillary forces enhance recovery by gas displacement and leave less oil behind to be recovered by the vaporization/combustion process (see Fig. 2.9). There is a continuous change between the relative importance of gas displacement and MTO wave recovery. For high capillary coefficients, which are however, slightly above physically acceptable values, the appearance of the solution changes completely.

2.4.3. Effect of thermal conductivity

Thermal conductivity manifests itself through the value of the quotient of the thermal conductivity and the heat capacity, which is called the thermal diffusion coefficient. The temperature profiles for smaller conductivity (with $\lambda = 0.03 W/m\,K$, see Fig. 2.10) show steeper transitions than for the base case values (see Fig. 2.4). The lower the thermal diffusion coefficient, the thinner the reaction region (RR). For reasons of illustration we took thermal conductivity values that are unrealistically small. The ensuing temperature profile shows numerical fluctuations. At higher thermal conductivity, e.g., with $\lambda = 15 W/m\,K$ (Fig. 2.11), we see more smooth transitions. The temperature profile does not show fluctuations. The temperature and hydrocarbon vapor spikes in Fig. 2.4 widen and flatten for the higher thermal

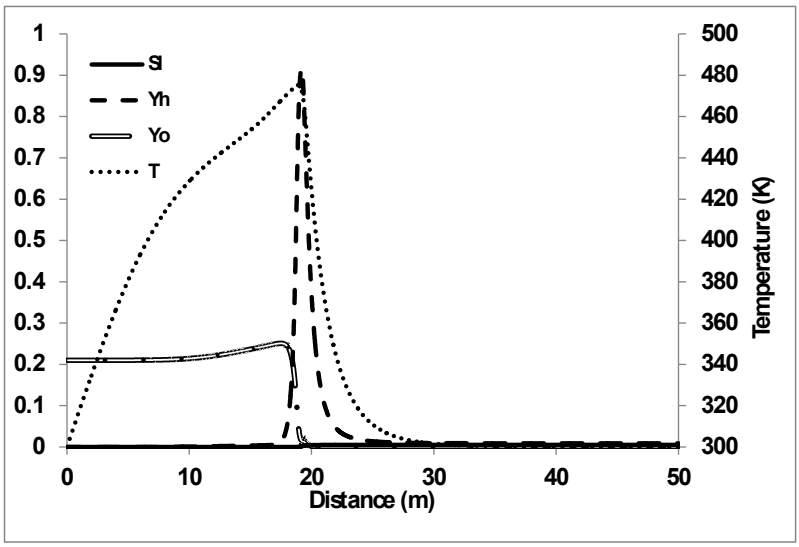

Figure 2.8.: Wave sequence solution with the thermal and MTO regions. Indicated are the distributions of the temperature T, liquid saturation s_l, oxygen mole fraction Y_o and gaseous hydrocarbon mole fraction Y_h at $t = 4 \times 10^7 sec$ in the case of large capillary diffusion $D_{cap} = 1 \times 10^{-4}[m^2/s]$.

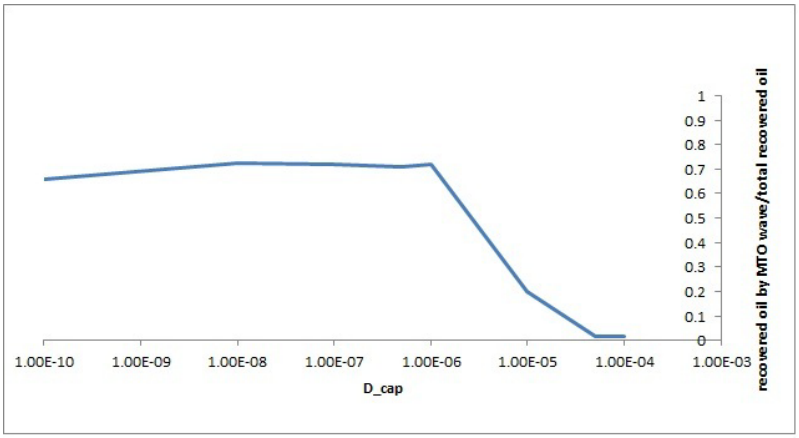

Figure 2.9.: Effect of capillary diffusion on the amount of oil recovered by the MTO wave.

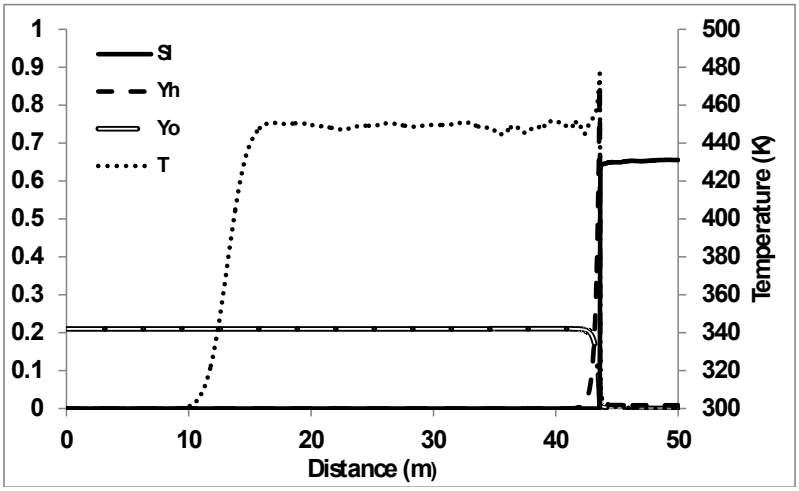

Figure 2.10.: Wave sequence solution with the thermal and MTO regions. Indicated are the distributions of the temperature T, liquid saturation s_l , oxygen mole fraction Y_o and gaseous hydrocarbon mole fraction Y_h at $t = 4 \times 10^7 sec$ in the case of small thermal conductivity $\lambda = 0.03[W/mK]$.

diffusion coefficient.

We distinguish three aspects. First, there is the rate of oil combustion, which is given by the oxygen injection rate, considering that the oxygen consumption is complete. The velocity of the combustion front is determined by the density of the fuel participating in the reaction process, which is not necessarily related to the amount of oil left behind by the gas displacement process, because part of the oil also evaporates. The oil left behind by the displacement process is removed due to a combination of evaporation and combustion in the MTO region. This can explain why for a higher gas displacement efficiency the velocity of the MTO region can become lower.

2.5. Conclusions

Air injection with the purpose of improving volatile oil recovery is a method that deserves investigation; it can be modeled as a medium temperature oxidation (MTO) process. A model was proposed to study the effect of diffusive processes (mass, thermal and capillary) on MTO of light oil in porous media. The proposed two-phase model considers evaporation, condensation and reaction with oxygen. This model includes three gaseous components (oxygen, gaseous hydrocarbon and remaining gas), the oil saturation and an energy balance equations. MTO combustion completely displaces the oil at a cost of small amounts of burned oil. We consider light oil recovery by air injection at medium pressures in a linear geometry, for the case when gas phase combustion and water are neglected. However, the effect of gas

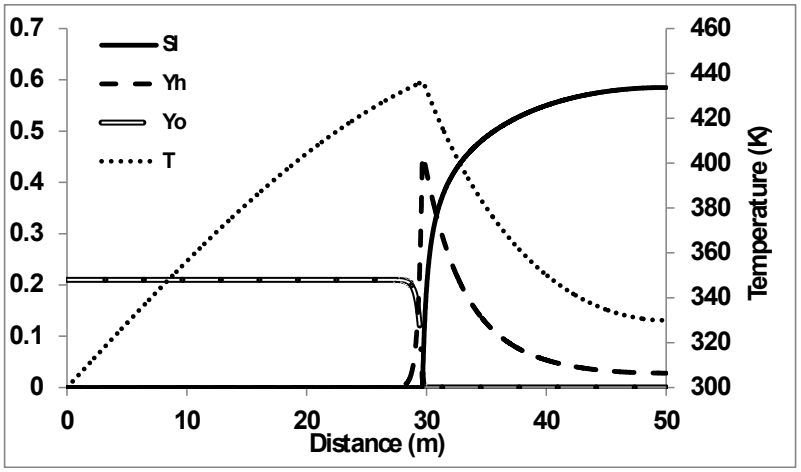

Figure 2.11.: Wave sequence solution with the thermal and MTO regions. Indicated are the distributions of the temperature T, liquid saturation s_l, oxygen mole fraction Y_o and gaseous hydrocarbon mole fraction Y_h at $t = 4 \times 10^7 sec$ in the case of large thermal conductivity $\lambda = 15[W/mK]$.

phase reactions and the presence of water need to be considered in the future.

We used a finite element package (COMSOL) to obtain a numerical solution for comparison with an analytical solution in a zero diffusion model obtained previously [67]. The numerical model uses fifth order Lagrangian base functions. Combined with a central difference scheme used in the finite element package, this makes it possible to model situations both at low diffusion and high diffusion coefficients. The numerical model is capable to quantify the effect of the diffusive processes, while the qualitative behavior of the numerical solution is similar to that of the analytical solution. The solution consists of three waves, i.e., a thermal wave, an MTO wave and a saturation wave, separated by constant state regions. The results show that vaporization occurs upstream of the combustion zone.

The effect of the diffusive terms is as follows. Molecular diffusion lowers the temperature in the MTO region, but creates a small peak in the vaporization region. Capillary diffusion increases the temperature in the upstream part of the MTO region. Higher capillary diffusion increases the recovery by gas displacement and lowers the recovery by the combustion mechanism. The analytical solution, without diffusive terms, and the numerical solution become completely different at very high capillary diffusion coefficients. The effect of thermal diffusion smoothes the thermal wave and widens the hydrocarbon vapor peak.

3. Compositional Effects in Light Oil Recovery: Vaporization vs. Combustion

Abstract[1]

Combustion can be used to enhance recovery of heavy, medium or light oil in highly heterogeneous reservoirs. Such broad range of applicability is attained because not only do the high temperatures increase the mobility of viscous oils but also does the high thermal diffusion spread the heat evenly and suppress heterogeneity effects. For the latter reason, combustion is also used for the recovery of light oils. The reaction mechanisms are different for light oils, where vaporization is dominant, whereas for medium non-volatile oils combustion is dominant. We will only consider combustion of medium and light oils. Therefore we ignore coke formation and coke combustion. It is our goal to investigate the relative importance of vaporization and combustion in a two-component mixture of volatile and non-volatile oils in a low air injection rate regime. By changing the composition we can continuously change the character of the combustion process. We derive a simplified model for the vaporization/combustion process, and implement it in a finite element package, COMSOL. For light oil mixtures, the solution consists of a thermal wave upstream, a combined vaporization/combustion wave in the middle (with vaporization upstream of combustion) and a saturation wave downstream. For heavier mixtures the vaporization/condensation sequence is reversed and vaporization moves ahead of the combustion. Due to its low viscosity, the light oil is displaced by the gases to a region outside the reach of oxygen and therefore less oil remains behind to reach the combustion zone. This leads to a high combustion front velocity, which is determined by the fuel consumption rate. For oil with more non-volatile components, vaporization occurs downstream of the combustion zone. As more oil stays behind to feed the combustion zone, the velocity of the combustion zone is slower, albeit the temperatures are much higher. The relative importance of vaporization/combustion depends also on the injection rate, pressure, initial temperature, and oil viscosity. Numerical calculations allow to estimate the bifurcation points where the character of the combustion changes from a vaporization-dominated to a combustion-dominated process.

[1]Accepted in Journal of Porous Media, 2014.

Nomenclature

A_{rl}	Light oil MTO reaction pre-exponential factor, 1/s
A_{rm}	Medium oil MTO reaction pre-exponential factor, 1/s
C_o, C_g	heat capacity of oil and gas, J/(mol·K)
C_m	heat capacity of porous matrix, J/(m^{3}K)
D_o	oil diffusion coefficient, m^2/s
D_g	gas diffusion coefficient, m^2/s
k_o, k_g	oil and gas phase permeabilities, m^2
k_{ro}, k_{rg}	oil and gas phase relative permeabilities
n	MTO reaction order with respect to oxygen
P_g	prevailing gas pressure, Pa
P_o	prevailing oil pressure, Pa
Q_{rl}	light oil MTO reaction enthalpy per mole of oxygen, J/mol
Q_{rm}	medium oil MTO reaction enthalpy per mole of oxygen, J/mol
Q_v	liquid fuel vaporization heat at reservoir temperature, J/mol
R	ideal gas constant, J/(mol·K)
s_o, s_g	saturations of oil and gas phases
t	time, s
T	temperature, K
T^{bl}	boiling temperature of light component, K
T^{ini}	reservoir temperature, K
T_l^{ac}	light oil MTO activation temperature, K
T_m^{ac}	medium oil MTO activation temperature, K
u_o, u_g, u	oil, gas and total Darcy velocities, m/s
$u_{gl}, u_{g\kappa}, u_{gr}$	Darcy velocity of gas components: hydrocarbon, oxygen, remaining, m/s
u_{ol}, u_{om}	Darcy velocity of light and medium component in oil phase, m/s
u^{inj}	injection Darcy velocity of gas, m/s
W_v, W_{rl}, W_{rm}	vaporization rate, light and medium oil MTO reaction rates, mol/(m$^3 s$)
x	spatial coordinate, m
X_l, X_m	oil molar fractions: light and medium components, mol/mol
Y_l, Y_κ, Y_r	hydrocarbons, oxygen and remaining gas molar fractions, mol/mol
Y_κ^{inj}	oxygen fraction in injected gas
φ	porosity
λ	thermal conductivity of porous medium, W/(m·K)
μ_o, μ_g	viscosity of oil and gas, Pa·s
ν_{ol}, ν_{gl}, ν_{om}, ν_{gm}	stoichiometric coefficients in the MTO reactions
ρ_o, ρ_g	molar densities of oil and gas, mol/m^3
ρ_{gl}, ρ_κ, ρ_r	hydrocarbon, oxygen and remaining gaseous densities, mol/m^3
ρ_{ol}, ρ_{om}	molar densities of light and medium hydrocarbon in oil phase, mol/m^3
ρ_L, ρ_M	pure oleic phase densities of light and medium hydrocarbon, mol/m^3
ψ_l, ψ_m	volume fractions in oleic phase: light and medium components, m^3/m^3

3.1. Introduction

In-situ combustion is generally considered as a technique that is applicable to heavy oils because of the significant reduction in oil viscosity. However, it also promotes production through thermal expansion, distillation and gas drive generated by the combustion gases, so it can also be used to recover light oils. In this case the air injection process is often referred to as "high pressure air injection" and can be applied to deep light oil reservoirs, whereas the term "in-situ combustion" traditionally has been used for heavy oil reservoirs. Our interest is in recovering relatively low viscosity oil from low permeability heterogeneous reservoirs using air injection leading to oil combustion. We will consider combustion of medium and light oils rather than of heavy oils. Air injection is very effective in heterogeneous permeability reservoirs as the oil evaporates away from the lower permeability parts to be collected in the higher mobility streaks. There is a large body of literature describing the use of HPAI (high pressure air injection, starting at $\sim$ 100 bars) to recover oil. Application of HPAI is confined to reservoirs at large depths, because high pressures need to be applied. However, at shallower depths, an alternative is to inject at medium pressures ($\sim 10-90$ bars) for light and medium oil in heterogenous low permeability reservoirs. De Zwart et al. [30] compare equation of state (EOS) models with multicomponent combustion models to assess their applicability to in-situ combustion under HPAI conditions. Even for HPAI, De Zwart et al. conclude that air injection cannot be modeled as a flue gas displacement process as such modeling results in an underestimate of the recovery, because certain thermal aspects are not adequately captured [72], such as stripping and condensation mechanisms. In other words, these thermal aspects play an important role also at medium pressures. These aspects are the focus of this paper.

Combustion of light oil and medium oil [3, 6, 23, 25, 26, 56, 62, 63, 64, 88, 93] are described by different mechanisms. Indeed, the mechanism actually responsible for oil displacement in the combustion process varies with the type of oil. For medium viscosity oils with medium boiling points, the oxygen in the air burns heavier components of the oil, generating heat leading to coking, cracking and vaporization of lighter components, in which lighter components move out of reach of oxygen. For light oil, the small amount of coke formation is usually disregarded, although it can occur [53]. Also, vaporization and condensation are just as important as the oxidation reaction [67]. As opposed to medium oil combustion, light oil combustion usually occurs at lower temperatures, because vaporization displaces part of the fluid out of reach of the combustion process and consequently the fuel concentration in the combustion zone becomes low. However, when little vaporization occurs, a larger part of the light oil is oxidized and relatively high temperatures can still occur.

At low temperatures, the crude oil can undergo oxidation reactions with or without small amounts of carbon mono- and dioxide generation. Rather, oxygenated hydrocarbons are formed. This is usually termed "low temperature oxidation" (LTO). As the temperature rises, distillation coupled with pyrolysis produces hydrogen gas

and some light hydrocarbons in the gas phase. A major part of light hydrocarbons are produced as they moved outside reach of oxidation process [34]. However, oxygen reacts with left behind light hydrocarbons and therefore medium-temperature oxidation (MTO) occurs, which produces, e.g., CO and CO_2. Further increase of temperature leads to deposition and combustion of coke and the combustion process is called HTO. When coke concentration is sufficient for complete consumption of air, the hydrocarbon ahead of the combustion front does not contact oxygen. In contrast, in the case of low fuel concentration a significant amount of oxygen moves ahead of the combustion zone [64, 65]. This results in an LTO process downstream. The viscosity of oxygenated crude oil is higher than the viscosity of the original crude [77]. The activation energy for LTO is generally lower than that for HTO [59].

In summary, we have high temperature oxidation (HTO), when cracking occurs and coke is formed, which is subsequently oxidized at high temperatures; low temperature oxidation (LTO), when the oxygen is incorporated in the hydrocarbon molecules to form alcohols, aldehydes, acids or other oxygenated hydrocarbons [44, 45, 48]; and medium temperature oxidation (MTO) [40, 45, 46], when the oxidation reaction leads to scission of the molecules and to the formation of small reaction products such as water, CO or CO_2. It is the purpose of this paper to quantify the relative importance of vaporization/condensation and oxidation for light oil in an MTO process, and relate it to the oil composition, air injection rate and pressure. We propose a simplified model considering light oil recovery through displacement by air at medium pressures. The presence of liquid fuel, which is mobile and can vaporize or condense, is a challenge for modeling the combustion process. We only consider the one dimensional flow problem, expecting that its solution contributes to understanding the MTO process [40, 45, 46].

Because the MTO process has been studied only in models with one hydrocarbon pseudo-component [67], we assert that our understanding of the oxidation/vaporization /condensation mechanisms in MTO wave can be improved by considering a simple model involving a two-component oil mixture, e.g., heptane and decane in dry porous rock. Heptane and decane represent pseudo-components as volatile and non-volatile components respectively, which are characterized by an average boiling temperature, density and viscosity for each. Heptane represents the light component, which is both evaporated and combusted, whereas decane represents the medium fraction of the mixed oil, which we assume to react with oxygen, but not vaporize. The main discerning factor in the MTO combustion process is the ratio between vaporization and combustion in the low injection rate regime. It turns out that the oxidation, vaporization and condensation often occur close to each other in the MTO wave in the case of larger presence of light components. Vaporization occurs upstream of the combustion zone. The temperature variation is bounded by the oil boiling temperature. Such regime is in a good agreement with the predictions based on a single pseudo-component model [67]. We show that adding more non-volatile components reverts the sequence of oxidation/vaporization in the MTO wave. This leads

to much higher temperatures, eventually changing the combustion regime to HTO. The overall flow consists of three waves, viz., the thermal, MTO, and saturation wave.

The paper is organized as follows. Section 3.2 describes the physical model and presents governing equations. Section 3.3 describes analytical solutions and the MTO wave profile for an oil model with one pseudo-component. Section 3.4 presents numerical solutions with several sets of conditions for the two-component oil model. We end with some conclusions.

3.2. Model

We study a two-phase flow problem including combustion when air is injected into porous rock filled with oil composed of light and medium fractions. The light oil (volatile component) can both evaporate and oxidize, whereas the medium oil (non-volatile component) can only oxidize. In our applications, we disregard gas-phase reactions, while it is still a matter of debate whether gas phase reactions play a significant role in porous media as annihilation of free radicals at the pore walls will drastically reduce the reaction rates [11, 49, 60, 81, 38]. We can summarize the reaction process in the following reaction equations:

$$\begin{aligned} \nu_{ol} \text{ light hydrocarbons} + \mathrm{O_2} &\rightarrow \nu_{gl} \text{ gaseous products}, \\ \nu_{om} \text{ medium hydrocarbons} + \mathrm{O_2} &\rightarrow \nu_{gm} \text{ gaseous products}, \end{aligned} \tag{3.1}$$

i.e., one mole of oxygen reacts with ν_{oi} moles of oleic (liquid) hydrocarbons ($i = l$, light and $i = m$, medium fractions) generating ν_{gi} moles of gaseous products (H_2O, CO_2, etc.). This system is studied in 1-D, allowing for the presence of oil and gas. The liquid oil saturation is s_o and the gas saturation is $s_g = 1 - s_o$. In the gaseous phase, we distinguish between the molar fraction of hydrocarbon gas Y_l and the molar fraction of oxygen Y_κ. The medium oil component does not exist in the gaseous phase. The remaining components with molar fraction $Y_r = 1 - Y_\kappa - Y_l$ consist of reaction products and inert components of the injected gas. X_m and X_l are the mole fractions of the medium (non-volatile) and light (volatile) components in the oleic phase ($X_m + X_l = 1$).

In the model that follows we will assume that the light oil and medium oil behave as an ideal mixture with neither heat nor volume effects due to mixing. Then the oil density can be expressed as $\rho_o = \psi_m \rho_M + \psi_l \rho_L$, where ψ_m and ψ_l are the volume fractions of the medium and light components ($\psi_m + \psi_l = 1$), and ρ_M and ρ_L are the pure oleic densities of the medium and light components respectively. The volume and molar fractions are related by

$$\rho_{om} = X_m \rho_o = \psi_m \rho_M, \quad \rho_{ol} = X_l \rho_o = \psi_l \rho_L, \tag{3.2}$$

where ρ_{om} and ρ_{ol} are molar densities of medium and light components in the oleic phase. For the ideal gas, the molar and volume fractions coincide. The molar densities of gas components are given by $\rho_{gl} = Y_l \rho_g$, $\rho_\kappa = Y_\kappa \rho_g$ and $\rho_r = Y_r \rho_g$.

The molar mass balance equations for liquid and gas components can be written as

$$\begin{aligned}
\partial_t(\varphi \rho_{om} s_o) + \partial_x(\rho_M u_{om}) &= -\nu_{om} W_{rm}, && (3.3)\\
\partial_t(\varphi \rho_{ol} s_o) + \partial_x(\rho_L u_{ol}) &= -\nu_{ol} W_{rl} - W_v, && (3.4)\\
\partial_t(\varphi \rho_{gl} s_g) + \partial_x(\rho_g u_{gl}) &= W_v, && (3.5)\\
\partial_t(\varphi \rho_\kappa s_g) + \partial_x(\rho_g u_{g\kappa}) &= -W_{rm} - W_{rl}, && (3.6)\\
\partial_t(\rho_r s_g) + \partial_x(\rho_g u_{gr}) &= \nu_{gm} W_{rm} + \nu_{gl} W_{rl}, && (3.7)
\end{aligned}$$

where $u_{\alpha j}$ means the Darcy velocity of component j in phase α. In summary, there are four components, viz., light oil (l), medium oil (m), oxygen (κ), and the rest (r). The light component can exist in the oleic phase (o) and the gaseous phase (g), the medium component only exists in the oleic phase (o), whereas oxygen and the remaining gases can only exist in the gaseous phase.

The oleic, gaseous phase and total Darcy velocities are

$$u_o = -\frac{k_o}{\mu_o}\frac{\partial P_o}{\partial x}, \quad u_g = -\frac{k_g}{\mu_g}\frac{\partial P_g}{\partial x}, \quad u = u_g + u_o. \tag{3.8}$$

In this equation $\mu_o(T, X_m)$ and $\mu_g(T)$ are the oleic and gaseous phase viscosities. For the gas viscosity μ_g composition dependency is disregarded. P_o is the oleic phase pressure and P_g is the gaseous phase pressure. We disregard capillary forces in what follows, i.e., we take $P_o = P_g$. We denote the permeability of phase α by k_α. We use the ideal gas law to relate the molar density ρ_g to the pressure P_g,

$$\rho_g = \frac{P_g}{RT}. \tag{3.9}$$

One can derive the following expressions for the velocity of the medium and light components in the oleic phase as [19]

$$u_{om} = \psi_m u_o - \varphi s_o D_o \partial_x \psi_m, \qquad u_{ol} = \psi_l u_o - \varphi s_o D_o \partial_x \psi_l \quad , \tag{3.10}$$

where D_o is the oleic liquid diffusion coefficient, which we take as $D_o = 10^{-10} m^2/s$.

Similarly we approximate the velocities of the components in the gas phase by

$$u_{gl} = Y_l u_g - \varphi s_g D_g \partial_x Y_l, \quad u_{g\kappa} = Y_\kappa u_g - \varphi s_g D_g \partial_x Y_\kappa, \quad u_{gr} = Y_r u_g - \varphi s_g D_g \partial_x Y_r. \tag{3.11}$$

The gas diffusion coefficient is of the order of $10^{-7} m^2/s$, i.e., much larger than the liquid diffusion coefficient.

The relative permeability functions depend on their respective saturations as

$$\begin{aligned} k_{ro}(s_o) &\equiv \frac{k_o(s_o)}{k} = \frac{(s_o - s_{or})^2}{(1 - s_{or})^2} \quad \text{if} \quad s_l \geq s_{or}, \quad 0 \quad \text{if} \quad s_l \leq s_{or}, \\ k_{rg}(s_g) &\equiv \frac{k_g(s_g)}{k} = s_g^2. \end{aligned} \tag{3.12}$$

The composition and temperature dependence of the viscosity μ_o is given by [57]

$$\frac{1}{\mu_o^b} = \frac{\psi_m}{\mu_m^b} + \frac{\psi_l}{\mu_l^b}, \quad \mu_j = \mu_{j0} \exp\left(-\frac{E_j}{RT}\right), \quad (j = m, l), \tag{3.13}$$

where we choose $b = 0.25$, see also Eq. (3.24). In this equation, E_m and E_l are the activation energies for the viscosity of medium and light components in the oleic phase. We use T^m and T^l to denote the activation temperature for the viscosity of medium and light components, which are equal to E_m/R and E_l/R.

By adding up the equations (3.5)-(3.7), the total balance of gas is

$$\partial_t(\varphi \rho_g s_g) + \partial_x(\rho_g u_g) = W_v + (\nu_{gm} - 1) W_{rm} + (\nu_{gl} - 1) W_{rl}. \tag{3.14}$$

The energy balance equation is

$$\begin{aligned} \partial_t((C_m + \varphi C_o \rho_o s_o + \varphi C_g \rho_g s_g)\Delta T) + \partial_x((C_o \rho_o u_o + C_g \rho_g u_g)\Delta T) \\ = \lambda \partial_x^2 T + Q_{rm} W_{rm} + Q_{rl} W_{rl} - Q_v W_v, \end{aligned} \tag{3.15}$$

where C_m, C_o, C_g are the heat capacities for the rock matrix, the oleic phase and gaseous phase respectively, which are all assumed to be constant and independent of composition. We use λ to denote the effective thermal conductivity. We neglect heat losses, which are usually very small in field applications (however, taking into account heat losses becomes essential for interpreting laboratory experiments). The full system of balance equations includes Eqs. (3.3)-(3.6), (3.14) and (3.15).

The partial pressure of the gaseous hydrocarbon assuming liquid-gas equilibrium is derived using the Clausius-Clapeyron relation and Raoult's law; it can be expressed

as

$$Y_l^{eq} P_g = X_l P_{atm} \exp\left(- \frac{Q_v}{R} \left(\frac{1}{T} - \frac{1}{T^{bn}} \right) \right), \tag{3.16}$$

where T^{bn} is the (normal) boiling point of the light component measured at atmospheric pressure P_{atm}. Taking $Y_l^{eq} = 1$ in (3.16), one recovers the actual boiling temperature $T = T^{bl}$ at the elevated gas pressure $P_g > P_{atm}$. We can see that Y_l^{eq} increases with temperature and $Y_l^{eq} \to 1$ as $T \to T^{bl}$. There are better boiling point relations than Clausius-Clapeyron (see [77]), but this relation is sufficiently accurate for our purposes.

We express the reaction rates for light and medium components by

$$\begin{aligned} W_{rl} &= A_{rl} \varphi X_l \rho_o s_o \left(\frac{P_g Y_\kappa}{P_{atm}} \right)^n \exp\left(- \frac{T_l^{ac}}{T} \right), \\ W_{rm} &= A_{rm} \varphi X_h \rho_o s_o \left(\frac{P_g Y_\kappa}{P_{atm}} \right)^n \exp\left(- \frac{T_m^{ac}}{T} \right) \end{aligned} \tag{3.17}$$

where A_{rl} and A_{rm} are the frequency factors for the oxidation rate of the light and medium components. We use T_l^{ac} and T_m^{ac} to denote the activation temperatures for these oxidation rates. The activation temperature is related to the activation energy E_{act-i} as $T_i^{ac} = E_{act-i}/R$, where $i = l$(light) and m(medium). Usually $0 < n < 1$, and we use $n = 1$ in our simulation. The vaporization-condensation rate is given by

$$W_v = k_l (Y_l^{eq} - Y_l) \rho_g s_o^{2/3} X_l, \tag{3.18}$$

where we assume that the vaporization rate is proportional to the deviation of the mole fraction of the light component in the gas phase Y_l from its equilibrium value Y_l^{eq}, the surface area $s_o^{2/3}$, the mole fraction of the light component in the liquid phase X_l, and an empirical transfer parameter k_l is equal to 1 which has a dimension of s^{-1} in our simulation. This formulation can be considered to be a consequence of non-equilibrium thermodynamics (see [78, 60]). The vaporization rate W_v vanishes under the conditions

$$W_v = 0 \qquad \text{when} \qquad s_o > 0,\ Y_l = Y_l^{eq} \quad \text{or} \quad s_o X_l = 0, \tag{3.19}$$

when either there is no liquid light component or it is in thermodynamic equilibrium with the gaseous phase. Note that when condensation occurs in our simulation, the

A_{rl}=A_{rm}	=	4060 1/s	Q_{rm}	=	400 kJ/mol O_2	u^{inj}	=	8.0×10^{-7} m/s
C_g	=	29 J/mol K	Q_v	=	31.8 kJ/mol	Y_κ^{inj}	=	0.21
C_m	=	2 MJ/m ^{3}K	R	=	8.314 J/mol K	ν_{gm}	=	1.36 [mol/mol]
C_o	=	224 J/mol K	s_{or}	=	0.1	ν_{om}	=	0.065 [mol/mol]
D_o	=	1×10^{-10} m^2/s	s_l^{ini}	=	0.9	ν_{ol}	=	0.090 [mol/mol]
D_g	=	1×10^{-7} m^2/s	T_l^{ac}	=	7066 K	ν_{gl}	=	1.36 [mol/mol]
k	=	10^{-10} [m^2]	T_m^{ac}	=	10050 K	ρ_L	=	6826 mol/m^3
n	=	1	T^{bn}	=	371 K	φ	=	0.3
P_{res}	=	10^6Pa	T^{bl}	=	478.5 K	ρ_M	=	5130 mol/m^3
Q_{rl}	=	400 kJ/mol O_2	T^{ini}	=	300 K	λ	=	3 W/m K

Table 3.1.: Values of reservoir parameters for heptane, decane as light, medium pseudo components.

oil saturation is bigger than zero.

3.2.1. Initial and boundary conditions

The initial reservoir conditions are taken as

$$t = 0,\ x \geq 0: \quad T = T^{ini}, \quad s_o = s_o^{ini}, \quad \psi_m = \psi_m^{ini},\ Y_l = Y_l^{eq},\ Y_\kappa = 0, \quad P_g = P_{ini}(x). \tag{3.20}$$

These conditions correspond to the reservoir filled by oil and gas (with no oxygen) at given oil saturation, composition and temperature. It is necessary to specify the initial pressure curve $P_{ini}(x)$ in the domain of interest, i.e., for $0 \leq x \leq l$, where l is the length of the system. For simulation purposes the following choice is convenient:

$$P_{ini}(x) = P_{res} + \frac{(l-x)\mu_g u_{inj}}{k_g(s_l^{ini})}\ . \tag{3.21}$$

We use the parameters from Table 3.1 and $l = 100$m.

The injection boundary conditions at $x = 0,\ t \geq 0$ are

$$T = T^{ini}, \quad s_o = 0, \quad \partial_x \psi_m = 0, \quad Y_l = 0, \quad Y_\kappa = Y_\kappa^{inj}, \quad u = u^{inj}, \tag{3.22}$$

corresponding to the injection of air at reservoir temperature. The condition $u = u_{inj}$ leads to an injected gas flux of $u_{inj}\rho_g$. It is assumed that there are no gaseous hydrocarbons in the injected gas, i.e., $Y_l = 0$. The production boundary conditions at $x = l$, $t \geq 0$ are

$$\partial_x T = \partial_x s_o = \partial_x \psi_m = \partial_x Y_l = \partial_x Y_\kappa = 0, \quad P_g = P_{res}, \tag{3.23}$$

where P_{res} is a constant reservoir pressure. Note that our simulation describes air

injection to a reservoir at constant initial temperature, with no use of any additional ignition mechanism.

3.3. Analytical solution for one-component oil

It is the purpose of this paper to understand the relative importance of vaporization/condensation vs. oxidation, by studying a two-component mixture of volatile and non-volatile oil. We first summarize the results of the analytical solution for the one-component system found in [67] for reasons of easy reference. The analytical solution [67] considers the combustion of a one-component light oil (heptane) by medium temperature oxidation (MTO). The numerical results for such oil including molecular diffusion, capillary and thermal conductivity effects can be found in [55]. Our interest is always in the behavior at large times, when the solution consists of a sequence of waves separated by constant states. It is shown in Fig. 3.1 and is composed of three waves, i.e., the thermal, the MTO, and the saturation wave. The thermal wave is the slowest wave due to the high heat capacity of the rock. The constant state at the upstream side of the thermal wave is determined by the injection boundary conditions. As shown in Fig. 3.1, the temperature in the thermal wave changes from $T = T^{ini}$ upstream to some value T^- further downstream. For calculating T^- one can see Eq. (3.26) in [67]. In the case of one-component oil (volatile oil), the MTO region contains the most interesting traveling waves, possessing the same speed v. In this region, all the dependent variables T, s_o, u, Y_l, Y_κ can be expressed in terms of a single traveling coordinate $\xi = x - vt$, i.e., in a frame of reference moving with speed v the profiles are stationary. Reference [67] uses the traveling wave solution to relate quantities at the upstream side (T^-, s_o^-, u^-, Y_l^-, Y_κ^-) to those at the downstream side (T^+, s_o^+, u^+, Y_l^+, Y_κ^+). It turns out that the wave speed v can be obtained from these quantities too [67]. The region

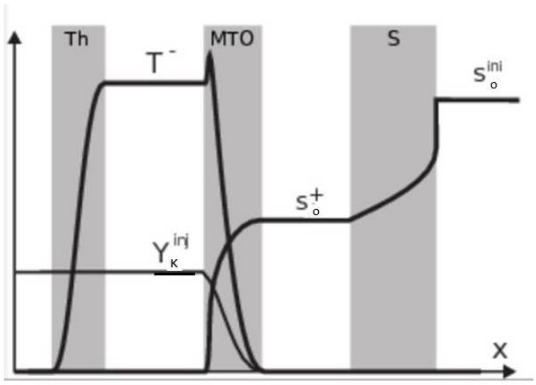

Figure 3.1.: Wave sequence solutions with the thermal (Th), MTO and saturation (S) region for light oil (heptane). Indicated are the schematic distributions of the temperature T, oleic saturation s_o and oxygen fraction Y_κ [67].

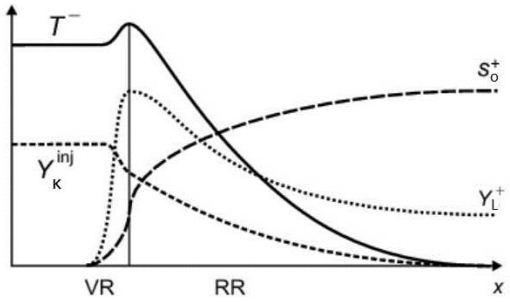

Figure 3.2.: Schematic graphs of the MTO wave profile in the one-component oil model. Indicated are changes in the temperature T, liquid fuel saturation s_o, oxygen fraction Y_κ and fuel fraction Y_l in the gas. The thin region VR is dominated by vaporization and the much wider region RR is dominated by the MTO reaction (with slow condensation). The VR is much thinner than the RR, because it is assumed that vaporization rate is much faster than the reaction rate [67].

upstream the MTO wave contains injected gas with an oxygen fraction $Y_\kappa^{inj} > 0$ and no gaseous hydrocarbon, $Y_l = 0$. Our interest is in situations where the reaction rate w_r vanishes both at the upstream and downstream sides of the MTO region; we find the condition $s_o^- = 0$ (no fuel) at the entrance and $Y_\kappa^+ = 0$ (no oxygen) at the production side.

Downstream of the MTO wave there is liquid hydrocarbon with a saturation $s_o^+ > 0$ and temperature $T = T^{ini}$. The equilibrium conditions $W_r = 0$, $W_v = 0$ require $Y_\kappa = 0$ and $Y_l = Y_l^{eq}(T^{ini})$, respectively. Finally, the saturation wave region travels downstream of the MTO wave, see Fig. 3.1. In this region, the temperature is constant and equal to $T = T^{ini}$. Therefore, we have thermodynamic equilibrium between liquid and vapor heptane, i.e., $Y_l = Y_l^{eq}(T^{ini})$, and there is no net vaporization or condensation. The injected oxygen has been consumed completely in the MTO region. Therefore, we have $Y_\kappa = 0$ in the saturation wave region and no reaction occurs. This region is described by a Buckley-Leverett solution, which uses the standard procedure involving the Welge tangent construction [89]. Briefly from upstream to downstream, the Buckley-Leverett solution consists of a rarefaction, a shock and a constant state, see also [73].

We continue to detail the behavior in the MTO region. The mathematical analysis is simplified in an essential way by the physical assumption that the vaporization rate is much faster than the reaction rate. Under this assumption the MTO region is divided into a vaporization region (VR) and a reaction region (RR), see Fig. 3.2. The VR is very thin. Its width is approximately proportional to the ratio between the reaction and vaporization rates. The surprising feature of MTO is that the thin vaporization region is located upstream of the RR. Here the fraction of gaseous fuel rises from $Y_l = 0$ in the injected gas to the equilibrium value $Y_l = Y_l^{eq}(T)$ at the downstream end of the VR (see Fig. 3.2). Since this region is very thin and the reaction rate is not large at the prevailing low fuel concentration, the oxygen

consumption in the VR is negligible. Downstream of the VR, we have the RR. In the RR, most of the MTO reaction occurs, as well as slow condensation due to temperature decrease in the direction of gas flow. Along the RR, the equilibrium condition $Y_l = Y_l^{eq}(T)$ holds approximately.

3.4. Numerical modeling of two component oil

Let us consider the reservoir parameters given in Table 3.1. These values correspond to heptane (C_7H_{16}) and decane ($C_{10}H_{22}$) as light (volatile) and medium (non-volatile) fractions of the fuel. In Table 3.1 we used MTO rate parameters compatible with the experimental results in [39]. We neglect the capillary effects in the model but the COMSOL software reintroduces numerical diffusion. For the viscosities (cp), we use Sutherland's formula for the gas (air) [77] and the Arrhenius model for liquid (heptane and decane) [77] given in $Pa \cdot s$ and for T in K as

$$\begin{aligned} \mu_g &= \frac{7.5}{T+120}\left(\frac{T}{291}\right)^{\frac{3}{2}}, \quad \mu_l = 1.32\times 10^{-2}\exp\left(\frac{1006}{T}\right), \\ \mu_m &= 1.423\times 10^{-2}\exp\left(\frac{1225}{T}\right). \end{aligned} \tag{3.24}$$

We use the quarter power rule for the oil mixture viscosity, see Eq. (3.13).

We utilize a fully implicit numerical solution approach based on finite-elements. We formulate and solve the finite element problem with the COMSOL software, which gives numerical results that can be compared to the analytical solution of the one-component model. We apply the mathematical module of COMSOL to introduce the model equations in weak form. We use fifth order Lagrange elements, which means that the basis functions in this finite element space are polynomials of degree five. In other words, on each mesh element the solution is a polynomial of degree five and the entire solution is a sum of piecewise fifth order polynomials. The grid size in the numerical simulation is 0.01 m, which is fine enough to capture the multi-scale processes and is capable of resolving salient features. Indeed, a spatial resolution of $100/0.01 = 10^4$ is enough to resolve qualitatively the fine structure.

3.4.1. Effect of the light (volatile) component fraction

As shown in Fig. 3.3 (left), the numerical solution exhibits a thermal and an MTO region in the same way as did the analytical solution for the one component system in Fig. 3.1. In this case the initial volume fraction of the volatile component (C_7H_{16}) is 0.8 in the oil mixture. The saturation region has moved out of sight to the right. For the parameter values used by us, the thermal wave is the slowest wave

(it lies between 0 and 25 m in Fig. 3.3). Therefore, the thermal wave travels in the region of the reservoir from which the light liquid and gaseous hydrocarbons were displaced, i.e., $s_o\psi_l = Y_l = 0$; however small amounts of medium oil remain behind (between $0 - 10m$), upstream of the MTO wave. The reaction rates W_{rl}, W_{rm} and the vaporization rate W_v are all zero or very small in the thermal wave region. Since there is no reaction in the upstream part of the MTO wave, the oxygen fraction $Y_\kappa = Y_\kappa^{inj}$ is constant. The temperature in the thermal wave changes from the injection value $T = T^{ini}$ upstream to some value T^- in the plateau. The gradual temperature increase is due to the non-zero value of the thermal conductivity in the first term of the right-hand side of Eq. (3.15). The Darcy velocity upstream the thermal wave is the injection Darcy velocity $u = u_{inj}$ and it increases downstream due to thermal expansion of gas.

The MTO region contains the most interesting wave in our solution, viz., the vaporization/combustion wave, see Fig. 3.3 (right). Downstream of the MTO region, the temperature is equal to the initial temperature $T = T^{ini}$. This implies the liquid-gas equilibrium $Y_l = Y_l^{eq}(T^{ini})$, and there are neither vaporization nor condensation, see (3.18). No reaction occurs downstream of the MTO region as the oxygen has been consumed completely in the MTO region ($Y_\kappa = 0$), see (3.17).

In summary when the volatile component represents a large fraction of the oil (in our case $\psi_l^{ini} = 0.8$), vaporization/condensation determines the effectiveness of the combustion process for oil recovery. This effectiveness is more pronounced at lower boiling points. As shown in Fig. 3.3, vaporization of the light component (heptane) occurs upstream of the region of the reaction (of light and medium oil) in the MTO wave (around $50m$ in Fig. 3.3). Most of the vaporized light component condenses further downstream as the temperature drops down. This fact emphasizes the effectiveness of vaporization/condensation in the displacement of the oil mixture (note the increase of the light component $s_o\psi_l$ as compared to the medium component $s_o\psi_m$ in the upstream side of the MTO wave in Fig. 3.3). However not all of the non-volatile oil is displaced by the volatile oil, but small amounts remain behind the MTO wave (between $0 - 10m$) because the MTO wave is not initially strong enough to displace the medium oil. This initialization effect causes a slow decrease in the oxygen profile in the first ten meters. The decrease is not visible in Fig. 3.3 because of the small amounts of fuel and low temperature in that region.

As shown in Fig. 3.3, the temperature profile is bounded by the boiling temperature ($T^{bl} = 478.5K$) of the volatile fraction at elevated pressure. Indeed, one can see that the temperature upstream of the MTO region increases to become close to T^{bl}, as was already conjectured in [67]. The oleic saturation downstream of the MTO region is about 0.67, and from this point, the flow continues with a constant state. The Buckley-Leverett profile may follow further downstream, and this profile passed the right end at the time of Fig. 3.3.

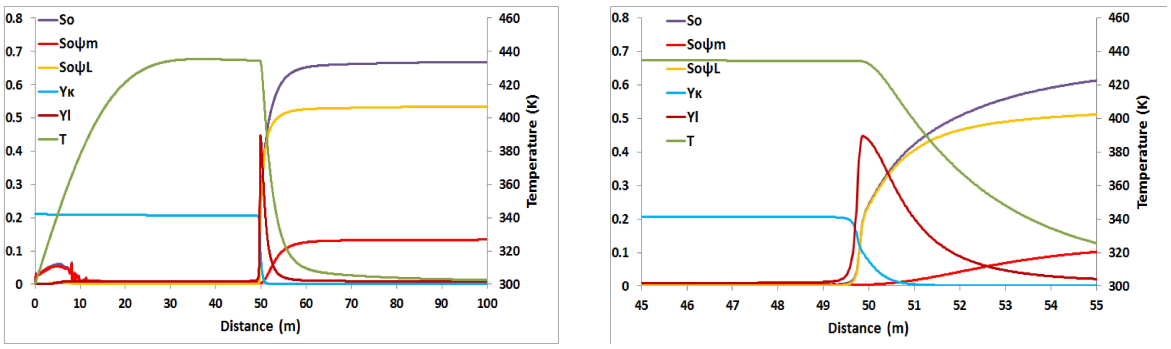

Figure 3.3.: Simulation for an initial medium component fraction of $\psi_m^{ini} = 0.2$. Wave sequence solution with the thermal and MTO regions. Indicated are the distributions of the temperature T, oleic saturation s_o, oxygen mole fraction Y_κ, gaseous hydrocarbon mole fraction Y_l, light oil concentration $s_o\psi_l$ and medium oil concentration $s_o\psi_m$ at $t = 9.7 \times 10^7 sec$ in the base case related to Table 3.1. Note the abrupt decay of the oxygen concentration, the narrow peak of the Y_l concentration, and the rapid decay in temperature representing the MTO region near $x = 50$.

3.4.2. Effect of the medium (non-volatile) component fraction

The two-component system in which one component evaporates and condenses at low or moderate temperatures shows pronounced enhancement of the combustion process effectiveness. Let us study the relative importance of vaporization and combustion in the medium pressure air injection process with different concentrations of the light component. In the base case with medium component volume fraction $\psi_m^{ini} = 0.2$, shown in Fig. 3.3, vaporization occurs upstream of the MTO wave. Single-component studies [67] showed that the combustion front moves considerably faster when vaporization/condensation occurs. In the two-component system $\psi_m^{ini} = 0.2$ shown in Fig. 3.3, the enhancement of oil recovery by distillation is confirmed.

In Fig. 3.4, where initial oil is a mixture of light ($\psi_l^{ini} = 0.4$) and medium component ($\psi_m^{ini} = 0.6$), thermal and MTO waves are distinguished. The saturation region has moved out of sight to the right. The general appearance of the solution (Fig. 3.4 and Fig. 3.3) is preserved even when the fraction of light component decreases to 0.4. The thermal wave travels in the region of the reservoir from which the light liquid and gaseous hydrocarbons were displaced. But a small fraction of medium component remains behind the MTO wave (between $0 - 30m$) because the MTO wave is not initially strong enough to displace the medium oil. This amount (see Fig. 3.4), however, is considerably larger than the amount in Fig. 3.3 as a consequence of the presence of three times more non-volatile component in the initial mixture (0.6 with respect to 0.2). The presence of left-behind medium oil (initialization effect) in Fig. 3.4 can explain the smooth temperature increase in the upstream part

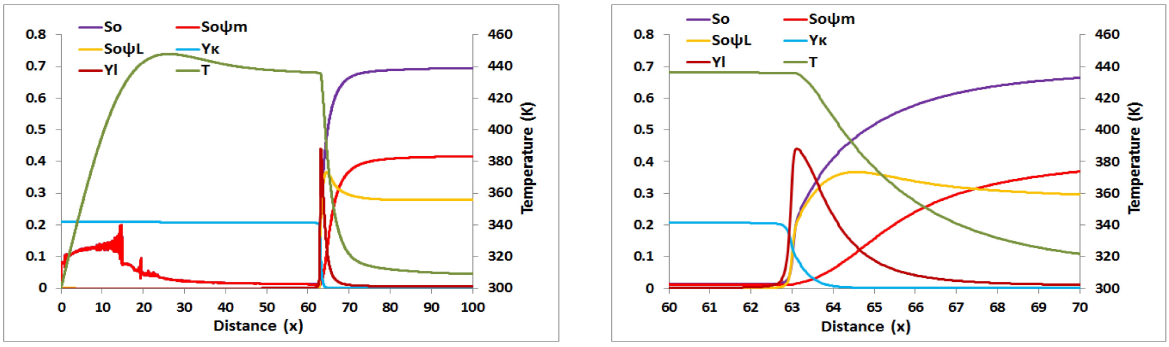

Figure 3.4.: Simulation for an initial medium component fraction of $\psi_m^{ini} = 0.6$. Wave sequence solution with the thermal and MTO regions. Indicated are the distributions of the temperature T, oleic saturation s_o, oxygen mole fraction Y_κ, gaseous hydrocarbon mole fraction Y_l, light oil concentration $s_o\psi_l$ and medium oil concentration $s_o\psi_m$ at $t = 1.4 \times 10^8 sec$ in the case related to Table 3.1. Note the abrupt decay of the oxygen concentration, the narrow peak of the Y_l concentration, and the rapid decay in temperature near $x = 63$.

of the thermal wave (between $10 - 30m$). Since there is some (small) reaction of medium component in the upstream part of the MTO wave, the oxygen fraction $Y_\kappa = Y_\kappa^{inj}$ decreases smoothly but very little before the sharp decline at $x = 63m$. The temperature in the thermal wave increases from the injection value $T = T^{ini}$ upstream to a peak due to the reaction of oil left behind and then reaches some value T^- in the plateau. The MTO region in Fig. 3.4 at $x = 63m$, i.e., the region characterized by the fast decrease in oxygen fraction Y_κ, consists of a region for reaction and another for vaporization. The vaporization region is located upstream of the reaction one. At the upstream side of the MTO region, hydrocarbon evaporates, whereas it condenses at the downstream side (see Y_l in Fig. 3.4 between $63 - 70m$). The gaseous hydrocarbon profile Y_l has a peak with a finite width.

In Fig. 3.5, the fraction of the medium component in the initial oil was increased to 0.8. As one can see comparing with Fig. 3.4, the general appearance of the waves is not preserved. The oil acts more like immobile fuel in the HTO process [65], though it moves slowly through the domain. Vaporization of the light component occurs downstream of the reaction zone (see the profile of Y_l that starts at $x = 40m$), so that the vaporization is not effective for oil recovery anymore. As shown in Fig. 3.5, most of the light component is swept away by vaporization, while the medium fraction remains behind and reacts with the oxygen in the injected air (at $x = 5m$). The two minima in oil saturation s_o in Fig. 3.5 (at $x = 5m$ and $x = 36m$) are related to combustion and vaporization; we have no correspondence to Fig. 3.1. In this case, reaction of a large amount of left-behind medium component with oxygen leads to a steep increase in temperature to almost $500°C$ before the latter decreases to its initial value T^{ini} downstream of the condensation region. Since there is no light component in the reaction zone, the temperature is not bounded by the boiling

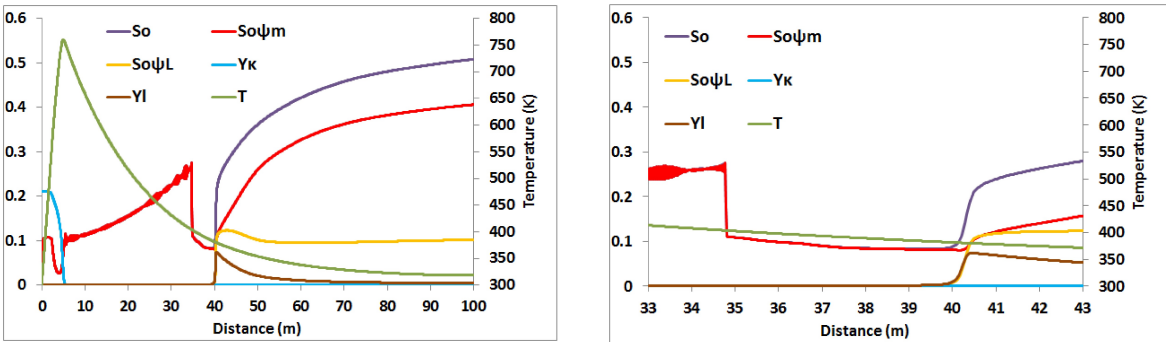

Figure 3.5.: Simulation for an initial medium component fraction of $\psi_m^{ini} = 0.8$. Indicated are the distributions of the temperature T, oleic saturation s_o, oxygen mole fraction Y_κ, gaseous hydrocarbon mole fraction Y_l, light oil concentration $s_o\psi_l$ and medium oil concentration $s_o\psi_m$ at $t = 2.1 \times 10^8 sec$.

point of the light component T^{bl}. The gaseous hydrocarbon fraction Y_l increases steeply (at $x = 40m$ in Fig. 3.5) and then condenses gradually downstream to the equilibrium value at the initial temperature. The slow condensation of hydrocarbon from the gas leads to increase in the light oil profile in Fig. 3.5. Note that the behavior near the vaporization region, shown in amplified form in Fig. 3.5 (right), leads to a large oscillation (a large drop followed by an increase downstream) in non-volatile oil component $s_o\psi_m$. The described process has much common with the HTO description in [64, 65]. However there are differences like oscillations in the saturation profile.

We conclude that the MTO wave structure depends drastically on the initial oil composition. When the light component fraction is sufficiently large, the vaporization occurs in the upstream side, leading to effective temperature control and high recovery rate, Figs. 3.3 and 3.4. On the contrary, when light oil fraction is low, vaporization region moves to the downstream side of the combustion zone, Fig. 3.5. This leads to very high temperatures and slow recovery rate. We should note, however, that our two-component model of MTO is not valid for such high temperatures, because cracking and vaporization of the medium component becomes a relevant part of the process [64, 65]. Thus, our model is only capable to predict a qualitative change of the combustion regime, while a specific profile in the case of Fig. 3.5 must be confirmed using a different model; the latter is a topic for a future research.

3.4.3. Effect of air injection rate

Now let us study the relative importance of vaporization and combustion in an air injection process under different air injection rates. As shown by Fig. 3.6, the general appearance of the wave sequences is not preserved for the oil mixture of 0.8 volatile components at three times higher air injection rate ($u^{inj} = 2.4 \times 10^{-6} m/s$).

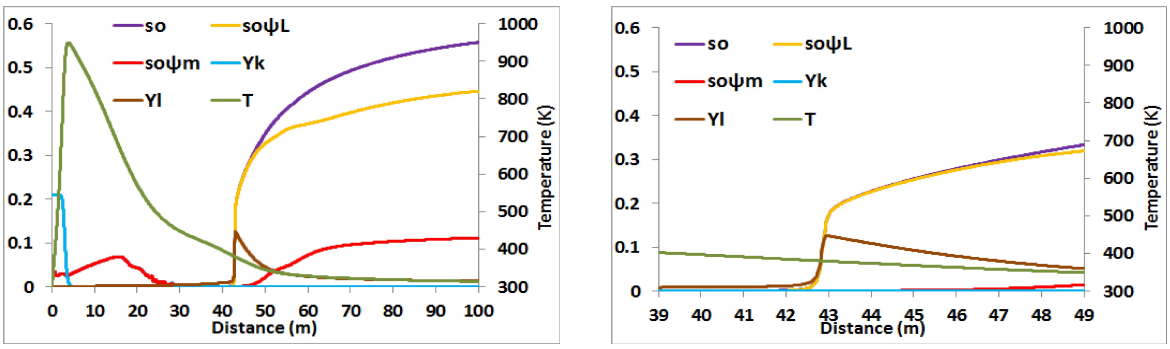

Figure 3.6.: Simulation for an initial medium component fraction of $\psi_m^{ini} = 0.2$. Indicated are the distributions of the temperature T, liquid saturation s_o, oxygen mole fraction Y_κ, gaseous hydrocarbon mole fraction Y_l, light oil saturation $s_o\psi_l$ and medium oil saturation $s_o\psi_m$ at $t = 4.6 \times 10^7 sec$ in the case related to Table 3.1 but with a higher air injection rate, $3 \times u^{inj}$.

Due to higher injection velocity, a large part of the light component is swept away by the injected gas (see $s_o\psi_l$ in Fig. 3.6). As shown in Fig. 3.6 compared to Fig. 3.3, the amount of evaporated light hydrocarbon (Y_l) decreases significantly with higher injection rates. The left-behind medium component reacts with oxygen (between $x = 0 - 30m$), and releases heat. Because the vaporization is not acting as dominant recovery method at higher injection rates, the released heat leads to high temperatures, although the initial mixture is light ($\psi_l^{ini} = 0.8$). As seen in Fig. 3.3 compared to Fig. 3.6, the downstream liquid saturation stays around the value $s_o^+ \approx 0.65$ for a lower injection rate rather than around $s_o^+ \approx 0.55$ for a higher injection rates. This decrease supports the conclusion that MTO process is less efficient for light oil recovery under higher injection rates.

Now, we investigate the air injection rate effect on the process effectiveness when the oil mixture is composed of large amounts of non-volatile component ($\psi_m^{ini} = 0.8$). As seen in Fig. 3.7, the recovery process is faster than at a lower injection rate (see Fig. 3.5). More left-behind oil is combusted and leads to higher temperatures in the domain. For both oil mixtures, Fig. 3.7 and Fig. 3.6, the oxygen decline is steeper than in the case of low injection rates. The minimum (at $x = 2m$) is related to the combustion of the medium component, while the second minimum related to vaporization in Fig. 3.5 (at $x = 36m$) is not seen in the high injection rate profile.

In summary, the increase of injection rate leads to the combustion regime, where reaction occurs upstream of vaporization, resulting in high temperatures and low efficiency of medium oil recovery. As in the previous section, we can rely on our model prediction about the transition to the regime with HTO, but a model with cracking is necessary for an adequate quantitative description at high temperatures.

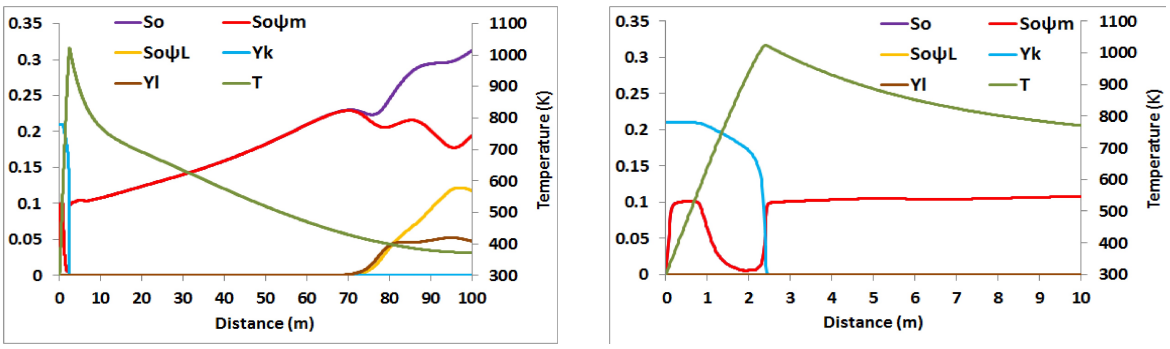

Figure 3.7.: Simulation for an initial medium component fraction of $\psi_m^{ini} = 0.8$. Indicated are the distributions of the temperature T, liquid saturation s_o, oxygen mole fraction Y_κ, gaseous hydrocarbon mole fraction Y_l, light oil saturation $s_o\psi_l$ and medium oil saturation $s_o\psi_m$ at $t = 1.26 \times 10^8 sec$ in the case related to Table 3.1 but with a higher air injection rate, $3 \times u^{inj}$.

3.4.4. Effect of pressure

This section considers the relative importance of vaporization and combustion in air injection processes under higher pressure in the reservoir. As shown in Fig. 3.8, the general appearance of the wave sequences is preserved for the oil mixture of 80% volatile components at higher pressure ($P_{res} = 30\ bar$). The thermal, MTO and saturation wave velocities get higher when the reservoir pressure increases from 10 *bar* (see Fig. 3.3) to 30 *bar* (see Fig. 3.8). We see that the downstream liquid saturation stays around the value $s_o^+ \approx 0.7$ for both pressures, albeit that this value slowly increases with increasing pressure, in agreement with the analytical result based on a single pseudo-component oil model [67]. Pressure increase leads to an increase of temperature as well as an increase of the MTO wave speed relative to the injection speed. When the oil mixture is light, the temperature in the thermal wave is still bounded by the boiling temperature of the volatile oil at elevated pressure. The width of the reaction region (RR) evaluated by the decline of oxygen concentration is of the order of 1.5 meter in the lower pressure model shown in Fig. 3.3, while the width in the higher pressure solution (Fig. 3.8) is of the order of 40 centimeters. Higher pressure leads to a higher reaction rate (see Eq. 3.17), and hence a rapid decline in oxygen fraction. It seems that the vaporization is slightly less effective in the high pressure regime (see Y_l in Fig. 3.8) than in the moderate pressure regime.

3.5. Conclusions

Oil recovery by air injection is a promising method to improve recovery of light/medium oil from highly heterogeneous low permeability reservoirs; it can be modeled as a medium temperature oxidation (MTO) process. We proposed a model consider-

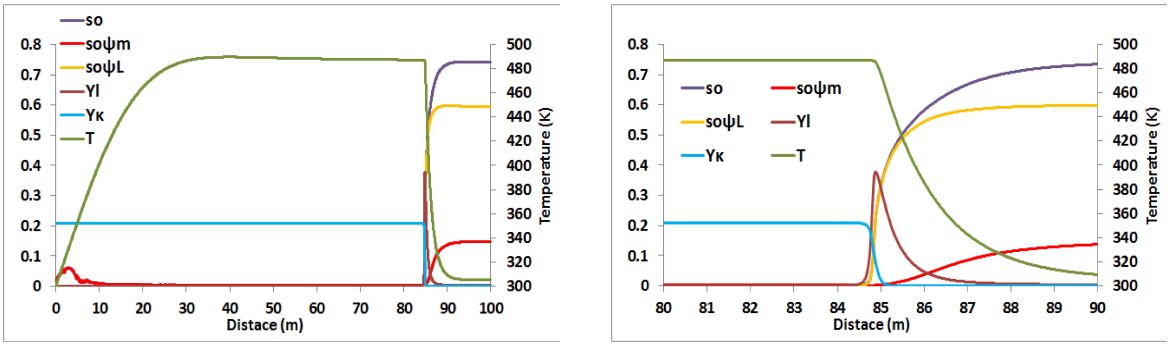

Figure 3.8.: Simulation for an initial medium component fraction of $\psi_m^{ini} = 0.2$. Wave sequence solution with the thermal and MTO regions. Indicated are the distributions of the temperature T, liquid saturation s_o, oxygen mole fraction Y_κ, gaseous hydrocarbon mole fraction Y_l, light oil saturation $s_o\psi_l$ and medium oil saturation $s_o\psi_m$ at $t = 8 \times 10^7 sec$ in the case related to Table 3.1 but with a higher pressure, $P_{res} = 30bar$.

ing vaporization, condensation and reaction with oxygen. It includes three gaseous components (oxygen, gaseous hydrocarbon and remaining gas) and two components (volatile and non-volatile) in the oil phase, and consists of the mass and energy balance equations. The MTO combustion completely displaces the oil at the expense of small amounts of burned oil. A mathematical model was proposed to study the effect of oil composition, air injection rate and pressure on the role of vaporization/condensation and combustion during oil recovery by MTO combustion in porous media.

We used a high order finite element software package (COMSOL) to obtain numerical solutions for different mixtures of volatile and non-volatile oil. The character of the MTO wave changes by altering the composition of the oil. Generally the solution consists of three waves, i.e., a thermal wave, an MTO wave and a saturation wave separated by constant state regions, while the order between vaporization and oxidation in the MTO wave changes for different sets of conditions. For a predominantly light oil mixture, vaporization occurs upstream of the combustion process, a fact that is also confirmed by previously obtained analytical and numerical solutions for one component volatile oil [67, 55]. The combustion front velocity is high as less oil remains behind in the combustion zone. For oil with more non-volatile component (0.8 in volume fraction), the vaporization moves to the downstream side of the combustion zone in the MTO wave. As more oil stays behind in the combustion zone, the velocity of the combustion zone is slower, albeit with much higher temperatures. Due to high temperatures, we conjecture a transition to the HTO region in this case, which should be confirmed using a more elaborate model.

The simulations show that there is a bifurcation point, determined by the fraction of the medium component, where the character of the combustion process changes from a vaporization-dominated to a combustion-dominated process. In a vaporization

dominated process less oil stays behind in the reservoir. Numerical calculations make it possible to establish a range of parameters for the bifurcation point, where the character of the combustion changes from a predominance of vaporization to a predominance of combustion. Finally, the MTO wave is less efficient for light oil recovery under higher air injection rates, but the recovery is faster at higher pressure.

4. Effects of Water on Light Oil Recovery by Air Injection

Abstract[1]

We formulate a mathematical model for one dimensional flow with chemical reactions resulting from injection of air into a porous medium initially filled with gas, water and volatile oil. Our goal is to investigate the effect of water and steam on oil recovery, and we do so for a medium pressure air injection process. We show that, when the boiling point of the volatile oil is below or slightly above the boiling point of water, the hot steam region moves upstream of the medium temperature oxidation (MTO) wave (where oil vaporization and combustion occur), while the volatile oil and steam condense at the same location; it leads to considerable improvement of oil recovery by the MTO wave. Remarkably, the recovery curves (recovery fraction vs. time) depend weakly on the initial water and light oil saturations. If the volatile oil boiling point is much higher than the boiling point of water, the steam region moves downstream of the MTO wave. In this case the water effect on recovery is weaker and becomes negative for high water saturations. Numerical calculations suggest the existence of an oil boiling point at which a bifurcation occurs that separates solutions with the steam region upstream or downstream of the combustion zone.

[1]Submitted in Fuel (minor revision), 2014.

Nomenclature

A_r	MTO reaction pre-exponential factor, 1/s
α	oleic (o), aqueous (w) and gaseous (g) phase
c_α	heat capacity of phase α (o, w, g), J/(mol·K)
C_m	heat capacity of porous matrix, J/(m^3·K)
D_g	gas diffusion coefficient, m^2/s
k	rock permeability, m^2
$k_{r\alpha}$	relative permeability of phase α
n	MTO reaction order with respect to oxygen
P_α	pressure of phase α, Pa
P_{res}	reservoir pressure, Pa
Q_r	MTO reaction enthalpy per mole of oxygen at reservoir temperature, J/mol
Q_{vh}, Q_{vw}	oil and water vaporization heat at reservoir temperature, J/mol
R	ideal gas constant, J/(mol·K)
s_α	saturations of phase α
s_o^{ini}, s_w^{ini}	initial saturations of oil and water phase
T	temperature, K
T^{nh}, T^{nw}	normal boiling temperature of oil and water at atmospheric pressure, K
T^{ini}	initial reservoir temperature, K
T^{ac}	MTO activation temperature, K
u_α	Darcy velocity of phase α, m/s
u_{gj}	Darcy velocity of component $j = h, \kappa, w, r$ in gas phase, m/s
u_{inj}	Darcy velocity of injected gas, m/s
W_r	MTO reaction rate, mol/(m^3·s)
W_{vh}, W_{vw}	vaporization rate for hydrocarbon and water, mol/(m^3·s)
x, t	spatial coordinate, m, and time, s
Y_h, Y_κ, Y_w, Y_r	gas molar fractions: hydrocarbons, oxygen, steam, remaining components,
Y_κ^{inj}	oxygen fraction in injected gas
φ	porosity
κ_h, κ_w	phase transfer parameters, s^{-1}
λ	thermal conductivity of porous medium, W/(m·K)
μ_α,	viscosity of phase α, Pa·s
ν_l, ν_g	stoichiometric coefficients in the MTO reaction
ρ_α	molar density of phase α, mol/m^3

4.1. Introduction

Air injection leading to in-situ combustion is generally considered applicable to recovery of heavy oils because it causes a significant reduction in oil viscosity. However, it can also be used to recover light oils by mechanisms such as combustion gas drive recovery, distillation and thermal expansion. The air injection process usually refers to "high pressure air injection" (HPAI), whereas the term "in-situ combustion" traditionally has been used for heavy oil reservoirs. Our interest is in recovering relatively low viscosity oil from low permeability reservoirs that contain initially water and oil, using air injection leading to combustion, vaporization and condensation. Note that air injection can be very effective in heterogeneous light oil reservoirs as the oil evaporates away from low permeability parts to be collected in the higher mobility streaks; this occurs in HPAI (starting at ~ 100 bars), for which there is a large body of literature [6, 25, 26, 56, 62, 63, 93], including a field example [42]. De Zwart et al. [30] conclude that air injection cannot be modeled solely as a flue gas displacement process because disregarding combustion leads to an underestimate of the recovery efficiency. HPAI is confined to reservoirs at large depths. However, at shallower depths, an alternative is to inject air at medium pressures ($\sim 10 - 90$ bars) in light and medium oil reservoirs, where thermal aspects play an important role.

The mechanism actually responsible for oil displacement in the combustion process varies with the type of oil. In summary, we have high temperature oxidation (HTO) [64, 65], in which cracking occurs forming coke, which is subsequently oxidized at high temperatures; low temperature oxidation (LTO), in which the oxygen is adsorbed or incorporated by the hydrocarbon molecules to form alcohols, aldehydes, acids or other oxygenated hydrocarbons [44, 45, 48]; and medium temperature oxidation (MTO) [40, 45, 46], when the oxidation reaction leads to scission of the molecules into small reaction products such as water, CO or CO_2.

It is the purpose of this paper to study the relative importance of vaporization/ oxidation of light oil versus the vaporization/condensation of water in an MTO air injection process [3, 23]. Some HPAI projects are planned or already carried out in water flooded reservoirs [28, 32, 47, 74]. Barzin et al. [14] observed higher fuel deposition when initial water was absent during ramped temperature experiments with light oil in combination with high flux air injection. Pascual et al. [74] performed a high pressure tube test using light crude oil to simulate the LTO process performed after waterflood of a light oil reservoir, in which the process sustained a stable front at a temperature of $250°C$. They showed that reservoir oil had excellent burning characteristics, which made the process technically feasible. When thermal losses through the rock are much higher than the heat provided by the oxidation reactions at reservoir temperature, or if the heat released by the oil is not sufficient to increase the temperature significantly (for instance in presence of large quantities of water), the oxidation reaction occurs at temperatures not far from the initial reservoir temperature [28]. In this case, oxidation reactions are slow and can be incomplete. Less carbon oxide (CO_2 or CO) is generated than in the absence of water. In this case,

oxygen consumption occurs in a larger reservoir zone; the size of which depends on the oil reactivity [44] but extinction can also occur [65].

The presence of water and oil that are both mobile and can vaporize or condense represent a challenge for numerical modeling of the combustion process. Because the MTO process has been mainly studied theoretically and numerically in the absence of water in [54, 55, 67], it is essential that the current understanding of oxidation/vaporization/condensation mechanisms in the MTO wave is improved by studying a simple three phase model involving water, gas and a single pseudo-component oil (e.g., heptane, pentane or dodecane) in porous rock. Such oil is characterized by an average boiling temperature, density and viscosity. We assume that the oil vaporizes/condenses and reacts with oxygen, whereas water only vaporizes and condenses.

The paper is organized as follows. Section 4.2 describes the physical model and presents governing equations. Section 4.3 describes analytical and numerical solutions when water was not present initially and originated from oxidation reactions. In section 4.4, the numerical solutions with several sets of conditions for the oil with different boiling temperatures in the presence of initial water are presented. Different mechanisms caused by steam condensation/vaporization are analyzed. Section 4.5 describes the recovery curves. We end with some conclusions.

4.2. Model

We study a three-phase flow problem (gas, oil and water) involving a combustion front when air is injected into thermally isolated porous rock filled with light oil and water. In this paper, we summarize the reaction process by the following reaction equation:

$$\nu_l(\text{hydrocarbons}) + \mathrm{O_2} \rightarrow \nu_w\,(\mathrm{H_2O}) + \nu_g\,(\text{other gaseous products}), \qquad (4.2.1)$$

i.e., one mole of oxygen reacts with ν_l moles of initial (liquid) hydrocarbons generating ν_w moles of water in vapor phase and ν_g moles of gaseous products (CO, CO_2, etc.). This reaction equation is an abbreviated form of a number of intermediate reactions leading to complete scission of hydrocarbon molecules (medium temperature oxidation). We disregard gas-phase reactions, though it is still a matter of debate whether such reactions play a significant role in porous media as annihilation of free radicals at the pore walls drastically reduces the reaction rates [11, 49, 60, 81, 38].

The system is studied for one-dimensional flow in the positive horizontal spatial direction x, allowing for the presence of oil, water and gas. The oil saturation is denoted by s_o, the water saturation by s_w and the gas saturation by $s_g = 1 - s_o - s_w$. In the gaseous phase, we distinguish the molar fraction of hydrocarbon gas Y_h, the

molar fraction of steam Y_w and the molar fraction of oxygen Y_κ. The remaining components with molar fraction $Y_r = 1 - Y_\kappa - Y_h - Y_w$ consist of inert components from the injected gas and reaction products. The molar mass balance equations for oil, water and the four gas components are

$$\begin{aligned}
\partial_t(\varphi\rho_o s_o) + \partial_x(\rho_o u_o) &= -\nu_l W_r - W_{vh}, && (4.2.2)\\
\partial_t(\varphi\rho_w s_w) + \partial_x(\rho_w u_w) &= -W_{vw}, && (4.2.3)\\
\partial_t(\varphi Y_h\rho_g s_g) + \partial_x(\rho_g u_{gh}) &= W_{vh}, && (4.2.4)\\
\partial_t(\varphi Y_\kappa\rho_g s_g) + \partial_x(\rho_g u_{g\kappa}) &= -W_r, && (4.2.5)\\
\partial_t(\varphi Y_w\rho_g s_g) + \partial_x(\rho_g u_{gw}) &= W_{vw} + \nu_w W_r, && (4.2.6)\\
\partial_t(\varphi Y_r\rho_g s_g) + \partial_x(\rho_g u_{gr}) &= \nu_g W_r, && (4.2.7)
\end{aligned}$$

where $u_{\alpha j}$ means the Darcy velocity of component j in phase α. Light oil can exist in the oil phase (o) and in the gas phase (g), water can exist in the water phase (w) and in the gas phase, whereas oxygen and the rest can only exist in the gas phase.

The oil, gas, water and total Darcy velocities are

$$u_o = -\frac{kk_{ro}}{\mu_o}\frac{\partial P_o}{\partial x}, \quad u_g = -\frac{kk_{rg}}{\mu_g}\frac{\partial P_g}{\partial x}, \quad u_w = -\frac{kk_{rw}}{\mu_w}\frac{\partial P_w}{\partial x}, \quad u = u_g + u_l + u_w. \tag{4.2.8}$$

In Eq. (4.2.8), $\mu_\alpha(T)$ and P_α are the viscosity and the pressure for oleic (o), aqueous (w) and gaseous (g) phase. We denote the relative permeability of phase α by $k_{r\alpha}$. We disregard the effect of capillary forces on the phase behavior, thus, $P_o = P_w = P_g$. Moreover we also disregard the effect of pressure variations on density and thermodynamic behavior of liquids. We use the ideal gas law to relate the total molar gas density ρ_g to the pressure P_g, i.e.,

$$\rho_g = \frac{P_g}{RT}. \tag{4.2.9}$$

The Darcy velocities for gaseous components are

$$u_{gj} = Y_j u_g - \varphi D_g s_g \partial_x Y_j, \quad (j = h, \kappa, w, r). \tag{4.2.10}$$

As a first approximation, we use the same diffusion coefficient D_g for all gas components (see, however, the Stefan–Maxwell relations in [19] for the full composition dependence).

The relative permeability functions for the oil, water and gas phases [21] are taken as

$$k_{ro}(s_l) = \left(\frac{s_o - s_{or}}{1 - s_{or}}\right)^2 \quad \text{for} \quad s_o \geq s_{or}, \quad \text{and} \quad 0 \quad \text{otherwise}, \tag{4.2.11}$$

$$k_{rw}(s_w) = 0.5 s_w^2, \quad k_{rg}(s_g) = s_g^2. \tag{4.2.12}$$

We assume that the residual gas and water saturations are zero. For the viscosities (in cP with T in K), we use Eqs. (4.2.13), viz., Sutherland's formula for gas (air) viscosity and the Arrhenius model for liquid viscosities [77] as

$$\begin{aligned}
&\mu_g = \frac{7.5}{T + 120}\left(\frac{T}{291}\right)^{3/2}, \qquad \mu_w = 5.78 \times 10^{-3} \exp\left(\frac{1509}{T}\right), \\
&\text{Heptane}: \quad \mu_o = 1.32 \times 10^{-2} \exp\left(\frac{1006}{T}\right), \\
&\text{Pentane}: \quad \mu_o = 1.58 \times 10^{-2} \exp\left(\frac{768.2}{T}\right), \\
&\text{Dodecane}: \quad \mu_o = 1.06 \times 10^{-2} \exp\left(\frac{1444}{T}\right).
\end{aligned} \tag{4.2.13}$$

By adding (4.2.4)–(4.2.7) and using (4.2.10) with $Y_h + Y_\kappa + Y_w + Y_r = 1$, the balance law for the total gas is given by

$$\partial_t(\varphi \rho_g s_g) + \partial_x(\rho_g u_g) = W_{vh} + W_{vw} + (\nu_g + \nu_w - 1) W_r. \tag{4.2.14}$$

Assuming that the temperature of solid rock, oil, water and gas are locally equal, we write the energy balance equation as

$$\begin{aligned}
\frac{\partial}{\partial t}\Big((C_m + \varphi c_o \rho_o s_o + \varphi c_w \rho_w s_w + \varphi c_g \rho_g s_g)\, \Delta T \Big) + \frac{\partial}{\partial x}\Big((c_o \rho_o u_o + c_w \rho_w u_w + c_g \rho_g u_g) \Delta T \Big) \\
= \lambda \frac{\partial^2 T}{\partial x^2} + Q_r W_r - Q_{vh} W_{vh} - Q_{vw} W_{vw},
\end{aligned} \tag{4.2.15}$$

where $\Delta T = T - T^{ini}$ is defined with respect to the initial reservoir temperature T^{ini}. In (4.2.15), C_m, c_o, c_w, c_g are the heat capacities for the rock, the oil phase, water

phase and gas phase respectively; they are all assumed to be independent of temperature and composition. We use λ to denote the effective thermal conductivity. We disregard heat losses, which are usually very small in field applications (however, taking into account heat losses becomes essential for interpreting laboratory experiments).

The partial pressure of the gaseous hydrocarbon and water in oil-gas and water-gas equilibria are given by combining the Clausius-Clapeyron relation with Raoult's law, which leads to

$$Y_h^{eq} P_g = P_{atm} \exp\left(-\frac{Q_{vh}}{R}\left(\frac{1}{T} - \frac{1}{T^{nh}}\right)\right), \quad Y_w^{eq} P_g = P_{atm} \exp\left(-\frac{Q_{vw}}{R}\left(\frac{1}{T} - \frac{1}{T^{nw}}\right)\right), \tag{4.2.16}$$

where T^{nh} and T^{nw} are the (normal) boiling points of hydrocarbon and water measured at atmospheric pressure P_{atm}. Taking $Y_h^{eq} = 1$ or $Y_w^{eq} = 1$ in (4.2.16), one recovers the actual boiling temperatures of hydrocarbon or water at the elevated gas pressure $P_g > P_{atm}$. We observe that Y_h^{eq} and Y_w^{eq} increase with temperature and $Y_h^{eq}, Y_w^{eq} \to 1$ at the boiling points of the respective liquids. Even though there are more accurate boiling point relations than Clausius-Clapeyron (see [77]), this relation is sufficiently accurate for our purposes.

We consider the MTO reaction rate as

$$W_r = A_r \varphi \rho_o s_o \left(\frac{P_g Y_\kappa}{P_{atm}}\right)^n \exp\left(-\frac{T^{ac}}{T}\right), \tag{4.2.17}$$

where A_r is the frequency factor for the oxidation rate of oil. We use $T^{ac} = E_{ac}/R$ to denote the activation temperature for the oxidation reaction, which is related to the activation energy E_{ac}.

We express the vaporization rates for hydrocarbon and water into the gas phase by

$$W_{vh} = \kappa_h (Y_h^{eq} - Y_h)\rho_g \times \begin{cases} 1 & \text{if} \quad Y_h \geq Y_h^{eq} \\ s_o^{2/3} & \text{if} \quad Y_h < Y_h^{eq}, \end{cases} \tag{4.2.18}$$

$$W_{vw} = \kappa_w (Y_w^{eq} - Y_w)\rho_g \times \begin{cases} 1 & \text{if} \quad Y_w \geq Y_w^{eq} \\ s_w^{2/3} & \text{if} \quad Y_w < Y_w^{eq}, \end{cases} \tag{4.2.19}$$

where we assume that the vaporization rate is proportional to the deviation of the mole fraction of the gas component Y_j $(j = h, w)$ from its equilibrium value. For

vaporization ($Y_j < Y_j^{eq}$) we assume that the rate is proportional to $s_j^{2/3}$, which is related to the surface area, while for condensation ($Y_j > Y_j^{eq}$) we ignore the dependence on the liquid saturation. The empirical transfer parameters are denoted by κ_h for hydrocarbon and κ_w for water, which are taken equal to 1 s^{-1} in our simulations. These values were chosen for numerical convenience, because they are large enough for numerical modeling near equilibrium situations, i.e., instantaneous vaporization [22]. This formulation can be considered a consequence of non-equilibrium thermodynamics (see for instance [60, 78]).

The initial reservoir conditions for $t = 0$, $0 \leq x \leq l$ are

$$T = T^{ini},\ s_o = s_o^{ini} R(x),\ s_w = s_w^{ini} R(x),\ Y_h = Y_h^{eq},\ Y_\kappa = 0,\ Y_w = Y_w^{eq},\quad P_g = P_{ini}(x), \tag{4.2.20}$$

where the ramp function, $R(x < x_e) = 0$, $R(x_e \leq x \leq x_e + 1) = x$ and $R(x > x_e + 1) = 1$, describes continuous change of saturations from zero to their initial reservoir values. In the entrance domain, $0 \leq x < x_e$ (we use $x_e = 15$m) with zero initial oil saturation, the pressure P_{ini} is taken as

$$P_{ini}(x) = P_{ini}(x_e) + \frac{(x_e - x)\mu_g(T^{ini})u_{inj}}{k}, \tag{4.2.21}$$

and in the rest of the domain, i.e., for $x_e \leq x \leq l$, we express the initial pressure by

$$P_{ini}(x) = P_{res} + \frac{(l - x)\mu_g(T^{ini})u_{inj}}{k k_{rg}(s_g^{ini})}, \tag{4.2.22}$$

where l is the length of the system. The injection conditions at $x = 0,\ t \geq 0$ are

$$s_o = s_w = Y_h = Y_w = 0,\quad T = T^{ini},\quad u_g = u_{inj},\quad Y_\kappa = Y_\kappa^{inj}, \tag{4.2.23}$$

corresponding to the injection of air at reservoir temperature T^{ini} and constant Darcy velocity u_{inj}. It is assumed that there are neither gaseous hydrocarbons nor water in the injected gas, i.e., $Y_h = Y_w = 0$. For numerical solutions, we need to state the production conditions at $x = l$, $t \geq 0$, which are taken to be

$$\partial_x s_o = \partial_x s_w = \partial_x Y_\kappa = \partial_x Y_w = \partial_x Y_h = \partial_x T = 0,\quad P_g = P_{res}. \tag{4.2.24}$$

We consider the reservoir parameters given in Table 4.1. The values correspond to heptane (C_7H_{16}), pentane (C_5H_{12}) and dodecane ($C_{12}H_{26}$), each representing an effective one pseudo-component oil with water initially present in the reservoir. Table 4.1 contains MTO rate parameters compatible with the experimental results in [39].

We utilize a fully implicit numerical solution approach based on finite-elements, i.e., we formulate and solve the finite element problem using COMSOL software for the

A_r	=	4060 1/s	Q_r	=	400 kJ/mol O_2
u^{inj}	=	8.0×10^{-7} m/s	Y_κ^{inj}	=	0.21
c_g	=	29 J/mol K	Q_{vh}	=	31.8(45)(25) kJ/mol
C_m	=	2 MJ/m ^{3}K	R	=	8.314 J/mol K
ν_g	=	0.63(0.648)(0.625)mol/mol	ν_l	=	0.09(0.054)(0.125)mol/mol
c_o	=	224 J/mol K	s_{or}	=	0.1
c_w	=	75 J/mol K	φ	=	0.3
ν_w	=	0.72(0.7)(0.75)mol/mol	T^{ac}	=	7066 (10050) K
D_g	=	10^{-9} m^2/ s	ρ_w	=	55000 mol/m^3
k	=	10^{-10} [m^2]	T^{ini}	=	300 K
ρ_o	=	6826(4411)(8694)mol/m^3	λ	=	3 W/m K
P_{res}	=	10^6Pa	T^{nh}	=	371 (489) (309) K
Q_{vw}	=	40 kJ/mol	T^{nw}	=	373 K

Table 4.1.: Values of reservoir parameters for heptane (dodecane) (pentane) as effective oil pseudo-component.

model equations in weak form. We use fifth order Lagrange elements, meaning that the basis functions in this finite element space are polynomials of degree five. In other words, the entire solution is a sum of piecewise fifth order polynomials. The grid size in the simulations is 0.01 m, which is fine enough to capture the multi-scale processes and capable of resolving salient features.

4.3. Air injection into a porous medium with oil, gas and no initial water

In this section, we consider air injection into a reservoir containing initially medium boiling point oil (heptane) and gas, in absence of water. Our goal here is to study the effect of water produced in the reaction. This also verifies a simplified model studied in [67], which allows an analytical solution for the wave sequence including the MTO wave. In this model, condensation of water produced in the reaction was neglected, which corresponds to a vanishing condensation rate $W_{vw} = 0$. In this case, the reaction Eq. (4.2.1) is simplified to

$$\nu_l(\text{hydrocarbons}) + O_2 \to \nu_g' \,(\text{gaseous products}), \tag{4.3.1}$$

where $\nu_g' = \nu_g + \nu_w$ and gaseous products include water, carbon oxides and other gases. Also, the simplified model neglected molecular diffusion, capillary and thermal conductivity effects. For numerical results that take into account diffusive effects, see [55].

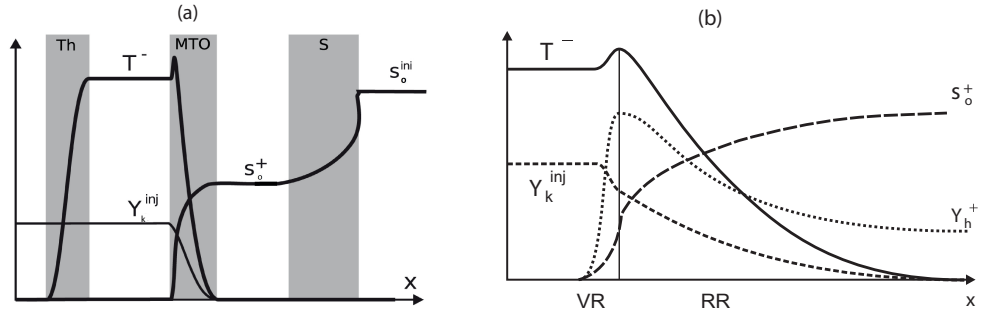

Figure 4.1.: (a) Wave sequence solutions of the thermal (Th), MTO and saturation (S) waves for the combustion of light oil [67]. Indicated are the schematic distributions of the temperature T, oleic saturation s_o and oxygen fraction Y_κ. Superscripts (-) and (+) represent the upstream and downstream side of the MTO wave respectively. The x-axis corresponds to T^{ini} for temperature and to zero for other variables. (b) Schematic graphs of the MTO wave profile. The thin vaporization region (VR) is dominated by vaporization and the much wider reaction region (RR) is dominated by the MTO reaction with slow condensation. The VR is much thinner than the RR, because it is assumed that vaporization is much faster than the reaction.

4.3.1. Structure of analytical solution

Here we briefly describe the analytical solution obtained in [67]. The solution corresponds to the long time behavior and consists of a sequence of moving waves separated by constant states. In Fig. 4.1a the solution is shown as a sequence of three waves, viz., a thermal, an MTO, and a saturation wave. Due to the high heat capacity of the rock, the thermal wave is the slowest. The constant state at the upstream side of the thermal wave is determined by the injection boundary conditions. The temperature in the thermal wave changes from a low value $T = T^{ini}$ upstream to some high value T^- downstream.

The MTO region contains the most interesting traveling wave, which has a constant speed v (Fig. 4.1b). In this region, all the dependent variables T, s_o, u, Y_h, Y_κ can be expressed in terms of a single traveling coordinate $\xi = x - vt$, *i.e.*, in a frame of reference moving with speed v. Reference [67] uses the traveling wave solution to relate quantities at the upstream side to those at the downstream side, and to obtain the wave speed v. The region upstream of the MTO wave contains injected gas with an oxygen fraction $Y_\kappa^{inj} > 0$ and no gaseous hydrocarbon, $Y_h = 0$. The reaction rate W_r vanishes both at the upstream and downstream side of the MTO region, which leads to the condition $s_o = 0$, (no oil) upstream, and $Y_\kappa = 0$, (no oxygen) downstream. Downstream of the MTO wave there is liquid hydrocarbon with a saturation $s_o^+ > 0$ and a temperature $T = T^{ini}$; here the equilibrium condition $W_{vh} = 0$ requires $Y_h = Y_h^{eq}(T^{ini})$.

The mathematical analysis of the MTO region is simplified in an essential way by the

reasonable physical assumption that the vaporization rate is much higher than the reaction rate. Under this assumption the MTO region is divided into a vaporization region (VR) and a reaction region (RR), see Fig. 4.1b. The VR is very thin due to high vaporization rate. Here the fraction of gaseous fuel rises from $Y_h = 0$ in the injected gas to the equilibrium value $Y_h = Y_h^{eq}(T)$ at the downstream end of the VR. Since this region is very thin and the reaction rate is not large at the prevailing low fuel concentration, the oxygen consumption in the VR is negligible. In the RR, most of the MTO reaction occurs. Moreover gaseous fuel condenses due to temperature decrease downstream in the direction of gas flow. Along the RR, the equilibrium condition $Y_h = Y_h^{eq}(T)$ holds approximately. The surprising feature of MTO is that the thin VR is located upstream of the RR.

Finally, the saturation wave travels downstream of the MTO wave, see Fig. 4.1a, where the temperature is constant and equal to $T = T^{ini}$. Therefore, we have thermodynamic equilibrium between liquid and vaporized hydrocarbon, i.e., $Y_h = Y_h^{eq}(T^{ini})$, and there is no net vaporization or condensation. The injected oxygen has been consumed completely in the MTO region. Therefore, we have $Y_\kappa = 0$ downstream of the MTO region, where no reaction occurs. The saturation region sustains a Buckley-Leverett solution, which is obtained using the standard procedure involving the Welge tangent construction [89]. Briefly, from upstream to downstream, the Buckley-Leverett solution consists of a rarefaction, a shock and a constant state with oil saturation s_o^{ini}, as its initial value.

4.3.2. Numerical solution and water condensation effect

We first explain the numerical simulation of air injection into a rock filled by an oil with medium boiling point (heptane) at initial saturation of $s_o^{ini} = 0.9$ in the absence of initial water, when condensation of water produced in the reaction is neglected [55]. As shown in Fig. 4.2a the numerical solution exhibits two regions (a thermal region $0 \leq x \leq 25m$ upstream, and an MTO region $32 \leq x \leq 40m$ downstream) in the same way as was found in the analytical solution. The analytical and numerical solution look similar, in spite of the presence of diffusion terms, which were required to obtain the numerical solution. The thermal wave travels in the region of the reservoir from which the liquid and gaseous hydrocarbons were displaced, i.e., $s_o = 0$ (purple curve) and $Y_h = 0$ (red curve), as the injected gas contains no gaseous hydrocarbons. Therefore the reaction rate W_r and the vaporization rate W_{vh} are both zero, and the (blue) oxygen fraction $Y_\kappa = Y_\kappa^{inj}$ is constant. The (green curve) temperature in the thermal wave changes from the injection value $T^{ini} = 300K$ upstream to the value $T^- \approx 450K$ in the plateau around $25 - 30m$. This gradual increase is due to thermal conductivity. The MTO wave contains vaporization and reaction regions. The wave profile is characterized by steep changes of all variables at higher temperatures, followed by slower variations at lower temperatures downstream (see Fig. 4.2a). Note also that the temperature T attains a

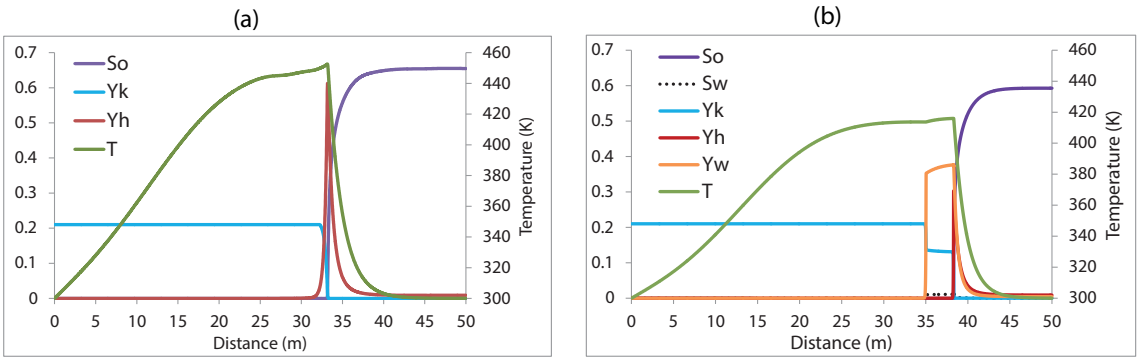

Figure 4.2.: Wave sequence in numerical solution with the thermal and MTO regions for heptane ($s_o^{ini} = 0.9$) when no water is present initially in the reservoir. Indicated are the distributions of the temperature T, oil saturation s_o, water saturation s_w, oxygen mole fraction Y_κ, steam mole fraction Y_w and gaseous hydrocarbon mole fraction Y_h at $t = 3.1 \times 10^7 sec$ in the base case (see Table 4.1). (a) Results of [55], where water condensation is neglected. (b) Simulations taking into account water condensation from reaction products.

maximum at a peak. At this state the heat consumption by the vaporization is balanced by the heat generation by the combustion process. Downstream of the MTO wave there is liquid-gas equilibrium $Y_h = Y_h^{eq}(T^{ini})$, so there is no net vaporization or condensation. The oxygen has been consumed completely in the MTO region, so no reaction occurs downstream of the MTO region. The saturation region (Fig. 4.1a) has moved away at the time corresponding to Fig. 4.2, but it was observed at earlier times. The above numerical simulation did not take into account condensation of water from reaction products, i.e., $W_{vw} = 0$. The simulations discussed below take this effect into account by means of the expression (4.2.19) for the water vaporization/condensation rate. Figure 4.2b and the zoomed region $30 - 50$ m in Fig. 4.3 show the numerical results for the combustion of heptane when water originates as a reaction product (see Eq. 4.2.1) but is not initially present in the reservoir ($s_o^{ini} = 0.9$ and $s_w^{ini} = 0$). The solution consists of a thermal wave, a water vaporization front, and a MTO wave merged with the steam condensation front. One observes that a steam bank, see the orange curve Y_w in Figs. 4.2b and 4.3a, is formed upstream of the MTO wave, which increases the total gas flux and, thus, speeds up oil recovery. This mechanism is supported by a water bank with very small saturation s_w in the region $35 - 38$ m, which collects the water produced from the reaction. The maximum temperature is lower than in Fig. 4.2a (for the case of no water condensation), which should be attributed to the increase of the MTO wave speed, as a larger amount of rock is heated up in the same time interval. The oxygen mole fraction Y_κ decreases abruptly from the injected value $Y_\kappa^{inj} = 0.21$ to $Y_\kappa = 0.13$ at $x \simeq 35m$ because at this point steam with concentration Y_w is produced. The oxygen is consumed comletely in the MTO wave at $x = 38$ m. As shown

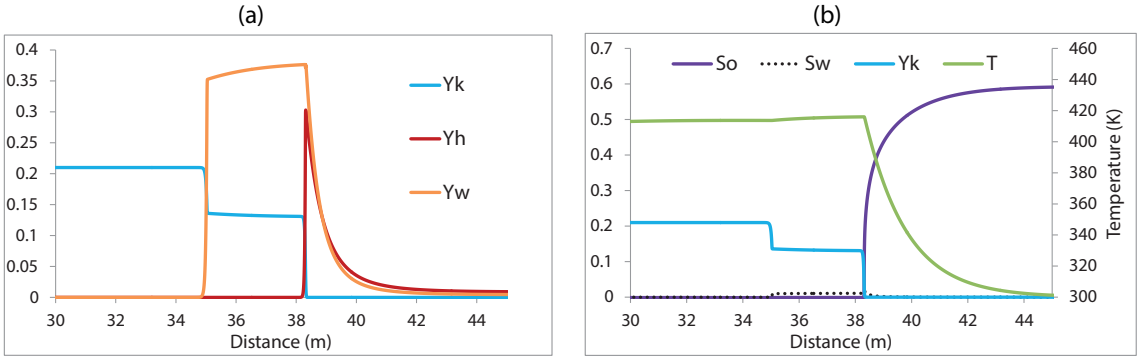

Figure 4.3.: Expanded version of Fig. 4.2b for air injection into reservoir with heptane and no initial water, but water as reaction product, (Eq. 4.2.1). Indicated are the distributions of the oxygen mole fraction Y_κ, steam mole fraction Y_w, gaseous hydrocarbon mole fraction Y_h at the left and the distributions of water saturation s_w, oil saturation s_o, and temperature T at the right, for $t = 3.1 \times 10^7 sec$.

in Fig. 4.3a, the steam and the vapor hydrocarbon both condense at the same location (around $38 - 40$ m). Condensed water accumulates upstream of the MTO wave, as we already mentioned. The oil saturation s_o downstream of the MTO wave in Fig. 4.2a is around 0.65, which decreases slightly to $s_o = 0.59$ in Fig. 4.3b due to the steam effect. We conclude that the water/steam produced by the reaction improve the MTO recovery.

4.4. Air injection into a porous medium with oil, gas and water

In this section, numerical results are presented for different cases of three phase (gas, water and oil) flow in the porous medium. The effects of the oil boiling point (heptane, dodecane and pentane) and of initial water saturation on oil recovery by the MTO wave are studied.

4.4.1. Medium boiling point oil

Figure 4.4 shows the numerical results for the combustion of heptane with the initial saturation $s_o^{ini} = 0.7$, when part of the water is initially present in the reservoir with $s_w^{ini} = 0.2$ and another part is generated by the reaction. The solution consists of a thermal wave, a water vaporization front, an MTO wave (reaction, vaporization and condensation of oil at the steam condensation front), and a saturation wave. As shown in Fig. 4.4, the (green) temperature in the slowest thermal wave increases from $T^{ini} = 300$K upstream to the value $T^- = 410$ K downstream. At $x = 16$ m,

there is a front where the steam is vaporized, and the porous medium contains water at almost initial saturation $s_w \approx 0.2$ downstream.

The MTO wave starts at $x = 41m$. Hydrocarbon vaporization and MTO occur in a very thin region in the upstream part of the MTO wave. All oxygen (blue curve) is consumed in this region. Further downstream at $x > 41$ m, the steam condenses abruptly generating a water jump. The gaseous hydrocarbon Y_h and steam Y_w condense at the same location, which means that the steam condensation front (SCF) moves with the same speed as the MTO wave. All oil is swept by the MTO wave, so that $s_o = 0$ and $Y_h = 0$ upstream of the MTO wave. No oxygen is left in the downstream side, $Y_\kappa = 0$. Overall mass balance considerations show that most of the steam originates from the initial water in the reservoir, while only about 10% comes from the combustion reaction.

Finally, the saturation wave travels downstream of the MTO wave at $x = 42.7$ m in Fig. 4.4. In this wave, the temperature is low. Therefore, we have thermodynamic equilibrium between vapor and liquid heptane and between steam and water, i.e., $Y_h = Y_h^{eq}(T^{ini})$ and $Y_w = Y_w^{eq}(T^{ini})$, and there is no net vaporization or condensation in the saturation wave. The water saturation drops down from $s_w = 0.5$ to the initial value $s_w = 0.2$, while oil saturation jumps from $s_o = 0.2$ to 0.4 followed by a slow increase till $s_o = 0.45$. This wave represents the slowest saturation wave. Recall that several saturation waves typically appear for three-phase flow [8, 69] and the faster saturation waves were only observed at earlier times and moved away to the right.

The behavior just described reveals a complex mechanism, where the coupling of MTO with vaporization/condensation of both steam and oil lead to enhanced recovery. This mechanism has multiple components. The steam vaporization upstream of the MTO wave with condensation downstream increases the gas drive and creates a water bank of high saturation (up to $s_w = 0.5$) in the interval $41 \leq x \leq 42.7$ m, see Fig. 4.4. The two-stage oil bank is created first by the oil vaporization/condensation mechanism ($s_o = 0.2$ in $41 \leq x \leq 42.7$ m), followed by the saturation shock wave leading to the plateau with $s_o = 0.45$. Figure 4.4 shows that for medium boiling point oil (heptane) the MTO wave and the SCF merge into a single wave; the first evidence for this mechanism was found by Bruining and Marchesin [24]. At the same time, the saturation wave is slightly faster than the MTO wave. So the water and oil banks get wider in time.

When the numerical results for heptane in the absence of initial water (Fig. 4.2b) are compared with the numerical results for a mixture of water and heptane (Fig. 4.4), one can observe that the presence of initial water has a positive effect on the recovery of light oil. Oil and water banks are built up, which does not happen in the absence of initial water. In the presence of water, the MTO wave speed is slightly higher, while maximum temperatures are almost the same in both cases.

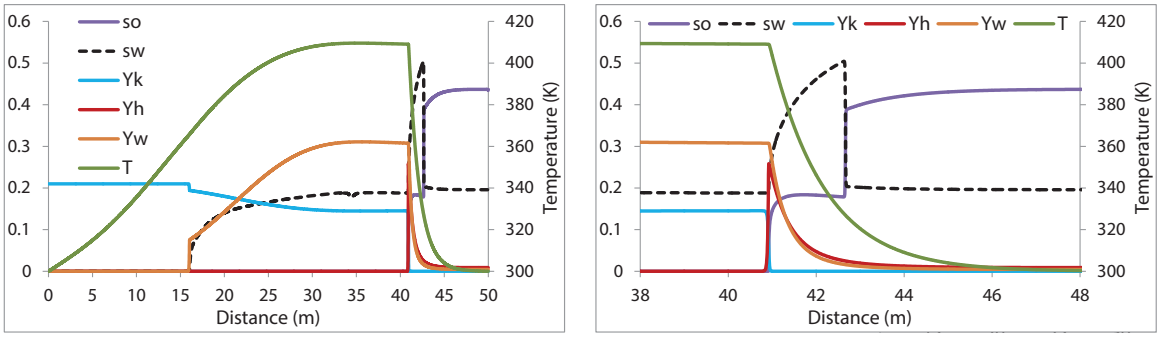

Figure 4.4.: Air injection into a heptane/water mixture with initial saturations $s_o^{ini} = 0.7$ and $s_w^{ini} = 0.2$. Indicated are the distributions of the water saturation s_w, oil saturation s_o, temperature T, oxygen mole fraction Y_κ, steam mole fraction Y_w, and gaseous hydrocarbon mole fraction Y_h at $t = 3.1 \times 10^7 sec$. The right figure shows the expanded region of the MTO and saturation waves.

4.4.2. High boiling point oil

Let us now consider the effect of water in the air injection process for the recovery of a high boiling temperature oil (dodecane), i.e., when the oil boiling temperature is much higher than that of water. For such oil, we need higher initial temperatures for ignition of the MTO process, and we use $T^{ini} = 350$K. Figure 4.5 shows the numerical results for the combustion of dodecane when water is initially present in the reservoir with saturation $s_w^{ini} = 0.2$. The initial oil saturation is $s_o^{ini} = 0.7$. The solution consists of a thermal wave, an MTO wave and a saturation wave. As shown in Fig. 4.5, the (green) temperature in the thermal wave increases from T^{ini} upstream to the value $T^- = 560$ K further downstream.

As one observes by comparing Figs. 4.4 and 4.5, the position of the steam region relative to the MTO wave changes. Both vaporization and condensation of steam occur downstream of the MTO wave for high boiling point oil. The reason is that the high boiling temperature volatile oil finds it difficult to vaporize and therefore the oil combustion and vaporization/condensation remains upstream. The oxygen mole fraction is constant ($Y_\kappa = Y_\kappa^{ini}$) upstream of the MTO wave, and decreases steeply to zero in the MTO wave at 55m due to the reaction. No oil exists upstream of the MTO wave ($x < 55$m in Fig. 4.5). The first increase of oil saturation s_o (purple curve) at $55m$ is a result of mechanisms involving the MTO wave. This includes the reaction as well as condensation of the oil, which was vaporized upstream and carried to colder region in gas form. The oil saturation increases to the maximum $s_o = 0.45$ at $x = 56$m, where it drops down to $s_o = 0.14$ at the boundary of the water region. Finally, there is a saturation wave in the region $70 \leq x \leq 81$ m where the oil saturation rises to $s_o = 0.45$, while water saturation drops to $s_w \approx 0.2$.

As opposed to the case of medium boiling point oil, in which oil and water condensation occur at the same location with the formation of an oil bank, in the case

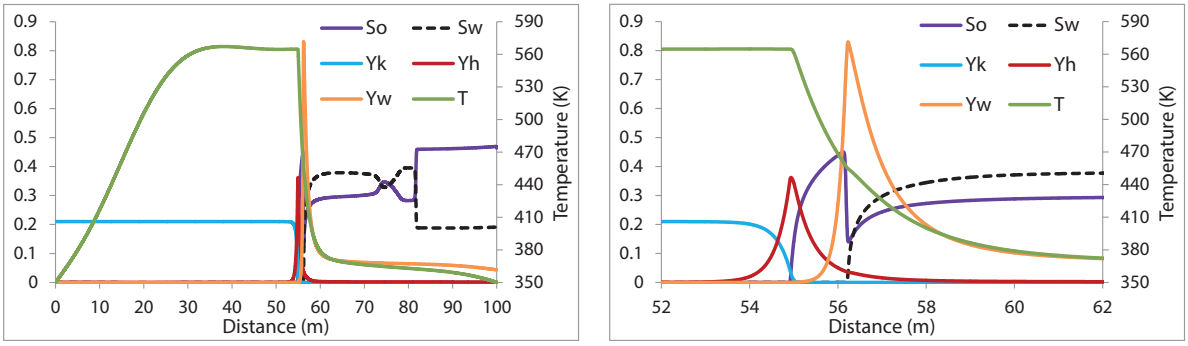

Figure 4.5.: Air injection into a dodecane/water mixture with initial saturations $s_o^{ini} = 0.7$ and $s_w^{ini} = 0.2$. Indicated are the distributions of the water saturation s_w, oil saturation s_o, temperature T, oxygen mole fraction Y_κ, steam mole fraction Y_w, and gaseous hydrocarbon mole fraction Y_h at $t = 5.5 \times 10^7 sec$. The right figure shows details of the region containing MTO wave.

oil with a high boiling point, oil condensation occurs at the location where water evaporates, and water condenses further downstream of the MTO wave. This leads to a negligible effect of water on the oil recovery, resulting in low ($s_o = 0.3$) oil saturation ahead of the MTO wave. Recovery is improved due to the presence of the saturation wave downstream. Unlike the case of Fig. 4.4, for higher boiling point oil, no steam and water remain behind the MTO wave.

Figure 4.6 shows the numerical results for the combustion of dodecane when water originates only from reaction (see Eq. 4.2.1), i.e., it is not initially present in the reservoir ($s_w^{ini} = 0$). As shown in this figure, negligible amounts of water s_w are produced, and the steam region is located downstream of the MTO wave. From

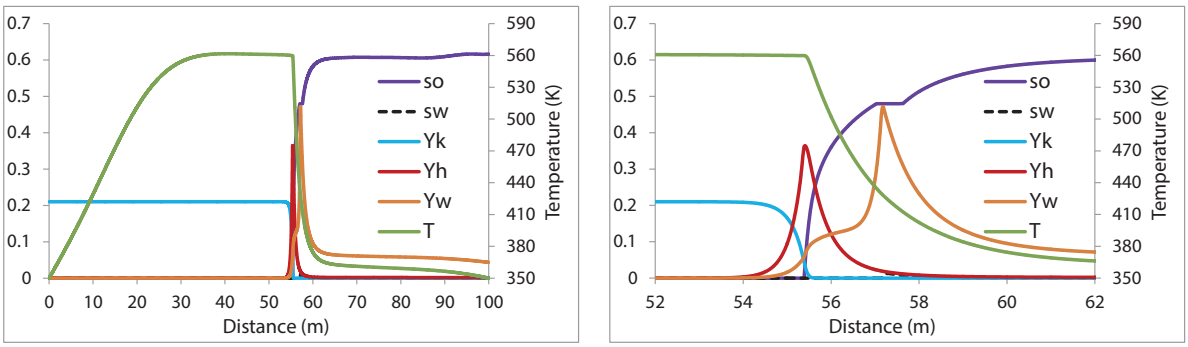

Figure 4.6.: Air injection into one pseudo-component oil (dodecane) of saturation $s_o^{ini} = 0.9$ with no initial water saturation, but water as reaction product (Eq. 4.2.1). Indicated are the distributions of the water saturation s_w, oil saturation s_o, temperature T, oxygen mole fraction Y_κ, steam mole fraction Y_w, and gaseous hydrocarbon mole fraction Y_h at $t = 5.5 \times 10^7 sec$. The figure at the right shows a blow-up of the Figure at the left near the MTO wave.

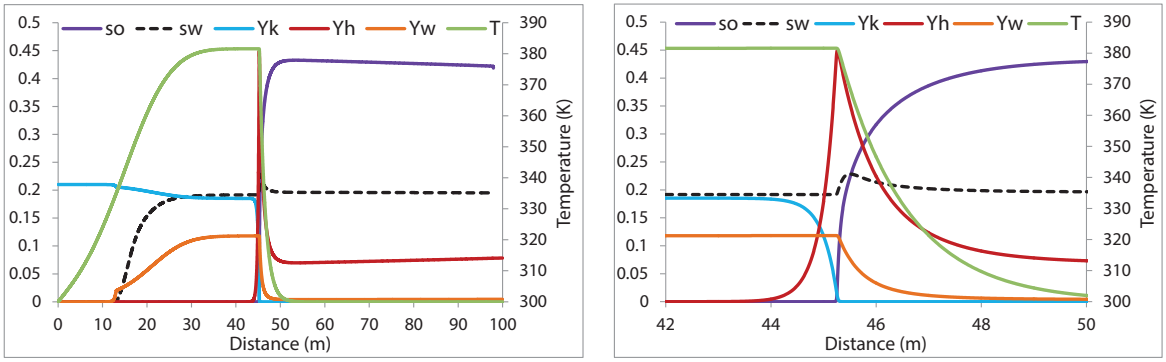

Figure 4.7.: Air injection into a pentane/water mixture with initial oil saturation $s_o^{ini} = 0.7$ and water saturation $s_w^{ini} = 0.2$. Indicated are the distributions of the water saturation s_w, oil saturation s_o, temperature T, oxygen mole fraction Y_κ, steam mole fraction Y_w, and gaseous hydrocarbon mole fraction Y_h at $t = 3.3 \times 10^7 sec$. The figure at the right shows a blow-up of the figure at the left near the MTO wave.

the profiles in Figs. 4.5 and 4.6, one observes that the presence of initial water decreases the oil saturation s_o in the MTO wave but is slightly improves the oil recovery.

4.4.3. Low boiling point oil

Figure 4.7 shows numerical results for the combustion of low boiling point oil (pentane) at saturation $s_o^{ini} = 0.7$ when water is initially present in the reservoir at saturation $s_w^{ini} = 0.2$. We see that the general structure of the solution is similar to the medium boiling point oil in Fig. 4.4. Both cases are characterized by a boiling temperature lower or close to the water boiling point. Figure 4.7 shows that more gaseous hydrocarbon is produced when the light oil is more volatile than water. The volatile oil is swept away and there is no oil upstream of the MTO wave. There is no oil bank build up in this case and the water condenses at the same location as oil. Part of the oil is produced as gas due to its low boiling temperature; note $Y_h > 0$ at the production side in Fig. 4.7. The MTO wave is responsible for more efficient oil recovery. As the oil is volatile and light, vaporization in the MTO wave plays an important role in this case.

4.4.4. High water saturation

Let us consider the effect of high initial water saturation on the wave sequence for an effective one-component oil representing heptane and dodecane. The numerical results show that the wave sequence is preserved for a mixture of water and oil when the initial water saturation is increased to $s_w^{ini} = 0.6$. As shown in Fig. 4.8 for a

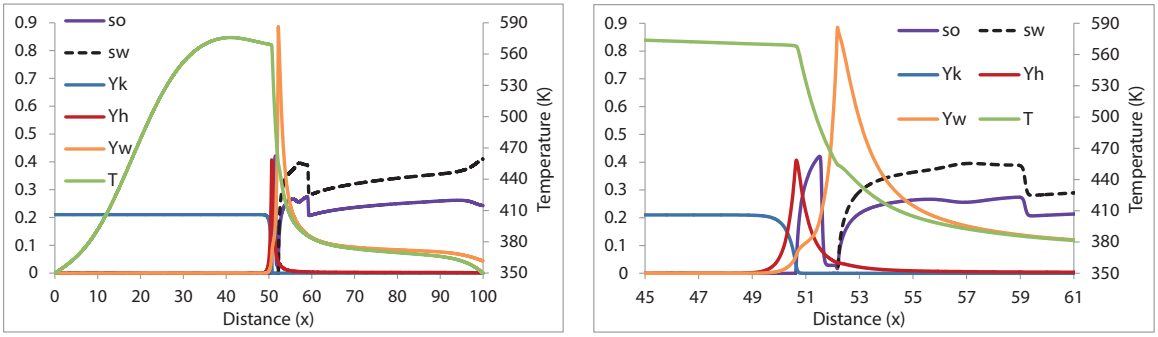

Figure 4.8.: Air injection into a dodecane/water mixture with initial oil saturation $s_o^{ini} = 0.3$ and water saturation $s_w^{ini} = 0.6$. Indicated are the distributions of water saturation s_w, oil saturation s_o, temperature T, oxygen mole fraction Y_κ, steam mole fraction Y_w, and gaseous hydrocarbon mole fraction Y_h at $t = 5.5 \times 10^7 sec$. The figure at the right shows a blow-up of the figure at the left.

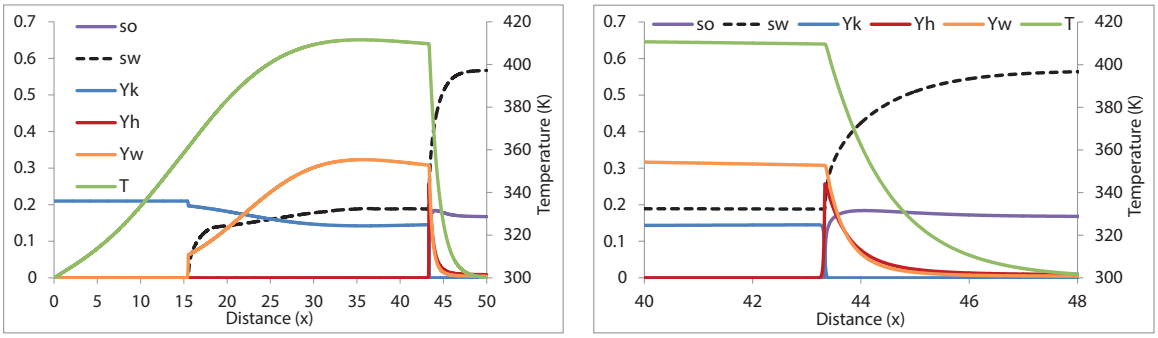

Figure 4.9.: Air injection into a heptane/water mixture with initial oil saturation $s_o^{ini} = 0.3$ and water saturation $s_w^{ini} = 0.6$. Indicated are the distributions of water saturation s_w, oil saturation s_o, temperature T, oxygen mole fraction Y_κ, steam mole fraction Y_w, and gaseous hydrocarbon mole fraction Y_h at $t = 3.1 \times 10^7 sec$. The figure at the right shows a blow-up of the figure at the left.

mixture of water and dodecane, the MTO wave is slower when the initial water saturation is high (compare with Fig. 4.5). In this case, because the dodecane has a higher boiling temperature than water and the water finds it easier to vaporize in the temperature range of the MTO wave, an increase in water saturation leads to longer time needed for vaporization and hence to a slower wave velocities. The MTO region and saturation wave speeds decrease and the steam region is located downstream of the MTO wave.

For a mixture of water and medium boiling temperature oil, Fig. 4.9 shows that the increase in the initial water saturation ($s_w^{ini} = 0.6$) speeds up the oil recovery because the SCF and the MTO wave move together, while water vaporization occurs upstream.

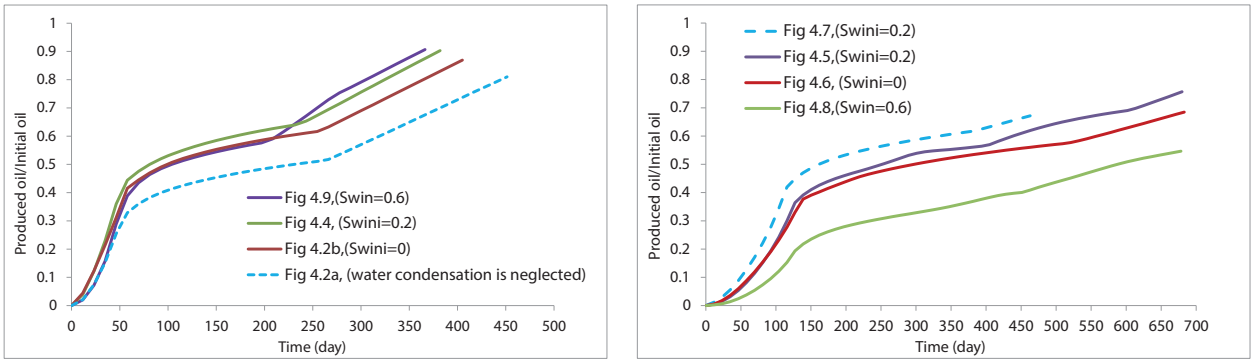

Figure 4.10.: The recovery fraction of oil versus time for (a) heptane and (b) dodecane (solid lines) and pentane (dashed line) for numerical simulations in Figs. 4.2–4.9. The times in Figs. 4.2–4.9 correspond to 358 days (heptane), 636 days (dodecane) and 381 days (pentane).

4.5. Efficiency of the steam region and MTO wave

The amount of oil recovered relative to the amount of initial oil in place versus time is shown for heptane, dodecane and pentane in Fig. 4.10, which correspond to the initial conditions shown in Figs. 4.2–4.9. Figure 4.10a shows the striking universality of the recovery curves for heptane in a wide range of initial water and oil saturation. One can see that the curves are almost identical to each other. The same figure shows that neglecting water condensation and vaporization in the MTO process (dashed curve) leads to underestimating the recovery, which is enhanced by the steam region. One can clearly distinguish three stages of the recovery history in Fig. 4.10a, which are characterized by approximately constant recovery rates (slopes). These three stages are the steepest initial part ($0-50$ days), the intermediate part with lower recovery rate ($50-240$ days) and the final part with a higher recovery rate (>240 days).

The reservoir states corresponding to the first and second stages are presented in Fig. 4.11, while the third stage is described in Fig. 4.4. One can see that the initial recovery (Fig. 4.11a) is a simple gas displacement in three-phase flow with almost no thermal effects due to reaction ($T \approx T^{ini}$). The recovery mechanism is based on the saturation wave (at 35m in Fig. 4.11a), which reaches the right end (production side) in about $t = 50$ days. At about the same time, the temperatures increases, leading to the formation of the MTO wave, Fig. 4.11b. Formation of this MTO wave triggers a secondary saturation wave with a higher speed and lower downstream oil saturation (at 36m in Fig. 4.11b). This wave is responsible for the small recovery rate in the second stage ($50-240$ days in Fig. 4.10a) due to a lower downstream oil saturation, and it reaches the right end in about $t = 240$ days. The rest of the recovery process is governed by the MTO wave with oil and water banks as described in section 4.4.1. Note that the last two stages of the recovery are based essentially on the MTO process leading to elevated temperatures. This

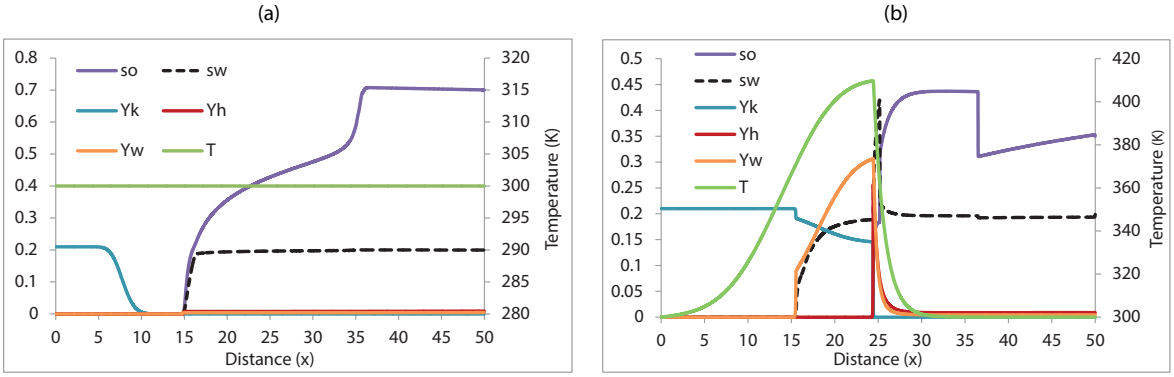

Figure 4.11.: Air injection into a heptane/water mixture with initial saturations $s_o^{ini} = 0.7$ and $s_w^{ini} = 0.2$. Indicated are the distributions of the water saturation s_w, oil saturation s_o, temperature T, oxygen mole fraction Y_κ, steam mole fraction Y_w, and gaseous hydrocarbon mole fraction Y_h at (a) $t = 3 \times 10^6 sec$ (35 days) and (b) $t = 1.6 \times 10^7 sec$ (185 days).

is why the steam vaporization/condensation plays an important role for improving the recovery rate for $t > 50$ days; compare with the dashed line in Fig. 4.10a when steam condensation is neglected in the model.

Figure 4.10b shows the relative recovery curves for dodecane and pentane. The case of pentane is similar to that of heptane (low boiling point) in Fig. 4.10a. However, we have a different situation for dodecane (high boiling point), where the steam region moves downstream of the MTO wave (Fig. 4.5). Several stages can be recognized in this process too. Though, in this case, high initial water saturations lead to considerable decline in oil recovery (green curve in Fig. 4.10b).

4.6. Conclusions

We formulated and simulated numerically a mathematical model for injection of air into a one-dimensional porous medium filled with gas, water and light oil. The numerical solution consists of a thermal wave, steam vaporization and condensation fronts, an MTO wave (oil reaction, vaporization and condensation), and three-phase saturation waves. It turns out that when the boiling point of the oil is near or slightly above the boiling point of water, the volatile oil condenses at the same location as the steam in the MTO wave, while steam vaporization occurs upstream. In this case the presence of water speeds up the oil recovery. The recovery curves (recovery fraction versus time) show the striking universal properties, as they are almost independent of initial water saturation. However the effect of water condensation/vaporization is important, because the recovery appears less efficient, when water condensation is neglected in the model. If the boiling point of the oil is much higher than the boiling point of water, the whole steam region moves ahead of the MTO wave. In this

case, the presence of water has only a minor effect on the recovery efficiency when initial water saturation is not high. However, the effect becomes negative, when the water saturation is high. Numerical simulations suggest that there is a bifurcation point (oil-boiling point) separating the case for which steam and oil condensation occur simultaneously in the MTO wave from the case where the steam region moves downstream of the combustion zone.

5. Recovery of Light Oil by Air Injection at Medium Temperature: Experiments

Abstract[1]

Volatile oil recovery through air injection is a promising method for highly heterogeneous low permeability reservoirs. Thermal effects due to oxidation reaction, vaporization/condensation and flue gas drive are the most important mechanisms for light oil recovery by medium pressure air injection. To gather evidence for this claim, we performed ramped temperature experiments with consolidated cores filled with hexadecane injecting either air or nitrogen at different injection rates at medium pressures. The experiments show that oxygen is removed from the injected air through physical and chemical sorption by the hydrocarbon at low temperatures. Most of the bonded oxygen is released later at higher temperatures and reacts to form carbon oxides. The amount of oil burned in the air injection process relative to the amount of oil recovered increased from 2% at 10 bar to 18% at 30 bar, and again decreased to 5% at 45 bar and 3% at 70 bar. This trend was predicted theoretically in an earlier study of the medium temperature oxidation process.

[1]Submitted for publication in Journal of Petroleum Science and Engineering, 2014.

5.1. Introduction

Recovery percentages from oil reservoirs range from 5% for difficult oil to 50% for light oil in highly permeable sandstone reservoirs. Due to the current difficulties encountered in the production of oil, in-situ combustion (ISC) and high pressure air injection (HPAI) are considered as effective ways to enhance the recovery of oil. When high pressures are impractical, an air injection method can be proposed that is effective at medium temperatures and pressures for light oil reservoirs [67]. The experiments described in this work explain the reasons for its effectiveness.

The air injection process is often referred to as HPAI when it is applied to deep light oil reservoirs, where other recovery methods are uneconomic or ineffective, whereas the term in-situ combustion traditionally has been used for heavy oil reservoirs. The effectiveness of HPAI depends on many oil recovery mechanisms [28] including sweeping by flue gases, field re-pressurization by the injected gas, oil swelling, oil viscosity reduction, stripping off light components from the oil by flue gas, and thermal effects generated by the oxidation reactions. The maximum amount of oil recovery in combustion processes is the initial oil-in-place exclusive the amount of fuel consumed in the combustion reactions [68], i.e., even residual oil may be produced.

The mechanism responsible for oil displacement by air injection varies with the type of oil. For light oil, vaporization and condensation are just as important as the oxidation reaction [67]. Air injection is very effective in heterogeneous permeability reservoirs as the oil evaporates away from the lower permeability parts to be collected at the higher mobility streaks. There is a large body of literature describing the use of HPAI to recover oil [3, 6, 25, 26, 56, 62, 63, 64], which is appropriate at high pressures (>100 bars) in reservoirs at large depths. However, at shallower depths ($300 \sim 1000$ m), an alternative is to inject at medium pressures ($10 \sim 90$ bars) for light and medium oil in heterogenous low permeability reservoirs. High temperatures and high heat generation are not necessary for the displacement of light oil by air injection [44]. However some form of oxidation is required in order to remove the oxygen from the injected air [44] to prevent it from reaching the production wells, which is considered a safety hazard.

In most of the experiments and simulation studies in the literature considered, scission reactions improve oil recovery, in which case oxygen is removed from the injected stream. However, it is suggested [94] that only about 20% of the light oils are good candidates for undergoing full oxidation at temperatures greater than $400°C$, and that the other 80% only incorporates the oxygen in the oil by low temperature oxidation (LTO) at lower temperatures. The mechanism for combustion of light or medium viscosity oils is fundamentally different from that for the combustion of heavy oils [3, 6, 23, 25, 26, 56, 62, 63, 93, 53], in which high temperatures are achieved. In the high temperature oxidation (HTO), the heat conducted out of the reaction zone converts the oil to coke before it is combusted. In the medium

temperature oxidation (MTO) [45, 46, 40] the oxidation reaction leads to scission of the molecules and formation of small reaction products such as water, CO or CO_2. In LTO, the oxygen is incorporated in the hydrocarbon molecules to form alcohols, aldehydes, acids or other oxygenated hydrocarbons. LTO is characterized by the production of little or no carbon oxides [45, 44, 48]. Dabbous et al. [29] also suggest that light crude oils appear to be more susceptible to partial oxidation at low temperatures because of their high hydrogen content. An increase in the viscosity of the oil subjected to LTO reactions was observed [7], while a decrease in the API gravity of the oil was reported [68].

Oxidation reaction mechanisms at reservoir conditions are complex. A number of conceptual combustion models describing ISC have been formulated in the past [7, 18, 34]. Most of the models assume liquid phase or coke combustion as the source of energy to sustain ISC. Some references indicate that gas-phase reactions in HPAI are relevant [13]. However, in view of the role played in these reactions [81] by free radicals [49, 60], which are easily annihilated at pore walls, it is still a matter of debate whether gas phase reactions are significant. Alexander et. al [7] found that LTO reactions have a pronounced effect on fuel deposition and composition. In the experiment [7] with crude oil 21.8° API and temperatures between $121°C$ and $345°C$, large values of apparent atomic hydrogen-carbon ratio was indicative for oxygen consumption in LTO reactions, which do not produce carbon oxides. Another important fact is that oxygen diffusion rate into the oil phase is greater than the oxidation reaction rate, so that oxygen is dissolved throughout the oil phase during LTO [29].

In the case of experiments in a combustion tube, the latter contains a mixture of oil and sand that is heated up, using nitrogen as a carrier gas. At initiation of the experiment the nitrogen is replaced by air and the combustion process starts [3, 6, 23, 25, 26, 56, 62, 63, 93]. For ramp temperature oxidation tests, such as the one we performed, the reactor is heated over the whole length of the tube. One set of experiments was carried out at high pressures (120 bar) and high injection rates with light oil (37° API) [13], in which combustion occurred at 220^oC. In another set of tests, combustion tube experiments were also performed at a low air flux rate [63], so that oxygen consumption was close to 100% (the oxygen contents in the produced gas phase were only 1 percent or less). Under these conditions, the combustion rate is controlled by oxygen mass transfer, and the kinetics of the oxidation reactions are not important except during the ignition period. Greaves et al. [45] carried out two tests on a light Australian oil (38.8° API) starting at initial oil saturations of $S_o = 0.41$ and 0.45, at an operating pressure of 70 bar and an initial bed temperature of $63°C$. The combustion temperature was about $250°C$ in both tests. High combustion velocities were achieved in all tests, varying from 0.15 to 0.31 m/hour.

Gillham et al. [42] show that for the deep Hackberry reservoir, air injection can increase the light oil recovery to economical significance. They distinguish between application of high and low pressures in the field trials. The low pressure trial is

conducted between $20 - 40$ bars. Unfortunately, supporting tube tests were only reported at high pressures (230 bar) incidentally. The paper reports two incidents of fire, one in the high pressure test and one in the low pressure test, both occurring in the injection well. Gutierrez et al. [47] describe a low pressure (14 bar) laboratory test with light oil, which gave rise to relatively high temperatures ($478°C$). The combustion is characterized initially by oxygen addition reaction followed by scission reactions. The authors conclude that high oxygen injection rates are required to stimulate the scission reactions. Germain et al. [40] describe combustion tube tests with light oil in heterogenous low permeability ($1 - 100$ mD) reservoirs using pressures of $40 - 45$ bars and leading to combustion temperatures between $260°C$ and $370°C$. Low pressure thermal gravity and differential scanning calorimetry test results [61] show that distillation is a dominant process for the recovery of light and medium oils at elevated temperatures. This may indicate that pressure effects need to be taken into account. They also found that pressure enhances exothermic reaction rates in a pressurized differential scanning calorimeter test with a sample weight of 10 mg.

In a previous theoretical study based on two-component oil model, we found that the ratio between vaporization and reaction determines the effectiveness of the air injection process [54]. If a large amount of heavy components is present in oil, the vaporization is weak and most oil is left behind for combustion. On the contrary, for a large amount of light component in the oil, most of the oil vaporizes and less oil is left behind for combustion. As a result, recovery of light oil is more efficient and requires less oxygen per amount of oil recovered. It is asserted that the oxidation mechanism also plays an important role in the effectiveness of the oil production, as partial oxidation of the light hydrocarbons forms oxygenated hydrocarbons with a higher boiling point [45, 44, 48] than the original hydrocarbons. In such a case vaporization will be hampered and the process may become less effective.

One of the purposes of our research is to investigate whether we can find experimental evidence for the medium temperature combustion mechanism described theoretically in [67, 54]. We perform and interpret experiments involving air injection in sandstone rock filled with n-hexadecane (modeling light oil) at medium pressures and conditions that are typical away from the injection well. The air fluxes used in typical combustion-tube experiments and accelerating-rate calorimetry [94] are much higher than in the field except in the near wellbore region of air-injection wells. At slower rates we expect to see details that are not visible in experiments operating at high rates and pressures [13, 47, 40, 63, 45]. The low air injection rate was chosen to mimic the processes in the main reaction zone (away from the injection well) in an oil reservoir, in which there is a long residence time for oxygen to be in contact with oil. The experiments were done to investigate the mechanisms in the air injection process at different pressures and injection rates. The important aspect in this study was to determine the nature of low temperature oxidation products prior to full combustion. The mechanism of initial uptake of oxygen for later release was established in this work.

The paper is organized as follows. Section 5.2 describes the experimental set-up and procedure. Section 5.3 describes operating conditions and modeling. Section 5.4 discusses the experimental results and interpretation. We end with some conclusions.

5.2. Experimental set-up and procedure

The experimental apparatus shown in Fig. 5.2 is a high pressure ramped-temperature oxidation reactor consisting of a combustion tube (a stainless steel reactor with an internal diameter of 5 cm and a length of 23 cm) equipped with heating devices, four internal thermocouples (see Fig. 5.2), and equipment for gas injection, sampling and analysis. This setup can be operated at either a predefined heating rate schedule or at a fixed temperature, medium pressure and low air injection rate. The reactor temperature is determined by thermocouples inserted along axis of the sandstone core. Two extra termocouples are added under the electrical-resistance band heater, wrapped around the outer wall of a pressure jacket in order to monitor the temperature change induced by the heating band. Heat is provided by a cylindrical electrical heater enclosing the tube. The heaters are controlled through an Eurotherm temperature regulator based on the temperatures underneath the heaters wrapped around the cell. The complete setup is insulated by thermal ceramic super-wool to minimize heat losses.

A vertically-positioned sandstone core in the high pressure stainless steel reactor is first evacuated and then is entirely saturated with the model oil (n-hexadecane), which was preheated to a desired temperature through a given heating schedule. One of the main favorable features of this type of test is being able to perform all experiments with Bentheimer consolidated sandstone cores, which are rather homogenous. This is opposed to most experiments reported in the literature, generally performed with crushed core or sand, which can alter the original permeability and porosity. The air is injected from the top, controlled by a mass flow meter; oil and exhaust gases are produced at the reactor bottom. The produced gas is analyzed by a gas chromatograph (GC). Liquids from the reactor are collected and analyzed to determine the produced oil viscosity and density. In order to prevent clogging of the GC column by heavier components as well as to collect the produced liquid, a cooling trap and separator are placed in front of the inlet port to the GC. An Agilent Cerity portable 3000 Micro gas chromatograph is used for the analysis of the produced gas. To analyze the gas stream, a GC is prepared to identify nitrogen, oxygen, carbon dioxide, carbon monoxide, methane, ethane, ethylene, and acetylene. Helium is used as a carrier gas.

The tubular reactor is made of steel (ASTM A269 TP316) and is located in a tubular pressure jacket. The annular space between reactor and jacket is pressurized by nitrogen, while the filled reactor is also pressurized by air. The pressure in the annulus is 10 bar higher than the reactor pressure for safety reasons. After pressurizing, the heating schedule is defined ($10°C$/10 min), while the injected gas

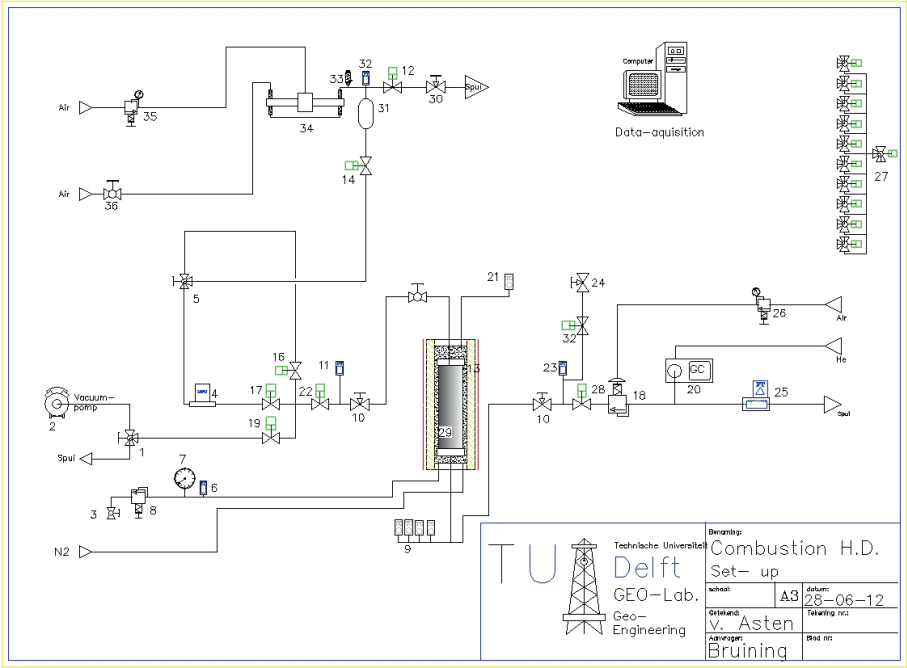

Figure 5.1.: Schematic drawing of the experimental set-up.

starts to flow through the reactor at a defined rate. At the top and bottom of the reactor two Swagelok safety valves are installed. The same heating schedule is used for all the experiments, because the heating rate has a direct effect on fuel availability [7]. Pressure transducers at the top and bottom of the reactor monitor pressure. Four thermocouples (TC) (ThermoCoax Type K) are installed in the reactor to allow monitoring the temperature at different locations in the tube, from TC-1 at the top to TC-4 at the bottom (see Fig. 5.2). A mass flow meter is used to control the rate of gas injection into the reactor. The back pressure valve is set to a desired pressure. A wet gas meter provides a cumulative reading of volumetric flow of the effluent gas stream. The data from the thermocouples, injection and production pressure, and the gas flow rate are collected every second on a computer using an in-house data acquisition system.

5.3. Description of the experiments

Six experiments were carried out. Some parameters varied from run to run, such as the system pressure, the injection flow rate and injected gas type. The temperature ranged from 25^oC to 450^oC. The pressure was maintained at 10, 30, 45 and 70 bar. The injection flow rates were 20 and 50 ml/min (measured at room temperature and atmospheric pressure). The core for the experiments is Bentheimer sandstone with a porosity around 30%. The model oil used in this work is n-hexadecane with a purity of 99 mol %. The injected gases were nitrogen and air. Nitrogen had a

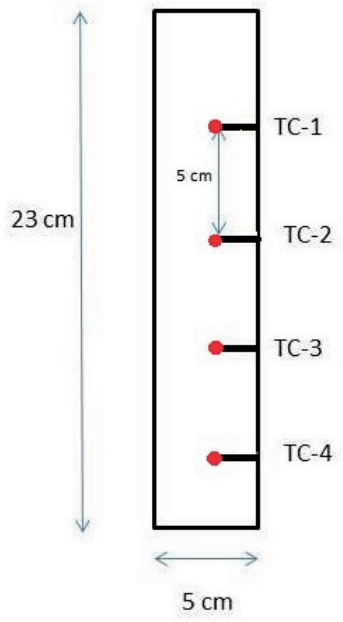

Figure 5.2.: Schematic drawing of the tube including thermocouples and their distances.

Run	Injected Gas	Injection rate	Pressure
Exp.1	Air	20 ml/min	30*bar*
Exp.2	Nitrogen	20 ml/min	30*bar*
Exp.3	Air	50 ml/min	30*bar*
Exp.4	Air	20 ml/min	10*bar*
Exp.5	Air	20 ml/min	45*bar*
Exp.6	Air	20 ml/min	70*bar*

Table 5.1.: Operation conditions of the experiments.

purity of 99.995 vol%. Compressed air was injected as oxygen source. Table 5.1 lists the operating conditions for each run in terms of injected gas, injection rate and pressure.

In the combustion process, oxygen in the injected air reacts with the hydrocarbon fuel to generate heat. Refering to the LTO reaction path proposed in [27], the hydrocarbon molecules are primarily oxidized to intermediate products, such as carboxylic acid, aldehyde, ketone, alcohol, ether and other products (exothermic); at the same time oxygen can also be dissolved in the oil or absorbed by the oil. Carbon dioxide is the main final gaseous product of LTO reactions. In our experiments, the composition of the produced gas is analyzed, where the molar concentrations of CO_2, CO, O_2 and N_2 are measured by GC and denoted as $[CO_2]$, $[CO]$, $[O_2]$ and $[N_2]$.

We propose the following overall oxidation reaction of hexadecane:

$$zC_nH_{2n+2} + qC_nH_{2n+2}O_2 + \frac{1}{\mathcal{R}}O_2 + N_2 \rightarrow \tag{5.3.1}$$

$$\hat{z}C_nH_{2n+2} + \hat{q}C_nH_{2n+2}O_2 + sH_2O + pCO_2 + vCO + fO_2 + N_2,$$

where the nitrogen/oxygen molar ratio in the injected air is denoted by $\mathcal{R}$, which is equal to 3.7. This model reaction describes sorption of oxygen or formation of oxygenated hydrocarbon when $\hat{q} > q$ and desorption or release of oxygen when $\hat{q} < q$. When $z+q > \hat{q}+\hat{z}$, it also describes full oxidation for a part of hydrocarbon molecules. Hydrogen concentration was not measured in the produced gas, which is a restriction for our GC setup. We disregard the hydrogen on the right-hand side of Eq. (5.3.1), which will lead to an underestimate of oxygen in the reaction products, but will not alter our main conclusions.

Initial hydrocarbon (C_nH_{2n+2}) with $n = 16$, oxygenated hydrocarbon (modeled effectively as $C_nH_{2n+2}O_2$) and water are produced in liquid phase, while other components are produced in gas phase. The stoichiometric coefficients p for CO_2, v for CO, and f for O_2 are found using the measured molar concentrations as

$$p = \frac{[CO_2]}{[N_2]}, \quad v = \frac{[CO]}{[N_2]}, \quad f = \frac{[O_2]}{[N_2]}. \tag{5.3.2}$$

Three balance equations for components C, H and O given by Eq. (5.3.1) are solved as

$$z - \hat{z} = \frac{1}{\mathcal{R}} + \frac{p+v}{2n} - \frac{3}{2}p - v - f, \tag{5.3.3}$$

$$\hat{q} - q = \frac{1}{\mathcal{R}} - \frac{p+v}{2n} - \frac{3}{2}p - v - f, \tag{5.3.4}$$

$$s = \frac{(n+1)}{n}(p+v). \tag{5.3.5}$$

The interpretation of the experiments is partly based on effective model in Eq. (5.3.1) and on analytical results for air injection in a reservoir with light oil [67], which will be summarized here for reasons of easy reference.

The mathematical analysis shows that the MTO reaction forms a wave traveling with constant speed, occupying a vaporization region and a reaction region, see Fig. 5.3. The vaporization region is very thin because vaporization is faster than reaction. The reaction region is much wider. The surprising feature is that the vaporization region is located upstream of the reaction region. In the vaporization region the

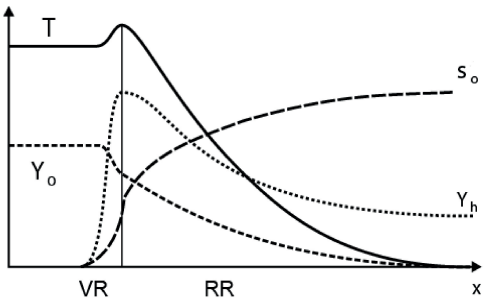

Figure 5.3.: A schematic graph of the MTO wave profile. Indicated are changes in temperature T, oil saturation s_o, oxygen fraction Y_o and hydrocarbon fraction Y_h in the gas. The thin vaporization region (VR) is dominated by vaporization and the much wider reaction region (RR) is dominated by the MTO reaction (with slow condensation) [67].

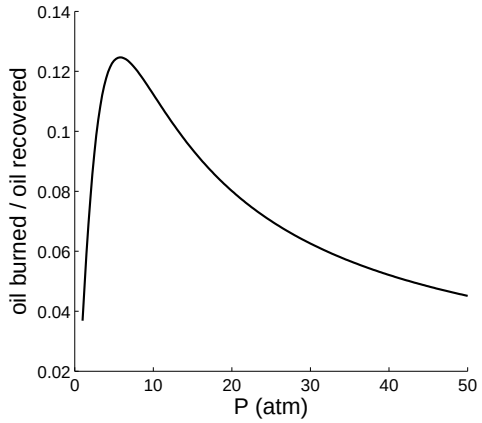

Figure 5.4.: Burned to recovered oil ratio for heptane depending on the reservoir pressure [67].

fraction of hydrocarbon in gas phase rises to the equilibrium value. In the reaction region most of the MTO reactions occur at medium temperatures. Moreover gaseous hydrocarbon condenses here due to temperature decrease in the direction of gas flow. The amount of oil burned in the MTO wave relative to the amount of oil recovered in front of the MTO wave was computed in [67].

Computations of this ratio for heptane depending on the reservoir pressure are reproduced in Fig. 5.4. The amount of burned oil varies in the range of $5-12\%$, decreasing at higher pressures.

5.4. Experimental results and interpretation

Figures 5.5 to 5.23 present the results of all experiments. These figures shows the temperature history at four locations in the reactor, produced gas composition history, reaction rate of hexadecane, production rate of oxygenated hydrocarbon, full oxidation rate and oil recovery curves. The results are interpreted right away.

5.4.1. Air injection Experiment (Exp. 1)

In the first experiment (Exp. 1), air was injected into the reactor, which was previously saturated completely with hexadecane as the model oil. The reactor was heated from room temperature to $400°C$ at a heating rate of $10°C/10min$. Figures 5.5 and 5.6 show the temperature and the produced gas composition histories. The gentle increase up to $150°C$ is due to heating interruption in the experiment because of problems with the back pressure valve, which were resolved after 150 minutes, recovering the initial heating rate.

Deviations of the temperatures along the tube (i.e., in different thermocouples) occur at temperatures above $200°C$, which is an indication of heat release due to sorption of oxygen in the hydrocarbon. Sorption of oxygen in the hydrocarbons within the porous medium [15, 51, 70] can be either physical (physisorption) or chemical (chemisorption); physical adsorption is caused by physical forces, i.e., van der Waals interaction between adsorbent and the adsorbate. The adsorption process is exothermic. The physisorption energy is below 40 kJ/mol. The chemical adsorption is due to chemical reaction between the adsorbent and the adsorbate, which changes the structure of the adsorbent. The chemisorption energy is comparable to the energy of chemical bonds in reactions and it is 80 kJ/mol or even more [52]. The solubility of gas in a liquid decreases as temperature increases [15, 51, 70].

The temperature peaks in Fig. 5.5 indicate that an exothermic reaction zone is formed at temperatures above $330°C$, which moves along the reactor passing through TC-1 (red curve) at the top to TC-4 (green) at the bottom in Fig. 5.2. The exothermic reactions resulted in an average temperature increase of $100°C$. It is shown that

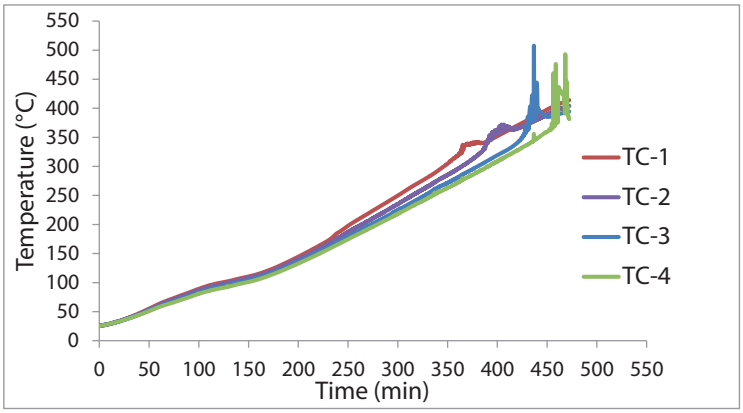

Figure 5.5.: Temperature history for air injection (Exp. 1).

the temperature increase is small and smooth at the top of the reactor (TC-1, TC-2), but less smooth at higher temperatures (TC-3, TC-4). A steep increase in temperature is an indication of a higher reaction rate at higher temperatures. The ultimate oil recovery for this experiment is 74%.

The effluent gas composition history is shown in Fig. 5.6. The oxygen fraction starts to decrease while the CO and CO_2 fractions start to increase, when the temperature reaches $200°C$, around $270min$ in Figs. 5.5 and 5.6. Very small amounts of hydrocarbon gases are produced starting at $230°C$; as the temperature rises, the produced amount of small molecule hydrocarbons increases, however their amounts are small in comparison to those of other produced gases. The nitrogen concentration increases in response to the consumption of oxygen, then starts to decrease to a constant value over the duration of the test, while more carbon oxides are produced. High nitrogen concentration is an indication of oxygen removal from the gas phase either by dissolution in the oil phase or by formation of oxygen containing compounds. These hydrocarbons (either with adsorbed oxygen or oxygenated) can partially provide fuel for combustion and oxidation reactions at later times. Moreover, adsorbed oxygen may also be released as the temperature increases (see Figs. 5.7 and 5.8). Figure 5.7 shows the produced atomic oxygen/nitrogen ratio in flue gas phase, which indicates that the consumption of oxygen from the injected gas does not correspond to the release of an equal amount of oxygen in gaseous reaction products (carbon oxides). Before oxygen uptake by the hydrocarbon, the molar ratio of $([CO]/2 + [CO_2] + [O_2])/[N_2]$ stays constant and equal its value in injected air. When the oxygen concentration begins to drop, the ratio decreases strongly and reaches the minimum, which means that part of oxygen oxygen is consumed while the production of carbon oxides is low. Later the ratio increases to a plateau value and the exothermic reaction zone is established as an indication of bond scission combustion reactions. In this final stage, the value of $([CO]/2 + [CO_2] + [O_2])/[N_2]$ is higher than the oxygen/nitrogen ratio in the injected air. This proves the release of oxygen from the oxygen containing hydrocarbon compounds. Subsequently the

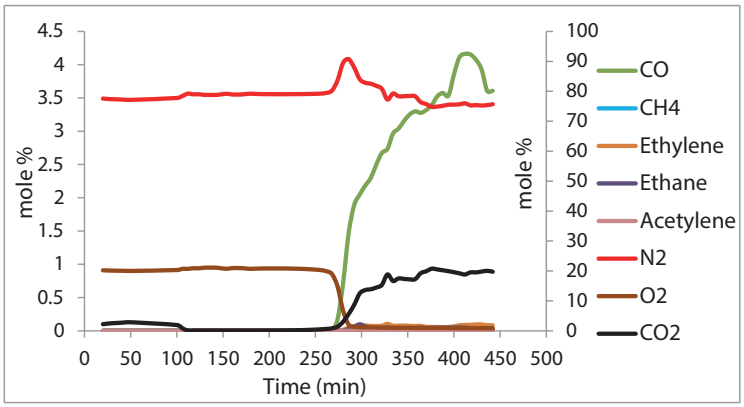

Figure 5.6.: Produced gas composition history for air injection (Exp. 1). Nitrogen, oxygen and carbon dioxide fractions are evaluated through the right vertical axis.

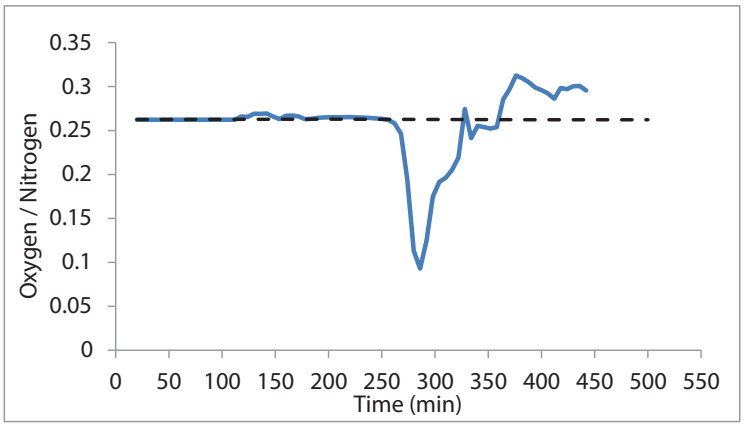

Figure 5.7.: History of the ratio of oxygen and nitrogen concentration in the produced gas for air injection experiment (Exp. 1). The dashed line indicates the ratio $1/\mathcal{R}$ in the injected air.

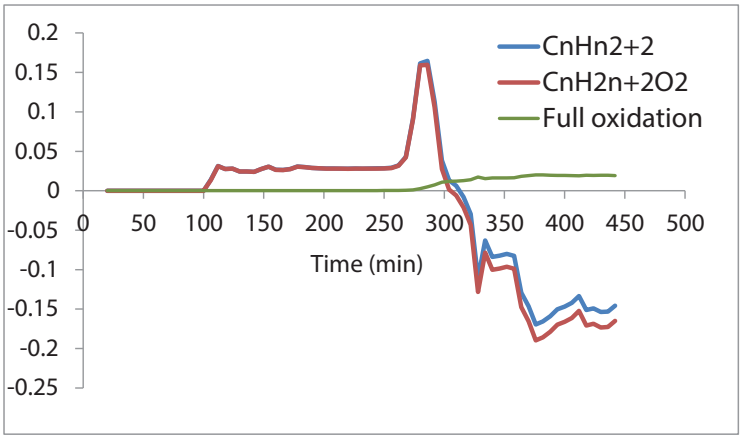

Figure 5.8.: Reaction rates for air injection experiments (Exp. 1) based on the reaction model (5.3.1). The blue curve shows the stoichiometric coefficient history $z - \hat{z}$ describing the reaction rate of hexadecane. The red curve corresponds to $\hat{q} - q$ describing the production rate of oxygenated hydrocarbon. The green stoichiometric coefficient $z + q - \hat{z} - \hat{q}$ describes the rate of full oxidation reaction. Negative values of $\hat{q} - q$ (red curve) imply that the oxygen-containing hydrocarbon is converted back to hexadecane.

oxygen reacts with the hydrocarbon locally to form mainly CO_2 and CO.

The viscosity and density of produced hydrocarbons are measured. These values turns out to be the same as the viscosity (2.9 cP) and density (761 kg/m^3) of hexadecane. This is intriguing evidence that the formation of oxygenated hydrocarbon may play a smaller role relative to oxygen dissolution in hydrocarbon than has been advocated in the literature.

Using the model reaction in Eq. (5.3.1), we can estimate the stoichiometric coefficient $\hat{q} - q$, which is proportional to the conversion rate of hexadecane to oxygen containing hexadecane, see Fig. 5.8. Similarly, we estimate and plot in Fig. 5.8 the stoichiometric coefficient $z + q - \hat{z} - \hat{q}$, which describes the rate of complete scission of hydrocarbons. Initially, no hexadecane reacts with air. Then (after 100 min) oxygen starts to react with hexadecane. As shown in Fig. 5.8, part of the hexadecane is converted to oxygen-containing hexadecane, because no carbon oxides are produced (Fig. 5.6). As temperature increases due to the external heater, more hexadecane is involved in chemical or physical adsorption of oxygen. After 300 min, a large part of oxygen-containing hexadecane is converted back to hexadecane, while the rest produces carbon oxides (note the increase of full oxidation rate in Fig. 5.8). This agrees with the exothermic temperature history in Fig. 5.5.

In summary, in the low temperature range (below 250°C), oxygen bonds physically or chemically in the low temperature oxidation zone with hydrocarbon. At a later stage, the oxygen containing compound desorbs the oxygen or further undergoes oxidation reactions.

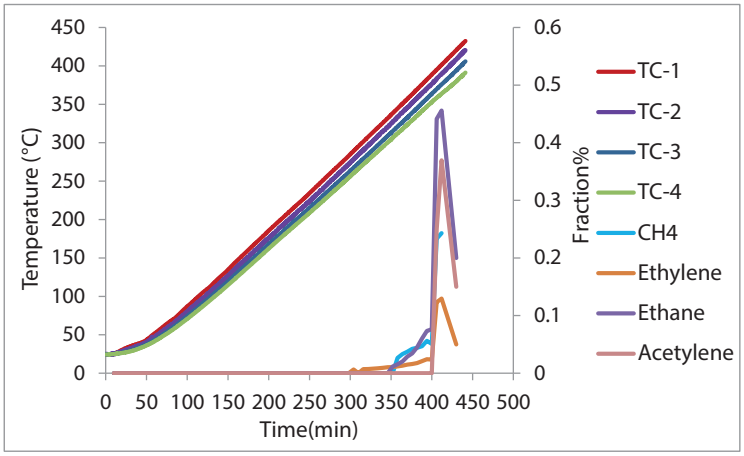

Figure 5.9.: Produced gas composition and temperature history for nitrogen injection experiment (Exp. 2).

5.4.2. Nitrogen injection experiment (Exp. 2)

The purpose of Exp. 2 is to determine the vaporization and the formation of cracking products in the absence of oxygen. In Exp. 2 nitrogen is injected from the top of the reactor while the reactor is heated according to a given heating schedule ($10°C$/10 min) starting at room temperature. Fig. 5.9 shows the temperature along the reactor and produced gas composition history. In the temperature profile, no endothermic front is visible due to vaporization or cracking, however small amounts of cracking products begin to be formed around $250°C$ (at 300 min). The amounts of cracking products during nitrogen injection are smaller than the amounts generated during air injection. This fact can be expected as air injection is accompanied by some heat releasing oxidation reactions, which lead to larger amounts of cracking products. However, even during air injection, the amount of cracking products would be too small to be a significant source of fuel for oxidation. The oil recovery for combined heating and nitrogen injection is 78%, which is larger than the recovery for combined heating and air injection (74%), a process in which part of the oil is consumed by combustion.

5.4.3. Effect of air injection rate (Exp. 3)

Figures 5.10 and 5.11 show the temperature profile and the produced gas composition for Exp. 3, which is similar to Exp. 1 but has a higher injection rate (50 ml/min). An exothermic reaction zone is visible in Fig. 5.10, which moves from TC-1 at the top of the reactor to TC-4 at the bottom. The first exothermic peak starts around $340°C$ as in the experiment with low injection rate (Fig. 5.5). The exothermic reactions result in an average temperature increase of $40°C$. The ultimate oil recovery for this experiment is 70%. The effluent gas composition is shown

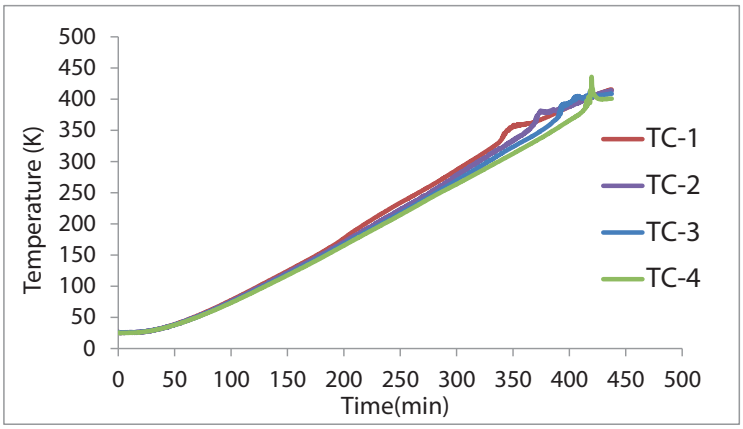

Figure 5.10.: Temperature history for air injection experiment with higher injection rate (50 ml/min) (Exp. 3).

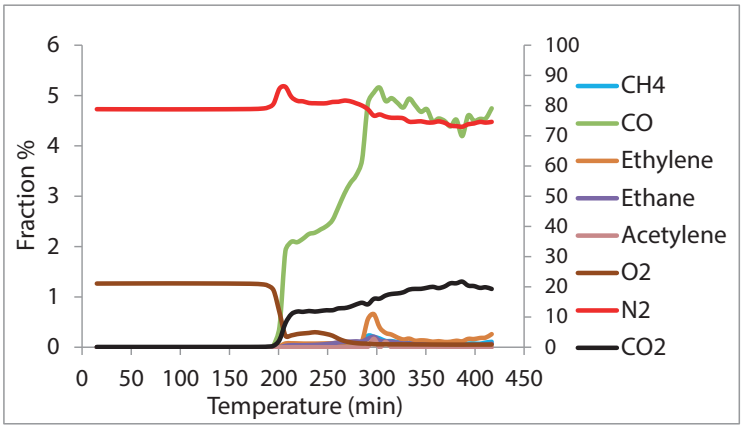

Figure 5.11.: Produced gas composition for air injection experiment with higher injection rate (50 ml/min) (Exp. 3). Nitrogen, oxygen and carbon dioxide fractions are evaluated through the right vertical axis.

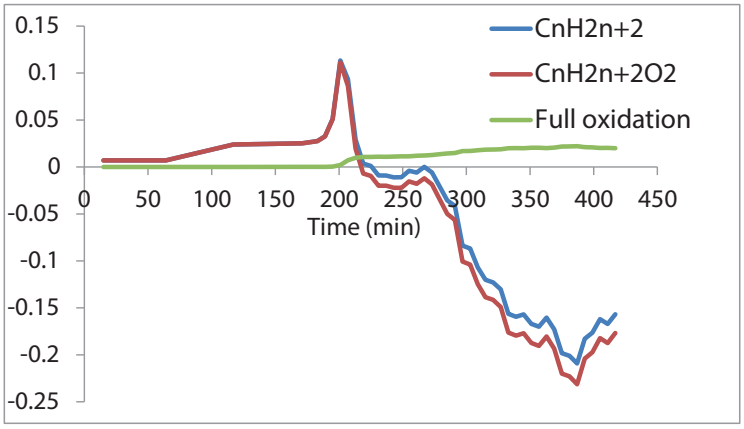

Figure 5.12.: Reaction rates for air injection experiment with high injection rate (50 ml/min) (Exp. 3) based on the reaction model (5.3.1). The blue curve shows the stoichiometric coefficient history $z - \hat{z}$ describing the reaction rate of hexadecane. The red curve corresponds to $\hat{q} - q$ describing the production rate of oxygenated hydrocarbon. The green stoichiometric coefficient $z + q - \hat{z} - \hat{q}$ describes the rate of full oxidation reaction. Negative values of $\hat{q} - q$ (red curve) imply that the oxygen-containing hydrocarbon is converted back to hexadecane.

in Fig. 5.11. The oxygen starts to drop around $180°C$ while CO and CO_2 fractions begin to rise. The oxygen fraction history in Fig. 5.11 shows that the oxygen uptake is not complete in the low temperature range as opposed to the results shown in Exp. 1. There are more cracking products. The nitrogen concentration increases in response to consumption of oxygen before it reaches a plateau. As shown in Figs. 5.12 and 5.8, the oxygen addition processes in hydrocarbon are favored when the air injection rate is low (Exp. 1). The smaller conversion is caused by the higher air speed, leading to smaller residence time; oxygen passes the hot region faster and has insufficient time to react with hexadecane. This reaction may be influenced by the ratio between the residence time of oxygen and the time available for diffusion, since higher injection air flux provides less time for the oxygen to sorb in the hydrocarbon. This leads to incomplete uptake of oxygen in the low temperature zone (see oxygen fraction history in Fig. 5.11).

5.4.4. Effect of reactor pressure (Exps. 4, 5 and 6)

We carried out several experiments on a core saturated with hexadecane at various pressures to study the effect of pressure on the air injection process. Figures 5.13 and 5.14 show the temperature and the produced gas composition history for Exp. 4, which is an air injection experiment at a reactor pressure (10 bar) lower than the ones used in the previous experiments. No exothermic reaction zone is visible in the temperature profile as the released heat is spread out, while oxygen in produced gas starts to decrease at much lower temperature around $170°C$ as apposed to the

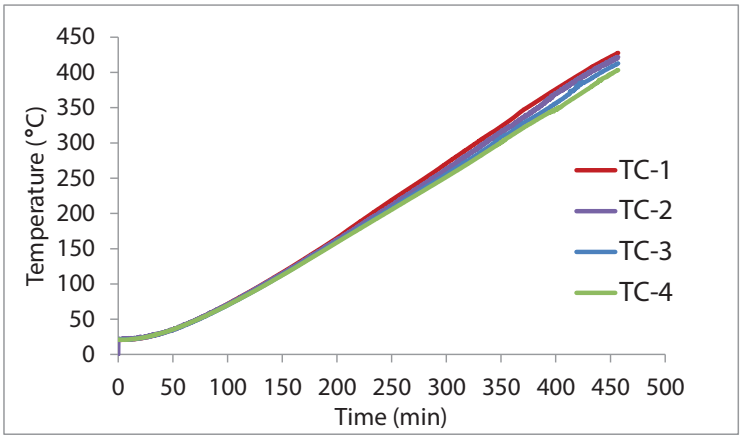

Figure 5.13.: Temperature history for air injection at pressure of 10 bar (Exp. 4).

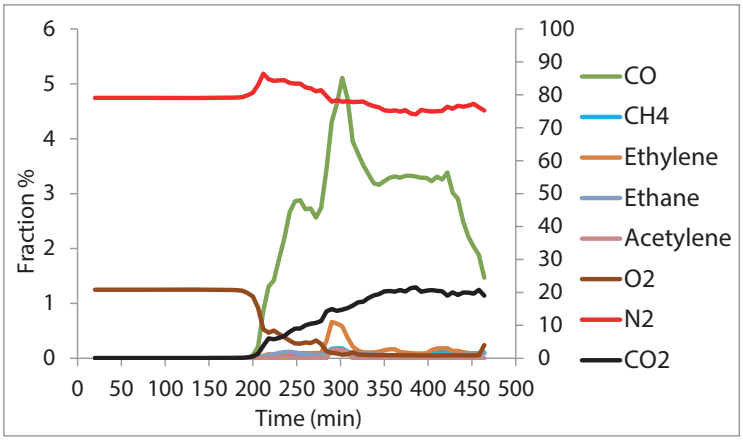

Figure 5.14.: Produced gas composition history for air injection at pressure of 10 bar (Exp. 4). Nitrogen, oxygen and carbon dioxide fractions are evaluated through the right vertical axis.

experiment at the higher pressure of 30 bar (Fig. 5.6). Oxygen is not completely removed from the air stream (Fig. 5.14) before the temperature reaches higher values around $250°C$. As shown in Fig. 5.15, hexadecane starts to release oxygen earlier than in the case of Exp. 1 (at 30 bar). The amount of cracking products (small molecule hydrocarbons) is negligible in air injection experiment at this lower pressure. Two other experiments were carried out at higher pressures, 45 and 70 bar. As observed in Figs. 5.16 and 5.19, no exothermic temperature effect (peaks) are visible. Two mechanisms may be responsible, viz., the effect of pressure on the reaction rate and the effect on the heat transfer. Increased pressure increases the chemical reaction rate,

$$W_r = A_r \varphi \rho_o s_o \left(\frac{P_g Y_o}{P_{atm}}\right)^n \exp\left(-\frac{E^{ac}}{RT}\right), \tag{5.4.1}$$

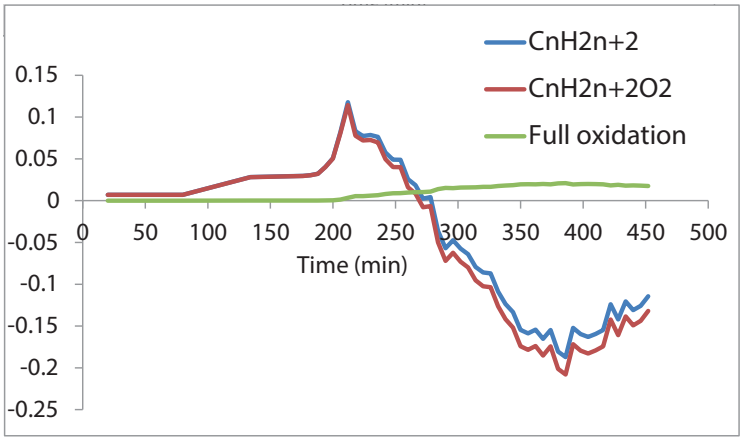

Figure 5.15.: Reaction rates for air injection experiment at pressure of 10 bar (Exp. 4) based on the reaction model (5.3.1). The blue curve shows the stoichiometric coefficient history $z - \hat{z}$ describing the reaction rate of hexadecane. The red curve corresponds to $\hat{q} - q$ describing the production rate of oxygenated hydrocarbon. The green stoichiometric coefficient $z + q - \hat{z} - \hat{q}$ describes the rate of full oxidation reaction. Negative values of $\hat{q} - q$ (red curve) imply that the oxygen-containing hydrocarbon is converted back to hexadecane.

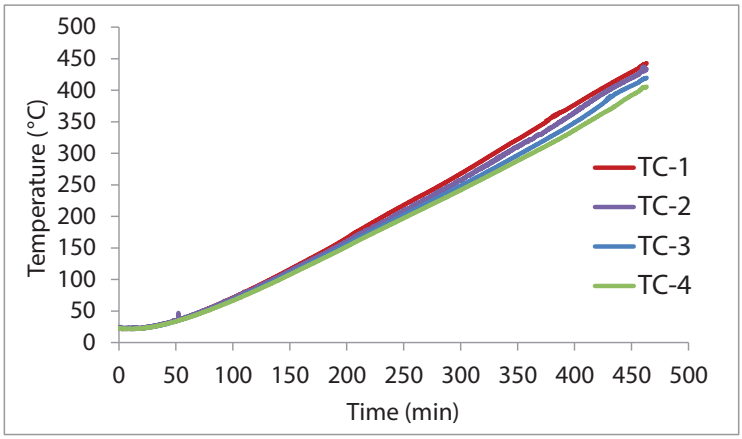

Figure 5.16.: Temperature history for air injection at pressure of 45 bar (Exp. 5).

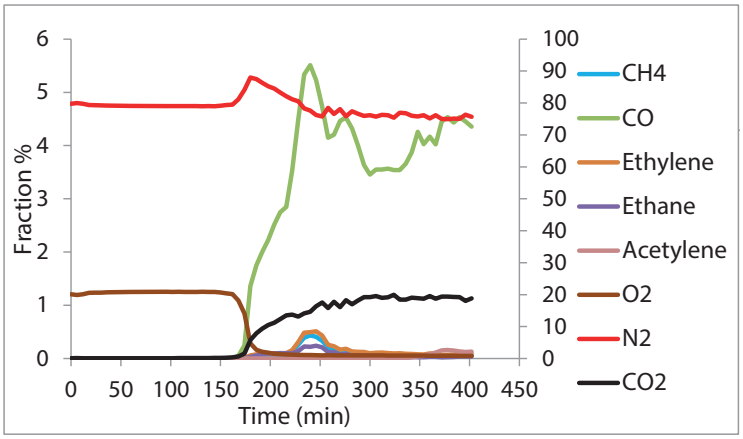

Figure 5.17.: Produced gas composition history for air injection at pressure of 45 bar (Exp. 5). Nitrogen, oxygen and carbon dioxide fractions are evaluated through the right vertical axis.

where A_r, ρ_o, s_o, P_g, Y_o, E^{ac} and R are oxidation reaction pre-exponential factor, oil molar density, oil saturation, gas pressure, oxygen mole fraction, activation energy and ideal gas constant respectively [67]. A higher pressure increases the concentration of oxygen in liquid oil. Increased pressure is conducive to both an enhanced chemical reaction rate and improved oxygen transport and would therefore increase the conversion rate of oxygen. This would lead to an increased visibility of the peaks in the temperature distribution, contrary to our observations. This leaves us with the effect of pressure on heat transfer. Increased pressure has only a small effect on thermal conductivity. However, it can increase the natural convection induced heat transfer, as the Grashof number is proportional to the square of the pressure [19]. Therefore one possible mechanism is that increased heat transfer spreads out the temperature and masks the temperature peaks.

The produced gas analysis (Figs. 5.17, 5.20 and 5.18, 5.21) showed the same mechanism as in the base case (30 bar), while cracking does not seem to be pressure dependent and remain small in all cases.

5.4.5. Efficiency of the air injection process

In the air injection process the amount of burned oil divided by the amount of recovered oil at the end of the experiment is shown in Fig. 5.22. The maximum ratio is attained at 30 bar (Exp. 1), while it gets smaller both for lower (10 bar) and higher (45 and 70 bar) pressures. This trend agrees qualitatively with the analytical results on medium temperature oxidation process [67], see Fig. 5.4. The amount of fuel burned is proportional to the injected oxygen flux. The recovered oil includes liquid and gaseous hydrocarbons. The mechanisms of liquid hydrocarbon recovery is flue gas displacement, (i.e., by nitrogen and combustion gases), while hydrocarbon

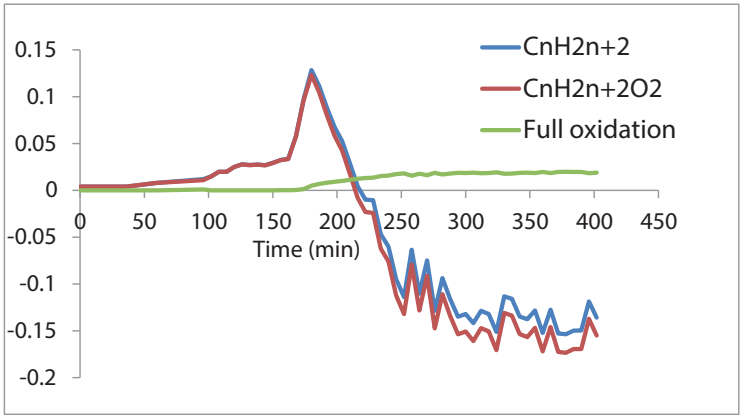

Figure 5.18.: Reaction rates for air injection experiment at pressure of 45 bar (Exp. 5) based on the reaction model (5.3.1). The blue curve shows the stoichiometric coefficient history $z - \hat{z}$ describing the reaction rate of hexadecane. The red curve corresponds to $\hat{q} - q$ describing the production rate of oxygenated hydrocarbon. The green stoichiometric coefficient $z + q - \hat{z} - \hat{q}$ describes the rate of full oxidation reaction. Negative values of $\hat{q} - q$ (red curve) imply that the oxygen-containing hydrocarbon is converted back to hexadecane.

recovery in gaseous phase is due to vaporization and distillation. The amount of burned oil varies in the range of $2 - 18\%$. As shown in Fig. 5.22, the maximum amount of oil is burned in the experiment at pressure of 30 bar. This mechanism is also confirmed by the exothermic temperature profile in Fig. 5.5.

Figure 5.23 shows the oil recovery versus time for four different pressures. We observe a rapid increase at early times. This early production is caused mostly by depressurization and gas flood effects. The MTO injection is more effective for oil recovery at higher pressures, as shown in Fig. 5.23, and confirmed theoretically in [67]. However, oil recovery at 30 bar is lower than oil recovery at 10 bar, but this may be attributed to some problems with the back pressure valve during initial part of the first experiment (Exp 1).

5.5. Conclusions

A set of experiments have been designed that enables investigation of the medium pressure air injection process in consolidated porous media saturated with oil using low injection rate. Air injection into light oil (modeled by hexadecane in this work) is a potentially attractive method for enhanced oil recovery. Our laboratory experiments indicate recoveries between $75 - 90\%$. The experiments show that an oxygen adsorption step takes place at low temperatures in the initial stage before the bond-scission combustion reactions occur. The sorbed oxygen bonds with hydrocarbon physically or chemically leading to complete uptake of oxygen from the injected

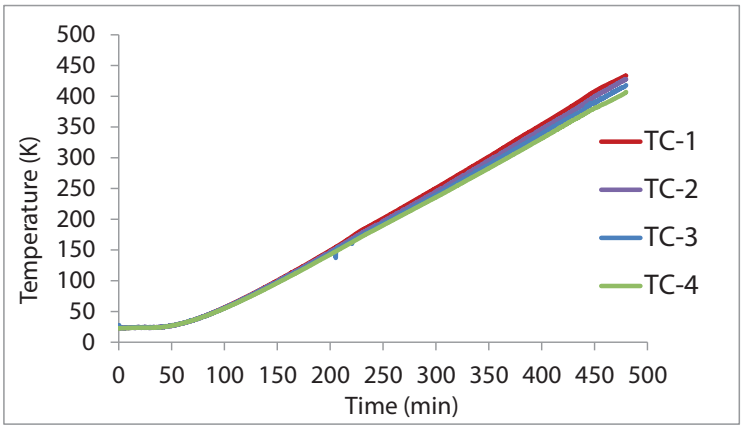

Figure 5.19.: Temperature history for air injection at pressure of 70 bar (Exp. 6).

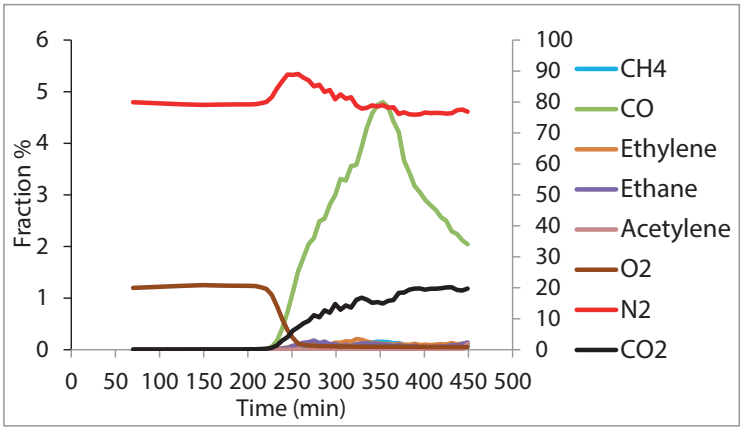

Figure 5.20.: Produced gas composition history for air injection at pressure of 70 bar (Exp. 6). Nitrogen, oxygen and carbon dioxide fractions are evaluated through the right vertical axis.

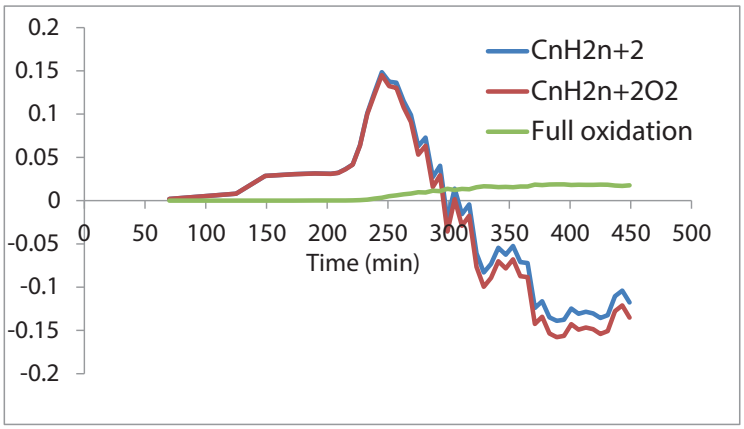

Figure 5.21.: Reaction rates for air injection experiment at pressure of 70 bar (Exp. 6) based on the reaction model (5.3.1). The blue curve shows the stoichiometric coefficient history $z - \hat{z}$ describing the reaction rate of hexadecane. The red curve corresponds to $\hat{q} - q$ describing the production rate of oxygenated hydrocarbon. The green stoichiometric coefficient $z + q - \hat{z} - \hat{q}$ describes the rate of full oxidation reaction. Negative values of $\hat{q} - q$ (red curve) imply that the oxygen-containing hydrocarbon is converted back to hexadecane.

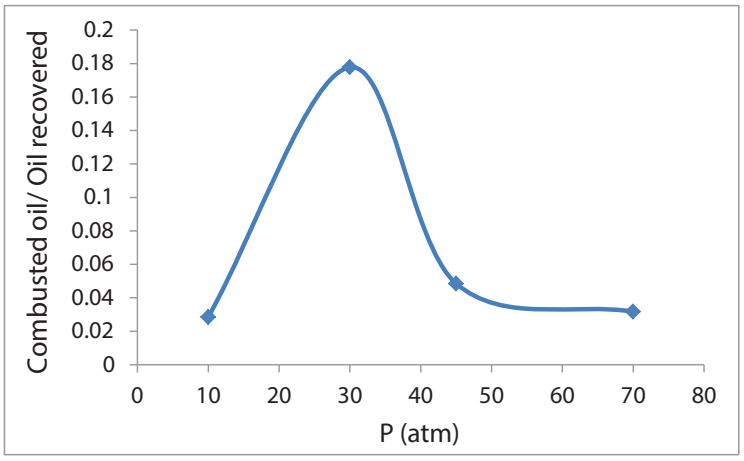

Figure 5.22.: Ratio of burned to recovered hydrocarbon at the end of the experiments depending on pressure. The curve shows a spline approximation through the four experimental points.

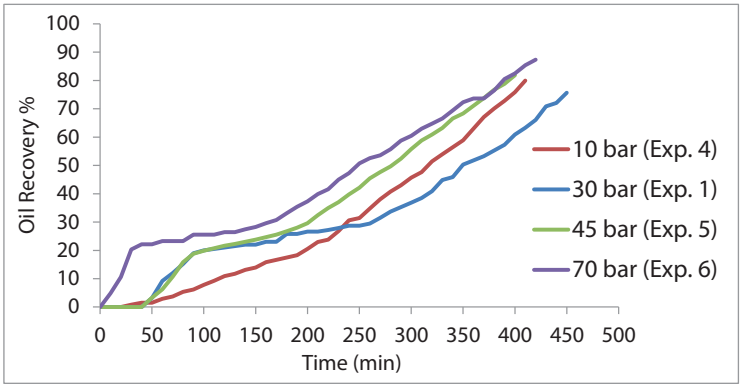

Figure 5.23.: Oil recovery versus time under different pressures.

air stream at low temperatures. Then the oxygen containing compound releases the oxygen at higher temperatures and partially reconverts to hexadecane, which is later produced, and partially undergoes a combustion reaction releasing carbon oxides and possibly also water. The produced liquid is not affected by the oxidation reaction and has the same viscosity and density as hexadecane. The amount of oil burned in the air injection process relative to the amount of oil recovered increases from 2% at 10 bar to 18% at 30 bar, and again decreases to 5% at 45 bar and 3% at 70 bar. This trend agrees with the previously obtained analytical results [67] for the medium temperature oxidation process.

6. Conclusions

1. The applicability of air injection in volatile oil reservoirs at medium pressures and the MTO (medium temperature oxidation) efficiency have been studied experimentally in the laboratory and mathematically using simple 1-D models. The models consider vaporization, condensation and reaction with oxygen. The models indicate displacement efficiencies of almost $82-98\%$ as opposed to $60-70\%$ water displacement efficiency. Combustion leaves no residual oil, but a small part of the oil is burnt. The laboratory experiments in this thesis concur, indicating displacement efficiencies between $75-90\%$ of the OIIP. The amount of oil burned in the air injection process relative to the amount of oil recovered in our laboratory experiments for hexadecane increased from 2% at 10 bar to 18% at 30 bar, and again decreased to 5% at 45 bar, after which it more or less remained constant. This trend was also predicted in previously obtained analytical results for the medium temperature oxidation process [67]. Finally, the MTO process is less efficient under higher air injection rates and the recovery is faster at higher pressures.
2. The following observations about the detailed combustion mechanisms in the presence of vaporization and condensation, based on a simple model with one volatile oil component and possibly a non-volatile component, can be made: vaporization occurs upstream of the combustion zone, which is also confirmed by previously obtained analytical solutions [67]. The MTO method is effective when oil contains an appreciable amount of volatile oil, more than 20% in the example considered by us. The effect of the interaction between volatile and nonvolatile components at various concentrations, air injection rates and pressures is obtained. The character of the MTO wave changes by altering the composition of the oil. Generally the solution consists of three types of waves, i.e., a thermal wave, an MTO wave and a saturation wave, all separated by constant state regions. The order between vaporization and oxidation in the MTO wave changes for different sets of conditions. For a predominantly light mixture, vaporization occurs upstream of the combustion process, a fact that confirms previously obtained analytical and numerical solutions for one component volatile oil [67, 55]. The combustion front velocity is high as less oil remains behind in the combustion zone. For oil with more non-volatile component (0.8 in volume fraction), the vaporization moves downstream of the combustion zone in the MTO wave. As more oil stays behind in the combustion zone, the velocity of the combustion zone is slower, albeit that the temperatures are much higher. Due to high temperatures, we conjecture a

transition to the HTO process in this case, which would need to be confirmed by further research.

3. Numerical calculations establish a range of parameters for the bifurcation point between MTO and HTO in a two-component oil mixture. Indeed, the bifurcation point is mainly determined by the fraction of the non-volatile component. At the bifurcation the character of the combustion process changes from a vaporization-dominated to a combustion-dominated process.

4. A numerical model was formulated to simulated an injection of air into a one-dimensional porous medium filled with gas, water and light oil. The numerical solution consists of a thermal wave, a steam vaporization and condensation fronts, an MTO wave (oil reaction, vaporization and condensation), and three-phase saturation waves. It turns out that when the boiling point of the oil is near or slightly above the boiling point of water, the volatile oil condenses at the same location as the steam in the MTO wave, while steam vaporization occurs upstream. In this case the presence of water speeds up the oil recovery. The recovery curves (recovery fraction versus time) show the striking universality properties, as they are almost independent of initial water saturation. However water condensation/vaporization effect is important, because the recovery curve is different (less efficient recovery), when water condensation is neglected in the model. If the boiling point of the oil is much higher than the boiling point of water, the whole steam region moves ahead of the MTO wave. In this case, the presence of water has only a minor effect on the recovery efficiency, when initial water saturation is not high. However, the effect becomes negative, when the water saturation is high. Numerical simulations suggest that there is the bifurcation point (oil-boiling point) separating the case for which steam and oil condensation occur simultaneously in the MTO wave from the case where the steam region moves downstream of the combustion zone.

5. User provided equation based commercial software (COMSOL in our case) is able to solve combustion model equations of interest and can be applied to quantify the effect of diffusive processes, such as capillary diffusion, thermal conductivity and molecular diffusion. We used this software to obtain a numerical solution for comparison with an analytical solution in a zero diffusion model obtained previously, one/two-component oil models including volatile and non-volatile components, and a one-component oil model including water. We used this software to obtain a numerical solution for comparison with analytical solutions in zero diffusion models obtained previously. The qualitative behavior of the numerical solution is similar to the analytical solution in the absence of diffusive processes. The solution consists of three types of waves, i.e., a thermal wave, an MTO wave and a saturation waves separated by constant state regions. The numerical model is capable to quantify the effect of the diffusive processes, oil composition, pressure, injection rates and presence of water. The central scheme used in the finite element package, makes it possible to model situations both for low and high diffusion coefficients. The

effect of the diffusive terms is as follows. Molecular diffusion lowers the temperature in the MTO region, but creates a small peak in the vaporization region. Capillary diffusion increases the temperature upstream of the MTO region. Higher capillary diffusion increases the recovery by gas displacement and lowers the recovery by combustion. The analytical solution, without diffusive terms, and the numerical solution become qualitatively different at very high capillary diffusion coefficients. The effect of thermal diffusion smoothes the thermal wave and widens the hydrocarbon vapor peak.

6. Experiments can validate various aspects of the developed models: A set of experiments have been designed that enables investigation of the medium pressure air injection process at low injection rate in consolidated porous media saturated with oil [67, 54]. The experiments used hexadecane. Our laboratory experiments indicate recoveries between $75 - 90\%$. Sufficient fuel is available to consume the injected oxygen, and only 0.5% of oxygen was found in the produced gas. The experiments show that an oxygen adsorption step takes place at low temperatures in the initial stage before the bond-scission combustion reactions occur. The sorbed oxygen bonds with hydrocarbon physically or chemically leading to complete uptake of oxygen from the injected air stream at low temperatures. Then the oxygen containing compound releases the oxygen at higher temperatures and partially reconverts to hexadecane, which is later produced, and partially undergoes a combustion reaction releasing carbon oxides and possibly also water. The produced liquid is hexadecane; it is not altered by an oxidation reaction because it has the same viscosity and density. It is recalled that oxygenated hydrocarbons have higher viscosities [68].

A. Diffusion flux

Here we derive Eqs (3.10), (A.0.4) and (A.0.6). Due to diffusion, the light component velocity and the medium component velocity will be different in the fluid system. Since Darcy's velocity is a volume averaged velocity, diffusion flux of the light molecules and the medium molecules should be defined with respect to the volume averaged velocity.

The averaged velocity v_o is related to the Darcy velocity u_o by following equation

$$v_o = \frac{u_o}{\varphi S_o}. \tag{A.0.1}$$

The diffusive flux for each component with respect to the volume averaged velocity v_o can be written as follows ([19])

$$j_l = \frac{\rho_{ol}}{\rho_L}\left(v_{ol} - v_o\right), \quad j_m = \frac{\rho_{om}}{\rho_M}\left(v_{om} - v_o\right). \tag{A.0.2}$$

where j_κ defines the volume flux of component κ. Here u_{om} is defined as $u_{om} = \varphi s_o \psi_m v_{om}$, where v_{om} is the interstitial velocity of the medium component. Defined in this way indeed u_{om} (u_{ol}) is a volume flux of medium (light) component. The Darcy velocity for medium component v_{oh} is calculated as $v_{oh}\psi_h\varphi S_o$ because it is volume based, the volume fraction needs to be included. Here $\rho_{ol} = X_l\rho_o$ is the molar concentration of the light oil, whereas ρ_L is the molar density of the pure light oil. In the same way we use $\rho_{om} = X_m\rho_o$ as the molar concentration of the medium oil, whereas ρ_M is the molar density of the pure medium oil. Using these definitions we also notice that the volume fraction of the medium component is $\psi_m = \rho_{om}/\rho_M$ while the volume fraction of the light component is $\psi_l = \rho_{ol}/\rho_L$. Here ρ_L and ρ_M mean the density of pure light and medium oil respectively. The flux with respect to the volume averaged velocity can be expressed as ([19])

$$j_m = -D\nabla\psi_m, \quad j_l = -D\nabla\psi_l.$$

Hence we end up with following expression which includes the diffusion for the component velocity in a phase

$$\rho_M u_{om} = \rho_{om} u_o - \varphi S_o D \rho_M \nabla \psi_m, \quad \rho_L u_{ol} = \rho_{ol} u_o - \varphi S_o D \rho_L \nabla \psi_l. \tag{A.0.3}$$

Dividing these equation by the pure density of the components we obtain

$$u_{om} = \psi_m u_o - \varphi s_o D \nabla \psi_m, \quad u_{ol} = \psi_L u_o - \varphi s_o D \nabla \psi_l. \tag{A.0.4}$$

Adding these two equations we get

$$\begin{aligned} &u_{om} + u_{ol} = \psi_m u_o - \varphi s_o D \nabla \psi_m + \psi_l u_o - \varphi s_o D \nabla \psi_l \\ &\Rightarrow u_{om} + u_{ol} = u_o \left(\psi_m + \psi_l\right) - \varphi s_o D \nabla \left(\psi_m + \psi_l\right). \end{aligned}$$

The sum of the volume fractions is equal to one, so the Equation simplifies as

$$u_{om} + u_{ol} = u_o \left(1\right) - \varphi s_o D \nabla \left(1\right), \quad u_o = u_{om} + u_{ol}. \tag{A.0.5}$$

Therefore, the fluid velocity can be expressed as a function of volume fraction of the components and their density in the mixtures.

For the gas phase we circumvent all complexities related to three component mixtures (see, however, the Stefan-Maxwell equations in [19]) and assume that the total gas flux is given by

$$\begin{cases} \rho_\Lambda u_{gl} = \rho_{lg} u_g - \varphi s_g D_g \rho_\Lambda \nabla \psi_l \\ \rho_K u_{g\kappa} = \rho_\kappa u_g - \varphi s_g D_g \rho_K \nabla \psi_\kappa \\ \rho_R u_{gr} = \rho_r u_g - \varphi s_g D_g \rho_R \nabla \psi_r. \end{cases} \tag{A.0.6}$$

where we used the subscripts (l, Λ) for the fraction of hydrocarbon gas, (κ, K) for oxygen and (r, R) for the rest.

Bibliography

[1] Enhanced oil recovery scoping study, final report, no. tr-113836. *Electric Power Research Institute, Palo Alto, CA, http://www.energy.ca.gov*, 1999.

[2] Enhanced oil recovery, CO_2 injection. *United States Department of Energy, Washington, DC,http://energy.gov*, 2011.

[3] J. H. Abou-Kassem, S. M. Farouq Ali, and J. Ferrer. Appraisal of steamflood models. *Rev. Tec. Ing.*, 9:45–58, 1986.

[4] G. Adagulu and I. Akkutlu. Influence of in-situ fuel deposition on air injection and combustion processes. *Journal of Canadian Petroleum Technology*, 46(4), 2007.

[5] L. Adetunji and R. Teigland. Light-oil air-injection performance: sensitivity to critical parameters. In *SPE Annual Technical Conference and Exhibition*, volume SPE-96844, 2005.

[6] S. Akin, M.V. Kok, S. Bagci, and O. Karacan. Oxidation of heavy oil and their SARA fractions: its role in modeling in-situ combustion. SPE 63230, 2000.

[7] J. Alexander, W. L. Martin, and J. Dew. Factors affecting fuel availability and composition during in situ combustion. *Journal of Petroleum Technology*, 14(10):1154–1164, 1962.

[8] A. V. Azevedo, A. J. deSouza, D. Marchesin, and B. Plohr. The solution by the wave curve method of three-phase flow in virgin reservoirs. *Transport in Porous Media*, 83(1):99–125, 2010.

[9] Tayfun Babadagli. Mature field development-a review. In *SPE Europec/EAGE Annual Conference*. Society of Petroleum Engineers, 2005.

[10] A. Bakry, A. Al-Salaymeh, A.H. Al-Muhtaseb, A. Abu-Jrai, and D. Trimis. Adiabatic premixed combustion in a gaseous fuel porous inert media under high pressure and temperature: Novel flame stabilization technique. *Fuel*, 90(2):647–658, 2011.

[11] C.H. Bamford and C.E.H. Tipper. *Comprehensive Chemical Kinetics, Vol. 17, Gas-phase Combustion*. Elsevier, 1977.

[12] Y. Barzin, R. Moore, S. Mehta, D. Mallory, M. Ursenbach, and F. Tabasinejad. Role of vapor phase in oxidation/combustion kinetics of high-pressure air injection (HPAI). In *SPE 135641*, 2010.

[13] Y. Barzin, R. Moore, S. Mehta, M. Ursenbach, and F. Tabasinejad. Impact of Distillation on the Combustion Kinetics of high pressure air injection (HPAI). In *SPE 129691-Improved Oil Recovery Symposium*, 2010.

[14] Yalda Barzin, Robert Moore, Sudarshan Mehta, Matthew Ursenbach, and Farshad Tabasinejad. Effect of interstitial water saturation and air flux on combustion kinetics of high pressure air injection (HPAI). In *SPE Western Regional Meeting*, 2010.

[15] Rubin Battino, Timothy R Rettich, and Toshihiro Tominaga. The solubility of oxygen and ozone in liquids. *Journal of physical and chemical reference data*, 12(2):163–178, 1983.

[16] A. Bayliss and B.J. Matkowsky. From traveling waves to chaos in combustion. *SIAM J. Appl. Math.*, 54:147–174, 1994.

[17] J. Bear. *Dynamics of Fluids in Porous Media*. Dover Publications, Inc., Dover, 1972.

[18] J.D.M. Belgrave and R.G. Moore. A model for improved analysis of in-situ combustion tube tests. *Journal of Petroleum Science and Engineering*, 8(2):75–88, 1992.

[19] R.B. Bird, W.E. Stewart, and E.N. Lightfoot. Transport Phenomena, 2002.

[20] Martin Blunt, F John Fayers, and Franklin M Orr Jr. Carbon dioxide in enhanced oil recovery. *Energy Conversion and Management*, 34(9):1197–1204, 1993.

[21] R. H. Brooks, M. Corey, and M. Asce. Properties of porous media affecting fluid flow. *J. Irrigation and Drainage Division*, 92:61–88, 1966.

[22] J. Bruining and C. J. van Duijn. Traveling waves in a finite condensation rate model for steam injection. *Computational Geosciences*, 10(4):373–387, 2006.

[23] J. Bruining, A.A. Mailybaev, and D. Marchesin. Filtration combustion in wet porous medium. *SIAM J. Appl. Math.*, 70:1157–1177, 2009.

[24] J Bruining and D Marchesin. Maximal oil recovery by simultaneous condensation of alkane and steam. *Physical Review E*, 75(3):036312, 2007.

[25] L.M. Castanier and W.E. Brigham. Modifying in-situ combustion with metallic additives. *In Situ*, 21(1):27–45, 1997.

[26] L.M. Castanier and W.E. Brigham. Upgrading of crude oil via in situ combustion. *Journal of Petroleum Science and Engineering*, 39:125–136, 2003.

[27] Zhenya Chen, Lei Wang, Qiong Duan, Liang Zhang, and Shaoran Ren. High-pressure air injection for improved oil recovery: low-temperature oxidation models and thermal effect. *Energy & Fuels*, 27(2):780–786, 2013.

[28] C. Clara, M. Durandeau, G. Quenault, and T.H. Nguyen. Laboratory studies for light-oil air injection projects: potential application in handil field. *SPE Reservoir Evaluation & Engineering*, 3(3):239–248, 2000.

[29] M. Dabbous and P. Fulton. Low-temperature-oxidation reaction kinetics and effects on the in-situ combustion process. *Old SPE Journal*, 14(3):253–262, 1974.

[30] A. De Zwart, D. van Batenburg, C. Blom, A. Tsolakidis, C. Glandt, and P. Boerrigter. The modeling challenge of high pressure air injection, 20-23 April 2008.

[31] D.N. Dietz and J. Weijdema. Wet and partially quenched combustion. *Journal of Petroleum Technology*, 20:411–415, 1968.

[32] M. Duiveman, H. Herwin, and P. Grivot. Integrated management of water, lean gas and air injection: the successful ingredients to ior projects on the mature handil field. In *SPE Asia Pacific Oil and Gas Conference and Exhibition*, 2005.

[33] A.A. Eftekhari, H. Van Der Kooi, and J. Bruining. Exergy analysis of underground coal gasification with simultaneous storage of carbon dioxide. *Energy*, 45(1):729–745, 2012.

[34] M. Fassihi, W. Brigham, and H. Ramey Jr. Reaction kinetics of in-situ combustion: Part 1-observations. *Old SPE Journal*, 24(4):399–407, 1984.

[35] M.R. Fassihi, D.V. Yannimaras, and V.K. Kumar. Estimation of recovery factor in light-oil air-injection projects. *SPE Reservoir Engineering*, 12:173–178, 1997.

[36] M.R. Fassihi, D.V. Yannimaras, E.E. Westfall, and T.H. Gillham. Economics of light oil air injection projects. In *SPE/DOE Improved Oil Recovery Symposium*, 1996.

[37] W. Fickett and W.C. Davis. *Detonation: Theory and Experiment*. Dover, Mineola, N.Y., 2011.

[38] E.M. Fisher, W.J. Pitz, H.J. Curran, and C.K. Westbrook. Detailed chemical kinetic mechanisms for combustion of oxygenated fuels. *Proceedings of the Combustion Institute*, 28(2):1579–1586, 2000.

[39] N.P. Freitag and B. Verkoczy. Low-temperature oxidation of oils in terms of SARA fractions: why simple reaction models don't work. *Journal of Canadian Petroleum Technology*, 44(3):54–61, 2005.

[40] P. Germain and J.L. Geyelin. Air injection into a light oil reservoir: the Horse Creek project. In *Middle East Oil Show and Conference, Bahrain*, 15-18 March 1997.

[41] M. Gerritsen, A. Kovscek, L. Castanier, J. Nilsson, R. Younis, and B. He. Experimental investigation and high resolution simulator of in-situ combustion processes; 1. simulator design and improved combustion with metallic additives. In *SPE International Thermal Operations and Heavy Oil Symposium and Western Regional Meeting*, 2004.

[42] T.H. Gillham, B.W. Cerveny, M.A. Fornea, and D. Bassiouni. Low cost IOR: an update on the W. Hackberry air injection project. In *Paper SPE-39642 presented at the SPE/DOE Improved Oil Recovery Symposium, Tulsa, Oklahoma, April, 19–22*, 1998.

[43] T.H. Gillham, B.W. Cerveny, E.A. Turek, and D.V. Yannimaras. Keys to increasing production via air injection in Gulf Coast light oil reservoirs. In *SPE Annual Technical Conference and Exhibition, SPE 38848-MS*, 1997.

[44] M. Greaves, S. Ren, R. Rathbone, T. Fishlock, and R. Ireland. Improved residual light oil recovery by air injection (LTO process). *Journal of Canadian Petroleum Technology*, 39(1), 2000.

[45] M. Greaves, T.J. Young, S. El-Usta, R.R. Rathbone, S.R. Ren, and T.X. Xia. Air injection into light and medium heavy oil reservoirs: combustion tube studies on west of Shetlands Clair oil and light Australian oil. *Chemical Engineering Research and Design*, 78(5):721–730, 2000.

[46] D. Gutierrez, F. Skoreyko, R. Moore, S. Mehta, and M. Ursenbach. The challenge of predicting field performance of air injection projects based on laboratory and numerical modelling. *Journal of Canadian Petroleum Technology*, 48(4):23–33, 2009.

[47] D. Gutierrez, A. Taylor, V. Kumar, M. Ursenbach, R. Moore, and S. Mehta. Recovery factors in high-pressure air injection projects revisited. *SPE Reservoir Evaluation & Engineering*, 11(6):1097–1106, 2008.

[48] W.C. Hardy, P.B. Fletcher, J.C. Shepard, E.W. Dittman, and D.W. Zadow. In-situ combustion in a thin reservoir containing high-gravity oil. *J. of Petroleum Technology*, 24(2):199–208, 1972.

[49] F.G. Helfferich. *Kinetics of Multistep Reactions*. Elsevier, 2004.

[50] http://www.worldenergyoutlook.org. International enegry agancy (IEA).

[51] Lu-Kwang Ju and Chester S Ho. Oxygen diffusion coefficient and solubility in n-hexadecane. *Biotechnology and bioengineering*, 34(9):1221–1224, 1989.

[52] J.U. Keller and R. Staudt. *Gas Adsorption Equilibria: Experimental Methods and Adsorptive Isotherms*. Springer, 2005.

[53] N. Khoshnevis Gargar, N. Achterbergh, S. Rudolph-Flöter, and H. Bruining. In-Situ oil combustion: processes perpendicular to the main gas flow direction. In *SPE Annual Technical Conference and Exhibition*, volume SPE 134655-MS, 2010.

[54] N. Khoshnevis Gargar, A.A. Mailybaev, J. Bruining, and D. Marchesin. Compositional effects in light oil recovery by air injection: Vaporization vs. combustion. *Accepted in Journal of Porous Media*, 2013.

[55] N. Khoshnevis Gargar, A.A. Mailybaev, J. Bruining, and D. Marchesin. Diffusive effects on recovery of light oil by medium temperature oxidation. *Accepted in Transport in Porous Media*, 2013.

[56] M.V. Kok and C.O. Karacan. Behavior and effect of SARA fractions of oil during combustion. *SPE Reservoir Evaluation and Engineering*, 3:380–385, 2000.

[57] EJ Koval. A method for predicting the performance of unstable miscible displacement in heterogeneous media. *Old SPE Journal*, 3(2):145–154, 1963.

[58] A.G. Kulikovskii and N.T. Pashchenko. Propagation regimes of self-supported light-detonation waves. *Fluid Dynamics*, 40(5):818–828, 2005.

[59] V. Kumar, D. Gutierrez, B.P. Thies, and C. Cantrell. Thirty years of successful high-pressure air injection: performance evaluation of Buffalo field, south Dakota. In *SPE Annual Technical Conference and Exhibition*, volume SPE 133494-MS, 2010.

[60] O. Levenspiel. *Chemical reaction engineering*. John Wiley & Sons, 1999.

[61] J. Li, S. Mehta, R. Moore, M. Ursenbach, E. Zalewski, H. Ferguson, and N. Okazawa. Oxidation and ignition behaviour of saturated hydrocarbon samples with crude oils using TG/DTG and DTA thermal analysis techniques. *Journal of Canadian Petroleum Technology*, 43(7), 2004.

[62] C.Y. Lin, W.H. Chen, and W.E. Culham. New kinetic models for thermal cracking of crude oils in in-situ combustion processes. *SPE Reservoir Engineering*, 2:54–66, 1987.

[63] C.Y. Lin, W.H. Chen, S.T. Lee, and W.E. Culham. Numerical simulation of combustion tube experiments and the associated kinetics of in-situ combustion processes. *SPE Journal*, 24:657–666, 1984.

[64] A.A. Mailybaev, J. Bruining, and D. Marchesin. Analysis of in situ combustion of oil with pyrolysis and vaporization. *Combustion and Flame*, 158(6):1097–1108, 2011.

[65] A.A Mailybaev, J. Bruining, and D. Marchesin. Analytical formulas for in-situ combustion. *SPE Journal*, 16(03):513–523, 2011.

[66] A.A. Mailybaev, D. Marchesin, and J. Bruining. Resonance in low-temperature oxidation waves for porous media. *SIAM Journal on Mathematical Analysis*, 43:2230, 2011.

[67] A.A. Mailybaev, D. Marchesin, and J. Bruining. Recovery of light oil by medium temperature oxidation. *Transport in Porous Media*, 97(3):317–343, 2013.

[68] DD Mamora. New findings in low-temperature oxidation of crude oil. In *SPE Asia Pacific Oil and Gas Conference*, 1995.

[69] D. Marchesin and B.J. Plohr. Wave structure in WAG recovery. SPEJ. 6 (2): 209-219. Technical report, SPE-71314-PA, 2001.

[70] EC Markham and Arthur F Benton. The adsorption of gas mixtures by silica. *Journal of the American Chemical Society*, 53(2):497–507, 1931.

[71] B.J. Matkowsky and G. Sivashinsky. Propagation of a pulsating reaction front in solid fuel combustion. *SIAM J. Appl. Math.*, 35:465–478, 1978.

[72] A.R. Montes, D. Gutierrez, R.G. Moore, S.A. Mehta, and M.G. Ursenbach. Is high-pressure air injection (HPAI) simply a flue-gas flood? *Journal of Canadian Petroleum Technology*, 49(2):56–63, 2010.

[73] O.A. Oleinik. Construction of a generalized solution of the cauchy problem for a quasi-linear equation of first order by the introduction of vanishing viscosity. *Uspekhi Matematicheskikh Nauk*, 14(2):159–164, 1959.

[74] Mario Pascual, D Crosta, P Lacentre, and D Coombe. Air injection into a mature waterflooded light oil reservoir–laboratory and simulation results for Barrancas field, Argentina (SPE94092). In *67th EAGE Conference & Exhibition*, 2005.

[75] D.W. Peaceman. *Fundamentals of Numerical Reservoir Simulation*, volume 6. Elsevier, 1977.

[76] F.M. Pereira, A.A.M. Oliveira, and F.F. Fachini. Asymptotic analysis of stationary adiabatic premixed flames in porous inert media. *Combustion and Flame*, 156(1):152–165, 2009.

[77] B.E. Poling, J.M. Prausnitz, O.C. John Paul, and R.C. Reid. *The Properties of Gases and Liquids*. McGraw-Hill, New York, 2001.

[78] I. Prigogine. Introduction to Non-equilibrium Thermodynamics. *Jonh Wiley & Sons, NY*, 1962.

[79] S.R. Ren, M. Greaves, and R.R. Rathbone. Air injection LTO process: an IOR technique for light-oil reservoirs. *SPE Journal*, 7(1):90–99, 2002.

[80] J. Sanmiguel, D. Mallory, S. Mehta, and R. Moore. Formation heat treatment process by combustion of gases around the wellbore. *Journal of Canadian Petroleum Technology*, 41(8), 2002.

[81] G.L. Schott. Kinetic studies of hydroxyl radicals in shock waves. iii. the OH concentration maximum in the hydrogen-oxygen reaction. *The Journal of Chemical Physics*, 32:710, 1960.

[82] D.A. Schult, B.J. Matkowsky, V.A. Volpert, and A.C. Fernandez-Pello. Forced forward smolder combustion. *Combustion and Flame*, 104:1–26, 1996.

[83] W. Schulte. Challenges and strategy for increased oil recovery. In *International Petroleum Technology Conference*, 2005.

[84] G.J. Sharpe and S. Falle. One-dimensional nonlinear stability of pathological detonations. *Journal of Fluid Mechanics*, 414(1):339–366, 2000.

[85] A.T. Turta and A.K. Singhal. Reservoir engineering aspects of light-oil recovery by air injection. *SPE Reservoir Evaluation & Engineering*, 4(4):336–344, 2001.

[86] D.U. Von Rosenberg. *Methods for the numerical solution of partial differential equations*, volume 16. Society of Petroleum Engineers, 1969.

[87] JR Waggoner, JL Castillo, Larry W Lake, et al. Simulation of EOR processes in stochastically generated permeable media. *SPE formation evaluation*, 7(02):173–180, 1992.

[88] C.W. Wahle, B.J. Matkowsky, and A.P. Aldushin. Effects of gas-solid nonequilibrium in filtration combustion. *Combust. Sci. and Tech.*, 175:1389–1499, 2003.

[89] H.J. Welge. A simplified method for computing oil recovery by gas or water drive. *Transactions of AIME*, 195:91–98, 1952.

[90] G.B. Whitham. Non-linear dispersion of water waves. *Journal of Fluid Mechanics*, 27(02):399–412, 1967.

[91] G.B. Whitham. *Linear and Nonlinear Waves*, volume 42. Wiley-interscience, 2011.

[92] W.W. Wood and Z.W. Salsburg. Analysis of steady-state supported one-dimensional detonations and shocks. *Physics of Fluids*, 3:549–566, 1960.

[93] Z. Xu, L. Jianyi, S. Liangtian, L. Shilun, and L. Weihua. Research on the mechanisms of enhancing recovery of light-oil reservoir by air-injected low-temperature oxidation technique. *Natural Gas Industry*, 24:78–80, 2004.

[94] DV Yannimaras and DL Tiffin. Screening of oils for in-situ combustion at reservoir conditions via accelerating rate calorimetry. *SPE Reservoir Engineering*, 10(1):36–39, 1995.

[95] C.H. Zheng, L.M. Cheng, T. Li, Z.Y. Luo, and K.F. Cen. Filtration combustion characteristics of low calorific gas in sic foams. *Fuel*, 89(9):2331–2337, 2010.

Summary

Using conventional production methods, recovery percentages from oil reservoirs range from 5% for difficult oil to 50% for light oil in highly permeable homogeneous reservoirs. To increase the oil recovery factor, enhanced oil recovery (EOR) methods are used. We distinguish EOR that uses chemical methods, (partially) miscible methods and thermal methods. Air injection is categorized as a thermal recovery method as it leads to combustion and therefore high temperature in the reservoir. However, many oil recovery mechanisms are involved in air injection process, including sweeping by flue gases, field re-pressurization by the injected gas, oil swelling, oil viscosity reduction, stripping off light components in the oil by flue gas and thermal effects generated by the oxidation reactions. Our interest is in recovering light oil from low permeability heterogeneous reservoirs using air injection leading to oil combustion, as the heated oil vaporizes away from the lower permeability parts to be collected in the higher permeability streaks. Due to simultaneous vaporization, the combustion at medium pressures, i.e., at medium depth, occurs at medium temperatures.

Our focus is on air injection at medium pressures ($\sim 10-90$ bars) to reduce the high compression costs and to avoid fracturing at shallower depth. We study this process at low air injection rates to mimic the processes in the main reaction zone (away from the injection well) in an oil reservoir, which provides a long residence time for the oxygen to be in contact with the oil. The main recovery mechanism that we consider for medium pressures is the interaction between vaporization and combustion of light oil. In the thesis, we consider exclusively modeling and simulation of air injection in light oil leading to medium temperature oxidation (MTO). In MTO, all physical processes, reaction, vaporization, condensation and filtration, are active. The main purpose of the thesis is to elucidate the prevailing mechanisms in MTO. Therefore we developed a 1-D model considering light oil recovery through displacement by air at medium pressures and low injection rates and performed both numerical and laboratory experiments to validate the MTO concept. The presence of liquid fuel, which is mobile and can vaporize or condense, is a challenge for modeling of the combustion process. We only consider the one dimensional flow problem, expecting that its solution contributes to understanding the MTO process and determine the displacement efficiency. The detailed mechanism depends on diffusive processes (capillary, molecular diffusion and heat conductivity), oil composition, air injection rate, pressure, and the presence of reaction water and initial water saturation. Each chapter is summarized as follows:

In Chapter 2, the modeling and simulation of the MTO process are exclusively studied including mass-, thermal and capillary-diffusion for air injection in light oil reservoirs. In this case, we consider only single pseudo-component oil, e.g., heptane as liquid fuel in dry porous rock, to improve the understanding of the oxidation/vaporization/condensation mechanisms. It turns out that the oxidation, vaporization and condensation often occur close to each other and move with the same speed in the porous medium (resonant structure). The temperature variation is bounded by the oil boiling temperature and thus not very large. We analyze the effect of capillary pressure, heat conductivity and diffusion and compare the results with the analytical solution in the absence of diffusion processes. The numerical simulation results and the analytical results with zero diffusion processes show qualitatively similar behavior. The solution consists of three types of waves, i.e., a thermal wave, an MTO wave and saturation waves separated by constant state regions. The effect of the diffusive terms is as follows. Molecular diffusion lowers the temperature in the MTO region, but creates a small peak in the vaporization region. Capillary diffusion increases the temperature upstream of the MTO region. Higher capillary diffusion increases the recovery by gas displacement and leaves less oil for combustion. The analytical solution, without diffusive terms, and the numerical solution become qualitatively different at very high capillary diffusion coefficients. The effect of thermal diffusion smoothes the thermal wave and widens the hydrocarbon vapor region.

In Chapter 3, we extended 1-D model involving a two-component oil mixture, e.g., light and medium oils as pseudo-components in dry porous rock. The light component (heptane) both vaporizes and combusts, whereas medium fraction in the oil mixture only reacts with oxygen, but its vaporization is disregarded. It was anticipated that at increasing medium oil content the nature of the combustion process would change from MTO to high temperature oxidation (HTO). The main discerning factor in the MTO combustion process is the ratio between vaporization and combustion in the low injection rate regime. It turns out that also with the two-component mixture, oxidation, vaporization and condensation often occur close to each other in the MTO wave. The character of the MTO wave changes by altering the composition of the oil. Vaporization occurs upstream of the combustion process when oil mixture is composed of a higher fraction of light component. This fact confirms previously obtained analytical and numerical solutions for one component volatile oil. The combustion front velocity is high as less oil remains behind in the combustion zone. Whereas, for a predominantly medium oil mixture (0.8 of medium component fraction in volume fraction), the vaporization moves downstream of the combustion zone in the MTO wave. As more oil stays behind in the combustion zone, the velocity of the combustion zone is slower, albeit that the temperatures are much higher. Due to high temperatures, we conjecture a transition to the HTO process in this case. To summarize, numerical calculations establish a range of parameters for the bifurcation point between MTO and HTO in a two-component oil mixture. Indeed, the bifurcation point is mainly determined by the fraction of the

non-volatile component. At the bifurcation the character of the combustion process changes from a vaporization-dominated (MTO) to a combustion-dominated process (HTO).

In Chapter 4, we investigate the effects of water on the oxidation/vaporization/ condensation mechanisms in the MTO wave by considering a simple three phase model involving a one-component oil (e.g., heptane, pentane or dodecane) and water in porous rock. The single pseudo-component oil vaporizes/condenses as well as combusts, whereas water only vaporizes and condenses. It was anticipated that only if the boiling point of oil is around or modestly higher (below 200^oC) than the boiling point of water, the presence of water is conducive to higher and faster oil recovery. The main emphasis of this Chapter is to investigate the relative importance of steam condensation, vaporization/condensation of oil and combustion in the low injection rate regime. The numerical solution consists of a thermal wave, a steam condensation front coinciding with or downstream of the medium temperature oxidation (MTO) wave (oil vaporization and combustion), and a three-phase saturation wave region involving oil, gas and water. Numerical calculations show that the presence of water makes the light oil recovery more efficient and faster and diminishes the adverse effect of high oil boiling points. When the boiling point of the volatile oil is about or slightly higher than the boiling point of water, the speed of the MTO wave (oil vaporization/combustion front) is equal to the speed of the steam condensation front. The volatile oil condenses at the same location as the steam, which leads to complete oil recovery. However, when the boiling point of the oil is much higher than the boiling point of water, the steam condensation front moves ahead of the MTO wave. Numerical calculations make it possible to estimate the bifurcation point (oil-boiling point) at which a solution for which steam condensation and combustion occur simultaneously changes to a solution where the steam condenses downstream of the combustion zone. We show that replacing the medium boiling volatile oil by a high boiling point oil (e.g., dodecane) decreases the MTO wave speed with respect to the steam condensation front and leads to delayed recovery.

In Chapter 5, a set of experiments have been designed that enables investigation of the medium pressure air injection process at low injection rate in consolidated porous media saturated with one-component oil in a ramped temperature reactor. The initial aim of the laboratory experiments was to validate various aspects considered in Chapters 2-4. The experiments were carried out to evaluate the mechanisms of the combustion reaction at different pressures and injection rates. At slower rates we expect to see details that are not visible for the experiments operating at high rates and high pressures. The most important aspect in this Chapter was to observe that an oxygen sorption step takes place at low temperatures prior to the full combustion reaction. The mechanism of initial uptake of oxygen for later release was established in this work. The sorbed oxygen bonds with hydrocarbon physically or chemically leading to complete uptake of oxygen from the injected air stream at low temperatures. At a later stage, the compound, which contains the chemically or physically adsorbed oxygen, desorbs the oxygen and further undergoes

oxidation reactions to produce CO and CO_2. The produced liquid is hexadecane; it is not altered by an oxidation reaction because it has the same viscosity and density, which argues against chemisorption. The laboratory experiments indicate displacement efficiencies between $75-90\%$ of the Oil Initially In Place. The amount of oil burned in the air injection process relative to the amount of oil recovered in our laboratory experiments for hexadecane increased from 2% at 10 bar to 18% at 30 bar, and again decreased to 5% at 45 bar, after which it more or less remained constant. This trend was previously obtained by the analytical results of medium temperature oxidation process. It was also shown that the oil recovery is faster at higher pressures.

Samenvatting

Bij gebruik van conventionele methoden, bedragen de winningspercentages uit oliereservoirs tussen de 5% voor moeilijke olie en 50% voor lichte olie in hoog permeabele homogene reservoirs. Om de winningsfactor te verbeteren gebruikt men verbeterde oliewinningstechnieken (EOR). We onderscheiden EOR methoden die gebruik maken van chemische methoden, gedeeltelijk mengbare methoden en thermische methoden. Luchtinjectie wordt gerekend tot de thermische methoden omdat het tot verbranding leidt en daarmee tot hoge temperaturen in het reservoir. Echter er zijn veel winningsmechanismen betrokken bij het luchtinjectieproces waaronder verdringing door rookgassen, het op druk brengen van het reservoir, oliezwelling, viscositeitsverlaging, verwijdering van lichte componenten door rookgassen en thermische effecten als gevolg van de oxidatiereacties. Onze belangstelling is gericht op winning van lichte olie uit laag permeabele heterogene oliereservoirs door luchtinjectie, die leidt tot olieverbranding, waarbij de moeilijk toegankelijke olie weg-dampt uit de laag permeabele gedeeltes en alsnog wordt gewonnen via de hoog permeabele gedeeltes. Door gelijktijdige verdamping, treedt verbranding bij middelgrote drukken, d.w.z., op middelgrote dieptes, bij middelhoge temperaturen op.

Onze aandacht gaat uit naar luchtinjectie bij middelgrote drukken ($\sim 10 - 90$ bar) om de samendrukkingskosten te verminderen en om breukvorming op minder grote diepte te voorkomen. Wij bestuderen dit proces bij lage injectiesnelheden om de processen in de belangrijkste reactiezone (ver weg van de put in het reservoir) na te bootsen; dit leidt tot lange verblijftijden voor zuurstof in contact met olie. Het belangrijkste winningsmechanisme dat we voor deze middelgrote drukken beschouwen is de wisselwerking tussen verdamping en verbranding voor lichte olie. In het proefschrift beschouwen we louter en alleen modelleren en simuleren van luchtinjectie voor middelhoge temperatuur oxidatie (MTO). In MTO zijn alle fysische processen, d.w.z., reactie, verdamping, condensatie en filtratie, actief. Het voornaamste doel van het proefschrift is om de voornaamste mechanismen in MTO te verhelderen. Daarom hebben wij een 1-D model ontwikkeld dat winning van lichte olie beschouwt door verdringing met lucht bij middelgrote drukken en lage injectiesnelheden en voerden hiervoor zowel numerieke berekeningen en laboratorium experimenten uit om het MTO concept te staven. De aanwezigheid van vloeibare brandstof die mobiel is en kan verdampen en condenseren is een uitdaging voor het modelleren van het verbrandingsproces. We beschouwen alleen het eendimensionale stromingsprobleem met de gedachte dat de oplossing hiervan bijdraagt aan het begrip van het MTO proces en de verdringings-efficiëntie kan bepalen. Het gedetailleerde mechanisme hangt af van diffusieachtige processen (capillaire, moleculaire diffusie en warmtegeleiding),

oliesamenstelling, luchtinjectiesnelheid, druk, en de aanwezigheid van reactiewater en een initiële water saturatie. Elk hoofdstuk wordt hierna kort samengevat:

In Hoofdstuk 2 worden louter en alleen het modeleren en het simuleren van het MTO proces bestudeerd, daarbij inbegrepen de massa-, thermische- en capillaire diffusie. In dit geval beschouwen slechts een pseudocomponent, bijvoorbeeld heptaan als vloeibare brandstof in droog poreus gesteente, om het begrip van de oxidatie/ verdamping/ condensatie mechanismen te vergroten. Het blijkt dat de oxidatie/ verdamping / condensatie vaak dicht bij elkaar optreedt en met dezelfde snelheid door het poreuze medium beweegt (resonantiestructuur). De temperatuur-variatie wordt begrensd door het kookpunt van olie en is dis niet erg hoog. We analyseren het effect van capillaire druk, warmte geleiding, en moleculaire diffusie en vergelijken de resultaten met de analytische oplossing in de afwezigheid van diffusieachtige processen. De numerieke simulatieresultaten met diffusie en de analytische resultaten in afwezigheid van diffusie laten een kwalitatief vergelijkbaar gedrag zien. De oplossing bestaat uit drie typen golven, d.w.z., een thermische golf, een MTO golf en saturatie golven, die van elkaar gescheiden zijn door gebieden waarin de afhankelijk variabelen constant zijn. Het effect van de diffusie termen is als volgt. Moleculaire diffusie verlaagt de temperatuur in het MTO gebied, maar veroorzaakt een kleine piek in het verdampingsgebied. Capillaire diffusie verhoogt de temperatuur bovenstrooms van het MTO gebied. Een hogere capillaire diffusie vergroot de winning door gasverdringing en laat minder olie achter voor verbranding. De analytische oplossing zonder diffusieachtige termen en de numerieke oplossingen met diffusie worden kwalitatief verschillend bij hoge capillaire diffusie coëfficiënten. Thermische diffusie maakt de thermische golf gladder en maakt het verdampingsgebied breder.

In hoofdstuk 3 hebben we het 1-D model uitgebreid met een oliemengsel dat bestaat uit twee-componenten, d.w.z. , een lichte en middelzware olie als pseudo componenten in een droog en poreus gesteente. De lichte component (heptaan) verdampt en verbrandt terwijl de middelzware fractie in het oliemengsel alleen met zuurstof reageert zonder verdamping te beschouwen. Het werd voorzien dat een verhoogd aandeel van de middelzware fractie het karakter van de verbranding van MTO naar HTO (hoge temperatuur oxidatie) zal veranderen. De voornaamste onderscheidende factor in MTO verbranding is de verhouding tussen verdamping en verbranding bij lage injectiesnelheid. Het blijkt dat ook met het twee-componenten mengsel, oxidatie, verdamping en condensatie in de MTO golf vlak bij elkaar plaatsvinden. Het karakter van de MTO golf verandert door de samenstelling van olie te wijzigen. Verdamping treedt bovenstrooms op wanneer de olie is samengesteld uit een hogere fractie van de lichte component. Dit feit bevestigt eerder verkregen analytische en numerieke oplossingen voor vluchtige olie met één component. De verbrandingssnelheid is hoog omdat er minder olie in de verbrandingszone achterblijft. Echter voor een voornamelijk middelzwaar oliemengsel (80 v/v% van de middelzware component), beweegt de verdamping benedenstrooms van de verbrandingszone in de MTO golf. Omdat er meer olie achterblijft, is de snelheid van de verbrandingszone lager, hoewel de temperaturen veel hoger zijn. Door de hoge temperaturen vermoe-

den wij in dit geval een overgang naar het HTO proces. Samengevat: numerieke berekeningen bepalen een verzameling parameter waardes voor het bifurcatiepunt tussen MTO en HTO in een twee-componenten oliemengsel. Inderdaad, wordt het bifurcatiepunt voornamelijk bepaald door de niet vluchtige oliefractie. Op het bifurcatiepunt verandert het karakter van het door verdamping beheerst MTO proces naar het door verbranding gedomineerde HTO proces.

In hoofdstuk 4, onderzoeken we de effecten van water op de oxidatie/verbranding/ condensatie mechanismen in de MTO golf door een eenvoudig driefasen model te beschouwen met een gasfase, een oliefase (bijv. heptaan, pentaan, of dodecaan) en water in poreus gesteente. De olie die bestaat uit een enkele pseudocomponent die verdampt/ condenseert en verbrandt, terwijl water alleen maar verdampt/ condenseert. Het werd voorzien dat alleen wanneer het kookpunt van olie ongeveer gelijk of enigszins hoger (beneden 200^oC) is dan het kookpunt van water, de aanwezigheid van water bevorderlijk is voor hogere en snellere oliewinning. De belangrijkste nadruk van dit hoofdstuk is om het relatieve belang van stoom condensatie en de verdamping/ condensatie/ verbranding van olie te onderzoeken. De numerieke oplossing bestaat uit een thermische golf, een stoom condensatiefront dat samenvalt of benedenstrooms van de MTO golf (olieverdamping en verbranding) optreedt, en een driefasen (olie, gas en water) saturatiegolf. Numerieke berekeningen laten zien dat de aanwezigheid van water, winning van lichte olie efficiënter en sneller maakt en het negatieve effect van hoge kookpunten van olie verkleint. Wanneer het kookpunt van de vluchtige olie gelijk of iets hoger is dan het kookpunt van water, is de snelheid van de MTO golf (olieverdamping / verbrandingsfront) gelijk aan de snelheid van het stoom condensatiefront. De vluchtige olie condenseert op dezelfde plaats als de stoom, en dit leidt tot volledige winning van de olie. Echter als het kookpunt van de olie veel hoger is dan het kookpunt van water, beweegt het stoomcondensatiefront voor de MTO golf uit. Numerieke berekeningen maken het mogelijk het bifurcatiepunt (oliekookpunt) te schatten waarvoor een oplossing waar de stoomcondensatie en de verbranding tegelijkertijd gebeuren verandert in een oplossing waar de stoom benedenstrooms van de verbrandingszone condenseert. Wij laten zien dat vervanging van de vluchtige olie met een middelhoog kookpunt door een olie met een hoog kookpunt (dodecaan) de snelheid van de MTO golf vertraagt ten opzichte van het stoom condensatiefront en tot vertraagde winning leidt.

Hoofdstuk 5 beschrijft laboratorium onderzoek naar het middelhoge druk luchtinjectie proces in geconsolideerde poreuze media verzadigd met één component olie in een oplopende temperatuur reactor. Het oorspronkelijke doel van de laboratoriumexperimenten was om verschillende aspecten in Hoofdstukken $2-4$ te bevestigen. Daarom zijn de experimenten ontworpen om de mechanismen van de verbrandingsreactie bij verschillende drukken en injectiesnelheden te evalueren. Bij de lagere injectiesnelheden verwachtten wij details te zien die niet zichtbaar zijn bij experimenten waarbij hoge injectiesnelheden en drukken worden toegepast. Het bleek echter dat het belangrijkste aspect in dit hoofdstuk was dat de experimenten leidden tot de waarneming dat voor volledige verbranding er eerst een zuurstof adsorptie stap bij

lage temperatuur plaats heeft. Het mechanisme van de initiële opname van zuurstof om later weer te worden afgegeven werd door de laboratoriumexperimenten bevestigd. De geadsorbeerde zuurstof bindt fysisch met de koolwaterstof, wat bij lage temperatuur leidt tot volledige opname van zuurstof uit de gasstroom. In een later stadium desorbeert de verbinding die de fysisch geadsorbeerde zuurstof bevat en ondergaat verder oxidatiereacties die CO en CO_2 produceren. De initiële en geproduceerde vloeistof is hexadecaan, die niet is omgezet door een oxidatiereactie omdat hij dezelfde viscositeit en dichtheid heeft, wat tegen chemisorptie pleit. The laboratorium experimenten geven aan dat de verdringing-efficiëntie tussen de $75 - 90\%$ van de oorspronkelijk aanwezige olie bedraagt. De hoeveelheid verbrande olie ten opzichte van de gewonnen olie in onze laboratorium experimenten neemt toe van 2% bij 10 bar tot 18% bij 30 bar, waarna het weer afneemt tot 5% bij 45 bar waarna het min of meer constant blijft. Deze trend werd eerder verkregen in analytische model resultaten van het oxidatieproces bij middelhoge temperatuur. Men kan ook aantonen dat oliewinning sneller gaat bij hogere drukken.

Acknowledgments

It would not have been possible to write this doctoral thesis without the help and support of the people around me, to only some of whom it is possible to give particular mention here. I would like to take this chance to state my gratitude.

First and foremost, I have been very fortunate to start working under honorific supervision of Prof. Hans Bruining and Prof. Dan Marchesin since October 2011, which was a milestone in my third year of PhD. This thesis is the yield of that period. Hans, I would like to express my sincere gratitude to you for your enthusiasm, knowledge, encouragement, guidance, dedication, persistence and support during my research that has been invaluable and priceless on both an academic and a personal level. Dan, my sincere appreciation is reserved for your vision, encouragement, advise, carefulness in editing and seriousness that helped me to proceed through the doctorial program and complete my dissertation.

I also would like to thank Dr. Alexei Mailybaev for his invaluable assistance, collaboration, very helpful comments and suggestions. I appreciate Dr. Susanne Rudolph for her supervision and new ideas for the first two years of my PhD. I am also grateful to rest of the examination committee members: Prof. Pacelli Zitha, Prof. Cor van Kruijsdijk, Dr. Karl Heinz Wolf, Dr. Diederik van Batenburg for participating in my Ph.D. defence and giving valuable comments.

The experimental part of this thesis would certainly not have been possible without the help of Henk Van Asten. Henk, I truly appreciate for your professional assistance, technical expertise and support for carrying out the difficult and novel combustion experiments here in Dietz lab. I truly enjoyed working with you. I would like to appreciate Dr. Karl Heinz Wolf for being positive, friendly and supportive during the difficult times in the lab. I would also thank to other technicians who were helping me, "Dick, Ellen, Jan, Jolanda, Karel, Marc, Micheil, and Wim" in Dietz Lab. My special thanks go to the secretaries and administrative side of Geoscience and Engineering department, Anke, Asha, Hannie, Lydia, Margot, Marja, Marijk, Marlijn and Ralf for their welcoming support and help with administrative works from the first day of my PhD. Hannie, thanks a lot for being always friendly and supportive. Lydia, Margot, and Marlijn, thanks for your consideration and kindness.

I would like to thank all my friends all around the world and also my colleagues of Petroleum engineering section, Geoscience and Engineering department that I shared good and memorable moments with them. I apologize that I did not mention them one by one, because I may forgot a name. In particular, I would like to mention my

close friend Rooja, who has gone above and beyond in terms of friendship. I would like to express my warmest feeling and thanks for my former teachers, instructors and supervisors during wonderful years of studying back home. I also acknowledge my teammates in SRC THOR rugby team for sharing good times as my mind was free from science and research.

Last but not least, I would like to pay high regards to my husband, my father, my mother, my brother and my sister for their sincere encouragement and inspiration throughout my research work. I owe everything to them. Roozbeh, I am truly grateful for your always being by my side, endless love, great patience, trust, care, support, unwavering belief in me and creating a pleasant atmosphere for me even in your busiest times of your PhD. Most of all, thank you for being my soulmate and best friend. I wish to express my love and gratitude to my wonderful parents, who raised me up with their extraordinary love, care, guidance and encouragement in all stages of my life and supported me in all my pursuits. They have been true and great supporters and have unconditionally loved me during my good and bad times. Mama and Baba, words are short to express my deep sense of gratitude towards you. You have willingly and selflessly sacrificed your lives for me and provided unconditional love and care. You have been a constant source of strength and inspiration. My grateful thanks are extended to my brother Behrouz and my sister Shalaleh for their loving, supportive and encouraging presence in my life. I know I always have my family to count on when times are rough. I love you so much, and I would not have made it this far without you. I am indebted to them for my entire life.

Negar Khoshnevis Gargar,

Delft, May 2014

Propositions

1. Air injection is an effective alternative for light oil recovery at shallow depths, medium pressures and low air injection rates (Thesis).
2. The character of the oil combustion process depends on composition of the multi-component oil. For an oil that consists predominantly of light components the process is vaporization dominated. When it consists of predominantly non-volatile components it becomes combustion dominated (Chapter 3).
3. In an oil mixture with a sufficient volatile fraction air injection leads to almost complete recovery of the heavy non-volatile fraction (Chapter 3).
4. In an MTO process in light oil recovery, an oxygen sorption (physical or chemical) step takes place at low temperatures prior to the full combustion reaction (Chapter 5).
5. In an air injection process (MTO) the presence of water, either initially or as an oxidation reaction product, improves the oil recovery, specially when the boiling temperature of the oil is close or slightly higher than that of the water (Chapter 4).
6. The initial saturation "at the end of the drainage cycle" used by Akbarabadi and Piri to find capillary trapping of carbon dioxide is much higher than the connate water saturation and is therefore not representative for long term field conditions.
7. Use of natural gas has only potentially a smaller carbon footprint than coal or oil. Therefore the advantage of using gas with the omnipresent leaking wells should not be overestimated.
8. The difference between the developing and developed countries is the governing system, not the people.
9. Also today, an investment in knowledge pays the best interest (Benjamin Franklin, Thomas Piketty).
10. There is no shortage of ugliness in the world. If man closed his eyes to it there would be even more (Furough Farrokhzad).

Stellingen

1. Luchtinjectie is een effectief alternatief voor de winning van lichte ondiep voorkomende olie bij middelhoge drukken en lage injectiesnelheden (Dit proefschrift).
2. Het karakter van het olieverbrandingsproces hangt af van de samenstelling van de multicomponenten olie. Voor een olie die voornamelijk bestaat uit lichte componenten wordt het proces overheerst door verdamping; wanneer het voornamelijk bestaat uit niet vluchtige olie wordt het proces overheerst door verbranding (Hoofdstuk 3).
3. In een oliemengsel met voldoende vluchtige olie leidt luchtinjectie tot bijna volledige winning van de zware niet-vluchtige oliefractie (Hoofdstuk 3).
4. In een middelhoog temperatuur oxidatie (MTO) proces, verbetert de aanwezigheid van hechtwater of reactiewater de oliewinning vooral als het kookpunt van de olie dichtbij of iets hoger ligt dan het kookpunt van water (Hoofdstuk 4).
5. In een middelhoog temperatuur oxidatie (MTO) proces voor lichte oliewinning, treedt eerst zuurstofsorptie (fysische of chemische) bij lage temperaturen op, voordat de volledige verbrandingsreactie begint (Hoofdstuk 5).
6. De initiële watersaturatie "aan het eind van de drainage cyclus" zoals gebruikt door Akbarabadi en Piri om de capillaire invanging van kooldioxide te vinden is veel hoger dan de hechtwater saturatie en derhalve niet representatief voor veldomstandigheden op de lange termijn. Akbarabadi, Morteza and Piri, Mohammad, Relative permeability hysteresis and capillary trapping characteristics of supercritical CO_2/brine systems: An experimental study at reservoir conditions, Advances in Water Resources, 52, 190-206 (2013).
7. Het gebruik van aardgas heeft slechts potentieel een lagere koolstofvoetafdruk dan kolen of olie. Daarom moet het voordeel van gebruik van gas met de alom aanwezige lekkende gasputten niet worden overschat.
8. Het verschil tussen ontwikkelingslanden en ontwikkelde landen ligt in het regeersysteem en niet in het verschil tussen mensen.
9. Ook vandaag de dag betaalt een investering in kennis de hoogste rente (Benjamin Franklin, Thomas Piketty).
10. Er is geen gebrek aan lelijkheid in de wereld. Als de mens daarvoor zijn ogen sluit zou er zelfs meer lelijkheid zijn. (Furough Farrokhzad).

Publications

1. Khoshnevis Gargar N., Mailybaev A.A., Marchesin D. and Bruining J., "Diffusive Effects on Recovery of Light Oil by Medium Temperature Oxidation", Accepted in Journal of Transport in porous Media (2014)
2. Khoshnevis Gargar N., Mailybaev A.A., Marchesin D. and Bruining J., "Compositional Effects in Light Oil Recovery: Vaporization vs. Combustion", Accepted in Journal of Porous Media (2014)
3. Khoshnevis Gargar N., Mailybaev A.A., Marchesin D. and Bruining J., "Effects of Water on Light Oil Recovery by Air Injection", Submitted (minor revision) to Fuel (2014)
4. Khoshnevis Gargar N., Mailybaev A.A., Marchesin D. and Bruining J., "Recovery of Light Oil by Air Injection at Medium Temperature: Experiments", Submitted to Journal of Petroleum Science and Engineering (2014)
5. Khoshnevis Gargar N., Mailybaev A.A., Marchesin D. and Bruining J., "Effect of Oil Composition on Light Oil Recovery by Air Injection", 6th International Conference on Porous Media and Annual Meeting of International society for porous media (Interpore), Milwaukee, USA (2014)
6. Khoshnevis Gargar N., Mailybaev A.A., Marchesin D. and Bruining J., "Role of Evaporation During Oil Recovery by Combustion", COMSOL conference, Rotterdam, The Netherlands (2013)
7. Khoshnevis Gargar N., Mailybaev A.A., Marchesin D. and Bruining J., "Numerical Simulation of Recovery of Light Oil by Medium Temperature Oxidation in Porous Media", COMSOL conference, Milan, Itally (2012)
8. Khoshnevis Gargar N., N., Achterbergh, N., Rudolph, E.S.J., and Bruining, J., "Modeling of In-Situ Combustion as Thermal Recovery Method for Heavy (Medium) oil", International Research NUPUS meeting, Freudenstadt, Germany (2010)
9. Khoshnevis Gargar, N., Achterbergh, N., Rudolph, E.S.J., and Bruining, J., "In-situ oil combustion: Processes perpendicular to the main gas flow direction", SPE Annual Technical Conference and Exhibition, (SPE 134655), Florence, Italy, (2010)
10. Mailybaev A.A., Khoshnevis Gargar N., Marchesin D. and Bruining J., "Oil Composition Effects in Light Oil Recovery by Air Injection", 14th European

Conference on the Mathematics of Oil Recovery (ECMOR XIV), Catania, Sicily, Italy (2014)

11. Mailybaev A.A., Marchesin D. and Bruining J., and Khoshnevis Gargar N. “Modelling of Recovery of Light Oil by Medium Temperature Oxidation“, EAGE, St. Petersburg, Russia (2013)

About the Author

Negar Khoshnevis Gargar was born on November 21, 1980 in Tabriz, Iran. Negar obtained mathematics and physics diploma from Farzanegan high school, Tabriz in 1999. She received her B.Sc. degree in Chemical Engineering in 2004 from Amirkabir University of Technology (Tehran Polytechnic), Tehran, Iran. In 2006, she received her M.Sc. degree in Petroleum Engineering, Reservoir Engineering in a dual degree program from University of Calgary, Canada and Petroleum University of Technology, Tehran, Iran. From 2006 to 2009, She worked in research institute of petroleum industry as reservoir engineer. Then She moved to the Netherland to start her Ph.D of Petroleum Engineering in the department of Geoscience and Engineering at Delft University of Technology, where she conducted her research under supervision of Prof. Dr. J. Bruining and Prof. Dr. D. Marchesin. Her research includes experimental work, modeling and simulation of combustion for enhanced recovery of light oil at medium pressures and medium temperatures.